



UNIL | Université de Lausanne

Unicentre

CH-1015 Lausanne

<http://serval.unil.ch>

Year : 2022

PD-I preserves the stem-like properties of memory-like CD8+ T cells during chronic viral infection

Maier Julia Malaika

Maier Julia Malaika, 2022, PD-I preserves the stem-like properties of memory-like CD8+ T cells during chronic viral infection

Originally published at : Thesis, University of Lausanne

Posted at the University of Lausanne Open Archive <http://serval.unil.ch>

Document URN : urn:nbn:ch:serval-BIB_8F0F5A35E0569

Droits d'auteur

L'Université de Lausanne attire expressément l'attention des utilisateurs sur le fait que tous les documents publiés dans l'Archive SERVAL sont protégés par le droit d'auteur, conformément à la loi fédérale sur le droit d'auteur et les droits voisins (LDA). A ce titre, il est indispensable d'obtenir le consentement préalable de l'auteur et/ou de l'éditeur avant toute utilisation d'une oeuvre ou d'une partie d'une oeuvre ne relevant pas d'une utilisation à des fins personnelles au sens de la LDA (art. 19, al. 1 lettre a). A défaut, tout contrevenant s'expose aux sanctions prévues par cette loi. Nous déclinons toute responsabilité en la matière.

Copyright

The University of Lausanne expressly draws the attention of users to the fact that all documents published in the SERVAL Archive are protected by copyright in accordance with federal law on copyright and similar rights (LDA). Accordingly it is indispensable to obtain prior consent from the author and/or publisher before any use of a work or part of a work for purposes other than personal use within the meaning of LDA (art. 19, para. 1 letter a). Failure to do so will expose offenders to the sanctions laid down by this law. We accept no liability in this respect.



UNIL | Université de Lausanne

Faculté de biologie
et de médecine

Département d'Oncologie

PD-1 preserves the stem-like properties of memory-like CD8⁺ T cells during chronic viral infection

Thèse de doctorat ès sciences de la vie (PhD)

présentée à la

Faculté de biologie et de médecine
de l'Université de Lausanne

par

Julia Malaika MAIER

Master of Biological Sciences, University of Konstanz, Germany

Jury

Prof. Matthieu Perreau, Président
Prof. Werner Held, Directeur de thèse
Prof. Sanjiv Luther, Expert
Prof. Joerg Huelsken, Expert

Lausanne
(2022)



UNIL | Université de Lausanne

Faculté de biologie
et de médecine

Département d'Oncologie

PD-1 preserves the stem-like properties of memory-like CD8⁺ T cells during chronic viral infection

Thèse de doctorat ès sciences de la vie (PhD)

présentée à la

Faculté de biologie et de médecine
de l'Université de Lausanne

par

Julia Malaika MAIER

Master of Biological Sciences, University of Konstanz, Germany

Jury

Prof. Matthieu Perreau, Président
Prof. Werner Held, Directeur de thèse
Prof. Sanjiv Luther, Expert
Prof. Joerg Huelsken, Expert

Lausanne
(2022)

Acknowledgment

First and foremost, I would like to thank Prof. Werner Held for giving me this opportunity to work in his group, for sharing his immense knowledge to advance this project and allowing my personal scientific growth. I will be forever grateful for your kind support and motivation throughout the research phase but especially for the writing.

Additionally, I would like to express my gratitude to my thesis committee representative, Prof. Matthieu Perreau, as well as the remaining members of the thesis committee, for the useful comments and remarks.

I want to especially thank my lab-members, both former and recent, without them it would not have been the same. Particularly, I would like to thank Mélanie for her help, support and her open ear in times of need. Cathérine S. for her kindness, support and her help with the lentiviruses. I would like to thank Vijay for explaining me everything necessary to take over this project. Imran for his knowledge and his insightful discussions. I would also like to thank Joana and Daniela for welcoming me in the beginning and helping me to adapt to the new environment. I would like to thank everyone in the lab for the happy coffee and lunchbreaks together, their support and helpful discussions. I would also like to specifically thank Romain, Yannis and Alexandre for the laughs, lightness and French in the lab.

I would also like to thank Tania for her bioinformatic analysis, without her that would not have been possible in this way.

Particularly, I would like to thank Cathérine Fumey for her kindness and warm words. Additionally, I'm grateful for her mouse management together with Aline Decultot.

A huge thanks to all the members of the flow cytometry facility Francisco, Kevin and Romain for the great environment and for answering calls at impossible times.

Thank goodness I was able to spend most of my time in the Biopôle building before COVID, so I was able to enjoy great lunches with people from the second floor, such as Mathias Wenes, Céline Godfroid, Giusy Di Conza, Alison Jaccard, Daniela Cropp and many more. Specific thank goes to Elisabetta Cribioli for her kindness and patience.

I would like to thank my friends here in Lausanne for enjoying the weekends and evenings together. I would like to especially thank Nicole Albrecher, Dina Bonazzoli, Marika Zietak for their friendship and of course the rest of this KN group for the great times together. Additionally, I would like to thank Valeria Superti for taking me out of my shell and spending great times together, either skiing or partying.

A huge thanks to my friends back in Germany that I neglected a bit in the last months. Thank you for your support and patience with me Sarah Mross, Julia Ruffing with her lovely little family, Eva Schaefer, Laura Kerling, Julia Körner, Annette, Tobias & Anna and many others.

Last but not least I would also like to thank my family back at home for their support during my whole studies that allowed me to go to Konstanz and later here to Lausanne for my PhD. Vielen lieben Dank Mama und Papa, Benedikt, Oma Annemarie und Opa Helmut, Patrik & Nina ohne eure Liebe und Unterstützung wäre all das nicht möglich gewesen. Vielen lieben Dank Patrik und Nina für eure technische und moralische Unterstützung!! Worte können meine Dankbarkeit an euch Alle nicht ausdrücken. Vielen lieben Dank für Alles!!!

J'aimerai aussi remercier Frédéric pour me soutenir, me faire rigoler et toutes les aventures ensemble, sans toi je serai plus en Suisse. Merci beaucoup pour me montrer la beauté, qui est merveilleuse en partageant. Merci beaucoup pour ton patience avec moi ces dernier mois.

I'm sorry for anyone that I forgot to mention personally. I'm grateful for every single word or gesture of encouragement.

PD-1 maintient les propriétés des cellules semblables à la mémoire T CD8⁺ pendant une infection virale chronique

Plusieurs virus résistent à la réponse immunitaire et causent une infection chronique, comme les virus des hépatites B (VHB) et C (VHC), le virus de l'immunodéficience humaine (VIH) chez l'homme ou le virus de la chorioméningite lymphocytaire (CMLV) chez les souris. C'est-à-dire que les cellules CD8⁺ spécifiques de l'antigène (T_{EX}) de l'infection sont moins efficaces qu'elles le seraient lors d'une infection aiguë. Ces cellules T_{EX} expriment des récepteurs sur leur surface, ce qui diminue leur efficacité et les épuise (récepteurs inhibiteurs). Cette population est maintenue par des cellules ancêtres (T_{ML}) qui possèdent non seulement des caractéristiques d'épuisement, comme l'expression des récepteurs inhibiteurs, mais aussi des caractéristiques de cellules souches, comme la capacité de s'auto-renouveler et de produire des cellules plus spécifiques. Le plus important récepteur inhibiteur est le récepteur « programmed cell death protein 1 » (PD-1). Ce dernier interagit avec son ligant PD-L1. Le résultat est l'inhibition de l'activité des cellules CD8⁺. Lorsque l'on empêche l'interaction de manière momentanée ou permanente entre PD-1 et PD-L1, la quantité de T_{ML} augmente et elles produisent plus de T_{EX} : les cellules sont plus efficaces. Il existe déjà des études sur l'effet de PD-1 sur les T_{EX}, mais pas sur les T_{ML}. C'est donc la question que nous avons abordée.

Pour répondre à cette question, nous nous sommes penchés sur le comportement des cellules CD8⁺ spécifiques de la CMLV déficientes en PD-1 (PD-1 ko) ou des cellules CD8⁺ correspondantes de type sauvage (WT) soumises au blocage de PD-1 à l'aide d'anticorps dans un modèle d'infection chronique par la CMLV. Les T_{ML} PD-1 ko ou traitées par anti-PD-L1 étaient, phénotypiquement et au niveau de l'expression des gènes, similaires aux T_{ML} WT. Cependant, les T_{ML} PD-1 ko présentes durant la phase chronique de l'infection avaient une capacité réduite à répondre à une re-stimulation, c'est-à-dire que leur « caractère souche » était réduit par rapport aux T_{ML} WT. Cette diminution, chez les T_{ML} PD-1 ko, n'a pas été observée lors la phase aiguë de l'infection, suggérant que le défaut a été acquis lors de l'infection chronique. Le « caractère souche » des T_{ML} était également réduit lorsqu'elles étaient soumises à une interruption du signal PD-1 durant la phase chronique. L'analyse de l'expression de gènes a révélé que les principales voies de signalisation en aval du récepteur des cellules T (TCR) avaient une activité réduite chez les T_{ML} PD-1 ko et aussi en partie chez les T_{ML} soumises au blocage de PD-1 par rapport aux T_{ML} WT. De plus, ces T_{ML} PD-1 ko présentaient une expression réduite des gènes liés au « caractère souche » des cellules CD8⁺ *Myb* et *Klf4*, identifiés précédemment. En effet, la diminution de l'expression de *Myb* et *Klf4* dans les cellules WT CD8⁺ spécifiques au virus a diminué la capacité d'auto-renouvellement et la production de cellules plus spécialisées, reproduisant dans une large mesure le phénotype des T_{ML} PD-1 ko.

Nos données montrent que l'expression de PD-1 protège le « caractère souche » des T_{ML}, et assure ainsi le maintien à long terme d'une réponse immunitaire nécessaire pour contenir l'infection. Nous suggérons que PD-1 servirait de mécanisme de rétroaction négative physiologique pour empêcher la surstimulation des T_{ML} durant la phase chronique de l'infection. Lorsqu'une surstimulation se produit sur une période prolongée, en raison de l'absence de PD-1, les cellules CD8⁺ s'adaptent en réduisant la transduction des signaux via le TCR. Cela pourrait se traduire par une réduction du « caractère souche » de ces cellules. Ces résultats ont des implications pour l'immunothérapie du cancer médiée par le blocage de PD-1. Il pourrait donc être bénéfique de limiter le nombre de cycles de blocage du PD-1 pour préserver la fonction des T_{ML} et ainsi maintenir une activité antitumorale à long terme.

PD-1 maintient les propriétés de type souche des cellules T CD8⁺ à mémoire pendant une infection virale chronique

La réponse immunitaire des lymphocytes T (LT) CD8⁺ est normalement capable d'éliminer les cellules infectées par un virus. Cependant, plusieurs virus, tels que le virus de l'hépatite B (VHB), le virus de l'hépatite C (VHC), le virus de l'immunodéficience humaine (VIH) ou certaines souches du virus de la chorioméningite lymphocytaire (CMLV) peuvent établir une infection chronique chez des individus/souris immunocompétents en dépit d'une réponse des lymphocytes T (LT) CD8⁺. Contrairement à une réponse protectrice, les LT CD8⁺ chroniquement activés perdent progressivement leurs capacités prolifératives et effectrices, subissent une différenciation terminale et augmentent l'expression de récepteurs inhibiteurs tels que « programmed cell death protein 1 » (PD-1). C'est ce qu'on appelle l'épuisement des LT. Récemment, il a été démontré que les LT CD8⁺ dits "de type mémoire" (T_{ML}) soutenaient la réponse immunitaire à une infection virale chronique. Les T_{ML} présentent des propriétés semblables à celles des cellules souches : ils conservent une capacité proliférative, s'auto-renouvellent et produisent des cellules différenciées (cellules épuisées ou T_{EX}) qui ont un potentiel lytique mais ont perdu leur potentiel prolifératif. Alors que le rôle de PD-1 dans l'épuisement des LT a été largement étudié, l'impact de son expression sur la fonction des T_{ML} n'a pas encore été abordé. Pour répondre à cette question, nous avons étudié le comportement des LT CD8⁺ spécifiques au CMLV déficients en PD-1 (PD-1 ko) ou des LT CD8⁺ correspondants de type sauvage (WT) soumis au blocage de PD-1 à l'aide d'anticorps dans un modèle d'infection chronique par le CMLV. Les T_{ML} PD-1 ko ou traitées par anti-PD-L1 étaient, phénotypiquement et transcriptionnellement, similaires aux T_{ML} WT. Cependant, les T_{ML} PD-1 ko présentes durant la phase chronique de l'infection avaient une capacité réduite à répondre à une re-stimulation, c'est-à-dire que leur "caractère souche" était réduit par rapport aux T_{ML} WT. Cette réduction, chez les T_{ML} PD-1 ko, n'a pas été observée lors de la phase aiguë de l'infection, suggérant que le défaut a été acquis pendant de l'infection chronique. Leur "caractère souche" était également réduit lorsque les T_{ML} étaient soumis à un blocage de PD-1 durant la phase chronique. L'analyse du transcriptome a révélé que les principales voies de signalisation en aval du récepteur des cellules T (TCR), y compris les voies NFAT, AP-1 et NF-κB, avaient une activité réduite dans les T_{ML} PD-1 ko par rapport aux T_{ML} WT. L'activité de la voie NF-κB était également réduite lorsque les T_{ML} étaient soumis au blocage de PD-1. De plus, ces T_{ML} PD-1 ko présentaient une expression réduite des gènes liés au "caractère souche" des LT CD8⁺ *Myb* et *Klf4*, identifiés précédemment. En effet, le knock down de *Myb* et *Klf4* dans les LT CD8⁺ spécifiques du virus a récapitulé dans une large mesure le phénotype des T_{ML} PD-1 ko. Nos données montrent que l'expression de PD-1 protège le "caractère souche" des T_{ML}, et assure ainsi le maintien à long terme d'une réponse immunitaire nécessaire pour contenir l'infection. Nous proposons que PD-1 servirait de mécanisme de rétroaction négative physiologique pour empêcher la surstimulation des T_{ML} durant la phase chronique de l'infection. Lorsqu'une surstimulation se produit sur une période prolongée, en raison de l'absence de PD-1, les LT CD8⁺ s'adaptent en réduisant la transduction des signaux via le TCR. Cela pourrait être responsable de la réduction du "caractère souche" de ces cellules. Ces résultats ont des implications pour l'immunothérapie du cancer médiée par le blocage de PD-1. Un excès de cycles de traitement par blocage du PD-1 peut finir par dégrader l'efficacité des T_{ML} spécifiques à la tumeur. Il pourrait donc être important de limiter le nombre de cycles de traitement afin de préserver la fonction des T_{ML} et de maintenir une activité anti-tumorale à long terme.

PD-1 preserves the stem cell-like properties of memory-like CD8⁺ T cells during chronic viral infection

An immune response by CD8⁺ T cells is normally able to clear virus infected cells. However, several viruses, such as hepatitis B virus (HBV), hepatitis C virus (HCV), human immunodeficiency virus (HIV) or certain lymphocytic choriomeningitis virus (LCMV) strains can establish chronic infection in immunocompetent individual/mouse strains despite the induction of a CD8⁺ T cell response. Compared to a protective response, chronically activated CD8⁺ T cells progressively lose their proliferative and effector capacities, undergo terminal differentiation and upregulate the expression of inhibitory receptors such as, programmed death protein 1 (PD-1). This is referred to as T cell exhaustion. Recently, so called memory-like (T_{ML}) CD8⁺ T cells were found to sustain the immune response to chronic viral infection. T_{ML} cells have stem cell-like properties i.e. they retain proliferative capacity and self-renew or yield differentiated cells (exhausted or T_{EX} cells) that have lytic potential but have lost proliferative potential. While the role of PD-1 for T cell exhaustion has been extensively studied, how PD-1 expression impacts the function of T_{ML} cells has not been addressed before.

To address this question, we investigated the behavior of LCMV-specific CD8⁺ T cells deficient of PD-1 (PD-1 ko) or of corresponding wild type (WT) CD8⁺ T cells subjected to PD-1 blockade using antibodies in a model of chronic LCMV infection. PD-1 ko and anti-PD-L1 treated T_{ML} cells were phenotypically and transcriptomically remarkably similar to WT T_{ML} cells. However, PD-1 ko T_{ML} present during the chronic phase of the infection had reduced capacity to respond to recall stimulation i.e. the stemness of these cells was reduced compared to WT T_{ML} cells. Reduced stemness of PD-1 ko T_{ML} cells was not observed at the acute phase of the infection suggesting that the defect was acquired during chronic infection. The stemness was also reduced when T_{ML} cells were subjected to PD-1 blockade during the chronic phase.

Transcriptome analysis revealed that key downstream T cell receptor (TCR) signalling pathways, including the NFAT, AP-1 and NF-κB pathways, had reduced activity in PD-1 ko compared to WT T_{ML} cells. The activity of the NF-κB pathway was also reduced when T_{ML} cells were subjected to PD-1 blockade. Moreover, PD-1 ko T_{ML} had reduced expression of the previously identified CD8⁺ T cell stemness genes *Myb* and *Klf4*. Indeed, knock down of *Myb* and *Klf4* in virus-specific CD8⁺ T cells recapitulated to a significant extent the phenotype of PD-1 ko T_{ML} cells.

Our data show that PD-1 expression protects the stemness of T_{ML} cells, and thus ensures the long-term maintenance of an immune response that is needed to contain the infection, although not sufficient to clear the infection. We propose that PD-1 serves as a physiological negative feedback mechanism to prevent overstimulation of T_{ML} cells during the chronic phase of the infection. When overstimulation occurs over a prolonged period of time, due to the absence of PD-1, CD8⁺ T cells adapt by reducing the transduction of signals via the TCR. This may be responsible for the reduced stemness of these cells. These findings have implications for PD-1 blockade-mediated cancer immunotherapy. An excess of PD-1 blockade treatment cycles may eventually degrade the effectiveness of tumor-specific T_{ML} cells. It may thus be important to limit the number of treatment cycles to preserve T_{ML} function in order to maintain anti-tumor activity long-term.

List of Abbreviations

°C: Grad celsius	Elovl6: Elongation of long-chain fatty acids family member 6
4-1BB: CD137	EDTA: Ethylene diamine tetra acetic acid
7AAD: 7-aminoactinomycin D	Eomes: Eomesodermin
αPD-1: anti-PD-1	ERK1/2: Extracellular signal-regulated protein kinase ½
αPD-L1: anti PD-L1	FasL: Fas-Ligand
ACK: Ammonium-Chloride-Potassium buffer	FCS: Fetal calf serum
Ab: Antibody	Foxo1: Forkhead box O1
ag: Antigen	GITR: Glucocorticoid-induced TNFR-Protein
AnnexV: AnnexinV	GLUT1: Glucose transporter 1
AP-1: Activator protein-1	GSEA: Gene set enrichment analysis
APC: Antigen-presenting cell	GzmB: Granzyme B
ATF: Activating transcription factors	gp: Glycoprotein
ATP: Adenosine triphosphate	h: Hour
Bcl-2/3/10: B cell lymphoma 2/3/10	HBV: Hepatitis B virus
Bcl-xL: B-cell lymphoma-extra large	HCV: Hepatitis C virus
BCR: B cell receptor	HDAC: Histone deacetylase
Blimp1: B lymphocyte-induced maturation protein 1	HIV: Human immunodeficiency virus
bZIP: Basic leucin-zipper	i.p.: intraperitoneal
Ca²⁺: Calcium	i.v.: intravenous
CAR T cell: Chimeric antigen receptor T cells	IFN: Interferon
CARD: Caspase recruitment domains	ICOS: Inducible T cell costimulator
Cardif: CARD adaptor inducing IFN-β	IFNα/β/γ: Interferon-α/β/γ
CARMA1: Caspase recruitment domain-containing membrane-associated guanylate kinase protein 1	IFNAR1: Interferon alpha and beta receptor subunit 1
CBM: CARMA1/Bcl10/MALT1	IFNAR2: Interferon alpha and beta receptor subunit 2
CCL2: CC-chemokine ligand 2	IkB: Inhibitor of nuclear factor kappa B
CPM: Counts per million	IKK: IkB Kinase
CCR7: C-C chemokine receptor 7	IL-2/7/12/15/18: Interleukin-2/7/12/15/18
CD3ζζ, δε, γε: Cluster of differentiation zeta-zeta, delta-epsilon, gamma-epsilon	IL7Ra: Interleukin 7 receptor alpha(CD127)
d0/8/27/28/41: Day 8/27/28/41	IL12Rb2: Interleukin 12 receptor beta 2
CD: Cluster of differentiation	IRF: Interferon regulatory factor
CD62L: CD62/L-selectin	ITAM: Immunoreceptor tyrosine-based activation motifs
Cx3cr1: C-X3-C motif chemokine receptor 1	ISG: Interferon stimulated genes
DAG: Diacylglycerol	JAK: Janus kinase
DAPI: 4',6-diamidino-2-phenylindole	Klf4: Kruppel like factor 4
DC: Dendritic cell	KLRG1: Killer-cell lectin like receptor G1
DEG: Differentially expressed genes	ko: Knock out
DG: α-Dystroglycan	Lag3: Lymphocyte-activation gene 3
DNA: Deoxyribonucleic acid	LAT: Linker for activation of T-cells family member
ds: Double-stranded	

Lck: Lymphocyte-specific protein tyrosine kinase

LCMV: Lymphocyte choriomeningitis virus

LCMV Arm: LCMV Armstrong

LCMV cl13: LCMV clone 13

LICOS: Ligand of ICOS

LSD-1: Lysine-specific demethylase 1

LV: Lentivirus

mAb: monoclonal antibody

MAF: Musculoaponeurotic fibrosarcoma

MALT1: Mucosa-associated lymphoid tissue lymphoma translocation protein 1

MAPK: Mitogen-activated protein kinase

MDR: MitoTracker® Deep Red

MFI: Mean fluorescence intensity

MG: MitoTracker® Green

MHC: Major histocompatibility complex

MDA5: Melanoma differentiation-associated gene 5

MPEC: Memory precursor effector cell

MSigDB: Molecular Signatures Database

mTOR: Mammalian target of rapamycin

NSCLC: Non-small cell lung cancer

NFAT: Nuclear factor of activated T cells

NF- κ B: Nuclear factor- κ B

np: Nucleoprotein

OE: over expression

OX40: CD134

OXPHOS: Oxidative phosphorylation

PBMCs: Peripheral blood mononuclear cells

PCA: Principal component analysis

PD-1: Programmed cell death protein 1

PD-L1: Programmed cell death protein ligand 1

PFU: Plaque forming units

PID: Pathway interaction database

Plxdc2: Plexin domain-containing protein2

p.i.: post infection

PKC θ : Protein kinase C theta

PLCy1: 1-phosphatidylinositol 4,5-bisphosphate phosphodiesterase gamma1

Prdm1: PR domain zinc finger protein 1

PRR: Pattern recognition receptors

PTK: Protein-tyrosine kinase

Ras: Rat sarcoma

RasGRP-1: Ras guanyl releasing protein-1

RCC: Renal cell carcinoma

RE: Response elements

RIG-I: Retinoic acid-inducible gene I

RNA: Ribonucleic acid

RNA-Seq: RNA Sequencing

ROS: Reactive oxygen species

RT: Room temperature

RTK: Receptor tyrosine kinase

RV: Retrovirus

Sca-1: Stem cell antigen-1

SD: Standard deviation

shRNA: short-hairpin RNA

SH2: Src homology 2

SIV: Simian immunodeficiency virus

SLEC: Short-lived effector cell

SLP-76: SH2 containing leukocyte phosphoprotein of 76 kDa

Smad1: Mothers against decapentaplegic homolog 1

ss: Single stranded

STAT: Signal transducer and activator of transcription

T_{CM}: Central memory CD8⁺ T cells

T_{fh}: T follicular helper cells

T_{EM}: Effector memory CD8⁺ T cells

T_{EX}: Exhausted effector CD8⁺ T cells

Th1: T helper 1 cells

T_M: Memory CD8⁺ T cells

T_{ML}: Memory-like CD8⁺ T cells

T_{Naive}: Naïve CD8⁺ T cells

T_{RM}: Tissue resident memory CD8⁺ T cells

Tbet: T-box transcription factor 21

Tcf1: T cell factor 1

TCR: T cell receptor

Tim3: T-cell immunoglobulin and mucin domain-containing protein 3

TLR: Toll like receptors

TNF- α : Tumour necrosis factor α

TNFR: Tumour necrosis factor receptor

TRIF: TIR domain-containing adaptor protein inducing IFN β

TRAFs: Tumour necrosis factor receptor-associated factors

TYK2: Tyrosine kinase 2

WT: Wild-type

ZAP-70: Zeta-chain-associated protein kinase-70

Zeb2: Zinc Finger E-box homeobox 2

List of Figures

FIGURE 1: T cell response during acute infection	4
FIGURE 2: Three signal model of T cell activation	5
FIGURE 3: Schematic illustration of TCR signalling	7
FIGURE 4: Bifurcative model of CD8 ⁺ T cell differentiation	8
FIGURE 5: Central memory CD8 ⁺ T cells derive from <i>Tcf7</i> ⁺ cells without passing through effector differentiation	9
FIGURE 6: T cell response during chronic infection	10
FIGURE 7: Hierarchical T cell exhaustion during chronic virus infection	12
FIGURE 8: Memory-like CD8 ⁺ T cells (T _{ML}) sustain the immune response in chronic viral infection	14
FIGURE 9: Populations of T _{ML} and T _{EX} cells during chronic infections	14
FIGURE 10: PD-1 signal inhibits T cell receptor (TCR) signalling pathway and CD28 co-stimulation pathway through several different mechanisms	18
FIGURE 11: Increased abundance of PD-1 ko T _{ML} cells in chronic LCMV infection	32
FIGURE 12: Similar phenotype and functionality of WT and PD-1 ko T _{ML} cells	33
FIGURE 13: Reduced recall expansion capacity of PD-1 ko T _{ML} cells	35
FIGURE 14: Increased expansion of PD-1 ko T _{ML} cells with reduced expression of memory and effector markers	37
FIGURE 15: PD-1 ko T _{ML} cells are phenotypically similar to WT T _{ML} in a competitive environment	38
FIGURE 16: Impaired stemness of PD-1 ko compared to WT T _{ML} cells	40
FIGURE 17: Increased primary expansion of acute phase PD-1 ko T _{ML} and T _{EX} cells	41
FIGURE 18: Similar phenotype and functionality of acute phase WT and PD-1 ko T _{ML} cells	42
FIGURE 19: Superior stemness of acute phase PD-1 ko T _{ML} cells	43
FIGURE 20: Increased expansion of PD-1 ko T _{ML} cells in a mixed environment	45
FIGURE 21: PD-1 ko and WT T _{ML} cells have comparable stemness in mixed transfers	47
FIGURE 22: Anti-PD-L1 treatment expands T _{ML} cells	48
FIGURE 23: Impaired stemness of T _{ML} from anti-PD-L1 treated mice	50
FIGURE 24: Increased cell cycling of acute phase PD-1 ko T _{ML} cells	51
FIGURE 25: Increased apoptosis of chronic phase PD-1 ko T _{ML}	52

FIGURE 26: Increased mitochondrial activity and cellular ROS production by chronic phase PD-1 ko T _{ML} cells	54
FIGURE 27: Transcriptome analysis reveals impaired downstream TCR signalling in PD-1 ko T _{ML} cells	56
FIGURE 28: Chronic phase PD-1 ko T _{ML} cells show reduced TCR signalling	58
FIGURE 29: Reduced <i>Myb</i> and <i>Klf4</i> expression in chronic phase PD-1 ko T _{ML} cells	60
FIGURE 30: Reduction of <i>Klf4</i> and <i>Myb</i> expression impairs stemness of P14 cells	62
FIGURE 31: PD-1 serves as a negative feedback mechanism to prevent overstimulation of T _{ML} cells	72

Table of contents

Acknowledgement	i
Résumé large public	ii
Résumé	iii
Summary	iv
List of Abbreviations	v
List of Figures	vii
1. Introduction	1
1.1 Immune response to infection	2
1.2 Innate immune response to viral infection	3
1.3 CD8 ⁺ T cell response to acute viral infection	4
1.4 CD4 ⁺ T helper cell response to acute viral infection	6
1.5 Signalling pathways involved in CD8 ⁺ T cell activation	6
1.6 CD8 ⁺ T cell differentiation during acute infection	8
1.6.1 Transcription factors involved in effector and memory differentiation	9
1.7 The CD8 ⁺ T cell response in chronic viral infection	10
1.8 CD4 ⁺ T cell response in chronic infection	13
1.9 Memory-like CD8 ⁺ T cells sustain the immune response in chronic infection	13
1.9.1 Transcription factors involved in T _{EX} and T _{ML} differentiation	15
1.9.2 Metabolism of CD8 ⁺ T cells during chronic virus infection	16
1.10 Importance and function of PD-1 in chronic infections	17
Aim of this study	20
2. Material and Methods	21
2.1 Mouse strain information	22
2.2 Antibodies	22
2.2.1 Flow cytometry	22
2.2.2 <i>In vivo</i> blocking antibodies	23
2.3 Lentivirus and Retrovirus constructs	23
2.4 Primers for qPCR	24
2.5 Chemicals	24
2.6 Cell Culture	24
2.7 Buffers and Solutions	25
2.8 Chemicals, Peptides, recombinant Proteins and Commercial assays	25
2.9 LCMV infections and viral titers	25
2.10 Adoptive T cell transfer	26
2.11 Plasmids, virus production and T cell transduction	26
2.12 Tissue preparation and cell suspension	27
2.13 Flow cytometry and cell sorting	27
2.14 RT-qPCR analysis	28
2.15 RNA-Seq analysis	28
2.16 Data analysis	29
2.17 Figure creation	30

3. Results	31
3.1 Increased abundance of PD-1 ko T _{ML} cells in chronic LCMV infection	32
3.2 Impaired stemness of PD-1 ko T _{ML} cells from chronic LCMV infection	34
3.3 Increased abundance of PD-1 ko T _{ML} cells in a competitive situation	36
3.4 Impaired stemness of PD-1 ko T _{ML} cells from a competitive situation	39
3.5 Increased abundance of PD-1 ko T _{ML} during the acute phase of chronic infection	40
3.6 Increased stemness of PD-1 ko T _{ML} cells present at the acute phase of chronic infection	43
3.7 Increased expansion of acute phase PD-1 ko T _{ML} cells in mixed transfers	44
3.8 Comparable stemness of acute phase PD-1 ko and WT T _{ML} cells in mixed transfers	46
3.9 PD-1:PD-L1 blockade reduces stemness of WT T _{ML} cells	47
3.10 Chronic phase PD-1 ko T _{ML} cells have a greater propensity to undergo apoptosis	51
3.11 Chronic phase PD-1 ko T _{ML} have an increased mitochondrial activity and cellular ROS	53
3.12 Transcriptome analysis of WT and PD-1 ko T _{ML} cells	55
3.13 PD-1 deficiency impairs the expression of TCR downstream genes	57
3.14 PD-1 deficiency impairs downstream TCR signalling	59
3.15 Reduced expression of the stemness genes <i>Myb</i> and <i>Klf4</i> in PD-1 ko T _{ML}	59
4. Discussion	64
4.1 Phenotypic changes in T _{ML} and T _{EX} cells lacking PD-1	65
4.2 Reduced stemness of PD-1 ko T _{ML} cells	67
4.3 Cycling, survival and metabolism of T _{ML} cells lacking PD-1	68
4.4 Transcriptome of T _{ML} cells lacking PD-1 or after PD-1 blockade	69
4.5 Reduced <i>Myb</i> and <i>Klf4</i> expression explains the impaired stemness of PD-1 ko T _{ML} cells	70
4.6 Perspective	72
5. References	73

1. Introduction

1.1 Immune response to infection

The first layer of protection against infection includes physical barriers, e.g. epithelial cell layers that express tight cell-cell contacts (e.g. tight junctions, cadherin-mediated cell interactions), the secreted mucus layer that overlays the epithelium in the respiratory, gastrointestinal and genitourinary tracts as well as the epithelial cilia that permit constant renewal of this mucus layer¹.

When pathogens cross barriers, such as epithelia, the immune system is responsible for clearing the infection. Initially, the innate branch of the immune system reacts to immediately inhibit pathogen spread and replication. Thereby, soluble, membrane-bound and intracellular receptors recognise molecular patterns specifically associated with invading pathogens, which induces an innate immune response (or an inflammatory response). In addition to soluble mediators, the innate branch consists of a variety of cells of myeloid origin, such as granulocytes, that are attracted to infected tissues where they can phagocytose pathogens. Additionally, monocytes immigrate into infected tissues that can differentiate into macrophages, which are specialised phagocytes, and which can promote inflammatory responses. The combined action of phagocytic cells and soluble mediators (antimicrobial peptides and complement) aims at rapidly controlling the infection. However, the innate immune system is often not sufficient to clear the pathogen completely and the induction of an adaptive immune response is necessary.

In order to induce an adaptive immune response, dendritic cells (DCs), that are tissue resident or derive from monocytes, function at the intersection between the innate and adaptive immune system. DCs are professional antigen-presenting cells (APC) and have the capacity to migrate from inflamed tissues to local lymph nodes where they induce an adaptive immune response. The adaptive immune system has the ability to remember previous pathogen encounter and to induce a more rapid and robust response upon re-infection with the same pathogen. This characteristic of the adaptive immune system is called immunological memory and is used in vaccination, in order to induce protective immunity². The adaptive immune response is based on clonally distributed antigen-specific surface receptors expressed by T- and B-lymphocytes i.e. T cell receptors (TCR) and B cell receptors (BCR), respectively. Following activation, pathogen-specific B lymphocytes differentiate into plasma cells that produce soluble pathogen receptors, so called antibodies. Antibodies can bind and neutralise pathogens, activate the complement system or facilitate phagocytosis³. In addition, antigen-specific naïve CD4⁺ T cells are activated to ensure optimal responses by other lymphocytes or macrophages via the secretion of cytokines. However, when pathogens hide inside host cells, the generation of cytotoxic CD8⁺ T cells is necessary to eliminate the pathogen. Rare antigen-specific naïve CD8⁺ T cells are activated upon the recognition of the cognate antigen presented on DCs. This leads to the clonal expansion of the antigen-specific CD8⁺ T cells and their acquisition of effector functions. These T cells will eventually migrate to the infected tissue and provide help to macrophages or kill infected cells by releasing cytotoxic molecules, such as perforin and granzymes⁴. Therefore, CD8⁺ T cell response is necessary to protect against intracellular pathogens, such as viruses, certain bacteria, fungi and parasites.

Unfortunately, several intracellular pathogens, such as human immunodeficiency virus (HIV) or hepatitis C virus (HCV) persist even though CD8⁺ T cell responses are induced.

1.2 Innate immune response to viral infection

Lymphocytic choriomeningitis virus (LCMV) is a mouse pathogen that belongs to the arenaviridae. It can be transmitted to humans or other animals through contact with droppings, urine and saliva of infected rodents. LCMV has been a key model to study viral infections in mice^{5,6}. LCMV is a spherical enveloped virus whose nucleocapsid contains two negative single-stranded ribonucleic acid (RNA) segments⁷. LCMV enters cells through attachment of the virion to the surface glycoprotein α -dystroglycan (DG) that is widely expressed in many tissues and appears to function as a transmembrane linker between the extracellular matrix and intracellular cytoskeleton⁸. The virion is endocytosed into the cytoplasm of the host cells where it fuses with the vesicle membrane and releases the ribonucleocapsid into the cytoplasm. LCMV's negative single-stranded RNA needs to be transcribed into positive-stranded RNA by the virus' RNA-polymerase.

The release of foreign RNA into the cytoplasm triggers an immediate immune response in the host cell by specific pattern recognition receptors (PRRs). The PRRs, retinoic acid-inducible gene I (RIG-I) and melanoma differentiation-associated gene 5 (MDA5) are the main cytosolic receptors that are responsible to recognize pathogen-derived RNA. RIG-I and MDA5 contain amino-terminal caspase recruitment domains (CARD) and a C-terminal region with a helicase domain⁹ and recognize double-stranded (ds)RNA or single-stranded (ss) RNA¹⁰. RIG-I preferentially recognizes single-stranded (ss) RNA, that contains a terminal 5' triphosphate (ppp), but not a 5'OH or a 5'-methylguanosine cap⁹. RIG-I binding to ppp induces a conformational change that activates it⁹. This induces downstream signalling by association with TRIF (TIR domain-containing adaptor protein inducing IFN β) and Cardif (CARD adaptor inducing IFN- β), respectively, leading to the activation of IRF3 (interferon regulatory factor 3) and IRF7. IRF3/7 induces the production of type I interferons (IFNs), IFN α and IFN β . Type I IFNs signal in an autocrine and paracrine manner to induce interferon-stimulated genes (ISGs), e.g. *Irf7*¹⁰ and other broadly acting effectors including *Irf1*, *C6orf150*, *HPSE*, *RIG-I* and *MDA5*¹¹. For the paracrine route, type I IFNs are secreted, and they then signal through a heterodimeric transmembrane receptor composed of IFNAR1 (interferon alpha and beta receptor subunit 1) and IFNAR2¹². Ligation of IFNAR induces phosphorylation of receptor-associated protein tyrosine kinases JAK1 (Janus kinase 1) and TYK2 (tyrosine kinase 2), which triggers a downstream signalling cascade to induce the transcription of ISGs. These restrict viral replication in already infected cells and promote an antiviral state in bystander cells¹².

Membrane bound TLRs (Toll like receptors) that recognize microbial RNA, such as TLR7 and TLR8 are not required to control acute LCMV infection, but are required for an efficient control of chronic LCMV infection¹³. In DCs and macrophages, LCMV enters the cell via the endosome, where TLR7 and -8 respond to single-stranded RNA¹⁰. Upon TLR7 and -8 engagement, the adaptor protein MyD88 binds and leads to a signal cascade that activates and leads to the translocation of the TF (transcription factors) AP-1 (activator protein) and NF- κ B (nuclear factor κ B) and induce the transcription of proinflammatory cytokines such as IL-1 β and TNF- α (tumour necrosis factor alpha) and immunostimulatory cytokines such as IL-12¹⁰.

In addition to induce an antiviral state, IFN α / β activate immature DCs by enhancing the cell-surface expression of major histocompatibility complex (MHC) and co-stimulatory ligands, e.g. CD80 and CD86¹². Additionally, IFN α / β promote the ability of DCs to cross-present antigens on MHC class I (MHC-I) to activate CD8⁺ T cells during viral infections, such as LCMV¹². Finally, Type I IFN acts as a third signal for T cell activation i.e. it further increases T cell expansion and it is responsible for the acquisition of effector functions by CD8⁺ T cells (see later).

1.3 CD8⁺ T cell response to acute viral infection

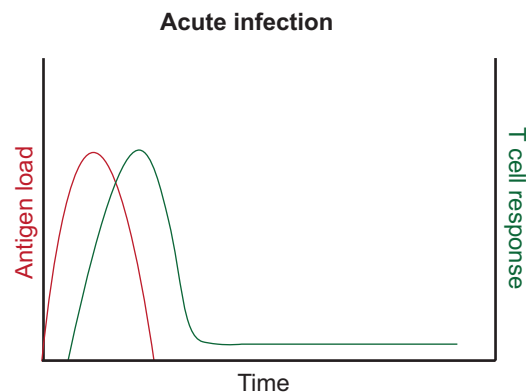


Figure 1: T cell response during acute infection. The CD8⁺ T cell response peaks with a delay after the peak of the virus titer, during which the innate immune response already inhibits the spread of infection. After the clearance of infection, a pool of stable long-lived memory T cells (T_M) remains in the absence of antigen in a cytokine-dependent way (IL-7 and IL-15) via self-renewal. These T_M cells remember previous pathogen encounter and induce a more rapid and robust response upon re-infection with this pathogen. Figure adapted from¹⁴.

Upon primary infection with LCMV Armstrong (Arm) or WE strains, which cause acute resolved infection, very rare naïve CD8⁺ T cells ($T_{Naïve}$) respond specifically to the invading pathogen. For example, it is estimated that mice have 50-100 naïve CD8⁺ T cells specific for the LCMV-derived gp33-41 epitope¹⁵. Upon activation, these naïve cells undergo between 15 to 20 cell divisions and expand in number up to 50'000-fold to efficiently clear the infection. In order to get activated, naïve CD8⁺ T cells need to interact with the antigen-MHC complex on the surface of DCs. However, for full activation, CD8⁺ T cells require three signals, 1) the interaction of their TCR with its specific antigen-MHC-complexes, 2) costimulation to ensure the functionality and the survival of proliferating cells and 3) inflammatory cytokines that promote the full acquisition of effector functions by CD8⁺ T cells¹⁵.

Signal 1: TCR

CD8⁺ T cells are activated when a naïve cell encounters an antigen presented by MHC class-I expressed by DC. Thereby, the TCR is responsible for the specificity of a T cell response and delivers the first activation signal¹⁶ (**Fig. 2**). The TCR complex consists of disulfide-linked TCR $\alpha\beta$ heterodimers. The TCR itself does not possess signalling domains and signals via the associated CD3 complex, i.e. noncovalently associated CD3 $\zeta\zeta$, CD3 $\delta\epsilon$, and CD3 $\gamma\epsilon$ subunits¹⁷. T cell activation occurs through phosphorylation of immunoreceptor tyrosine-based activation motifs (ITAMs) present in the intracellular portion of CD3, which leads to the recruitment of Lck (lymphocyte-specific protein tyrosine kinase) that belongs to the family of non-receptor tyrosine kinases^{18, 19, 20}. TCR binding alone fails to induce sustained proliferation and results in T cell apoptosis or anergy i.e. the cells become non-responsive to restimulation¹⁶.

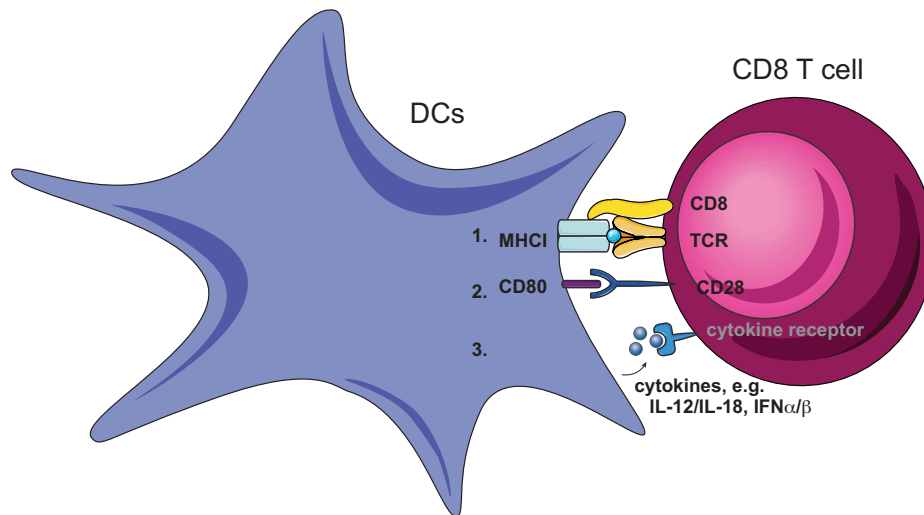


Figure 2: Three signal model of T cell activation. The first signal requires TCR binding to the MHC-I complex containing the antigenic peptide. The second signal includes costimulation via CD28 stimulation that induces cytokine production by T cells and their expansion. In order to obtain a fully functional effector response, a third signal through cytokine stimulation is required.

Signal 2: Co-stimulation

T cells require a second signal to achieve full activation, a so called co-stimulatory signal. CD28 is constitutively expressed by T cells and is the ligand to both CD80 and CD86 that are expressed by APCs¹⁶. Co-stimulation through CD28 is the most important pathway for the productive initial activation of naïve T cells. Costimulation ensures the survival of activated T cells and thus allows their productive expansion. It also promotes IL-2 production, which enhances proliferation in an autocrine and paracrine manner (**Fig. 2**)¹⁶.

Besides CD28, T cells simultaneously express an adjustable spectrum of co-stimulatory molecules that can deliver positive signals. The inducible T cell costimulator (ICOS, CD278) is a second co-stimulatory system that is upregulated upon T cell activation²¹. Its ligand, ligand of ICOS (LICOS, CD275) is predominantly expressed on DCs and B cells. ICOS activates the phosphoinositide 3-kinase (PI3K)²¹. Additional costimulatory receptors belong to the tumour necrosis factor receptor (TNFR) superfamily. These include CD27, glucocorticoid-induced TNFR-protein GITR (CD357), 4-1BB (CD137) and OX40 (CD134)²¹. These induce activation of NF-κB transcription factors. Overall, costimulatory signals augment T cell proliferation, survival and sustain T cell responses^{22,23,24}.

Signal 3: Inflammatory cytokines

TCR and costimulatory signals sustain the proliferation of naïve cells, but they fail to induce optimal effector functions²⁵. Certain inflammatory cytokines act as a third signal for CD8⁺ T cells by inducing the acquisition of effector functions (**Fig. 2**)²⁵.

One of the possible third signals during T cell activation is IL-12, which is produced by DCs and other cells during bacterial infections. Indeed, IL-12 can enhance proliferation, survival and effector differentiation i.e. it induces the expression of granzymes and perforin²⁶. IL-12 is also important for IFN-γ production by CD8⁺ T cells²⁶.

During viral infection IFN-α/β serves as a key third signal for CD8⁺ T cell function. IFNα/β directly supports survival of activated CD4⁺ T and CD8⁺ T cells in a Bcl-2 and Bcl-xL independent way²⁶. IFNAR-deficient CD8⁺ T cells transferred into WT host mice have a severe differentiation defect²⁶. Indeed, IFNα/β signalling via IFNAR1 induces the expression of Gzmb²⁷. While IFNα/β is an essential third signal in LCMV infection, IL-12 is dispensable²⁶. On the other hand IFNα/β is dispensable for the response to vaccinia virus while IL-12 is essential²⁶.

1.4 CD4⁺ T cell response to acute infection

In addition to CD8⁺ T cells, infection leads to the activation of CD4⁺ T cells. CD4⁺ T cell responses can be broadly grouped into T helper type 1 (Th1) cells, T helper type 2 (Th2) cells, T helper type 17 (Th17), regulatory T cells (Treg), T follicular helper (Tfh) cells and cytotoxic CD4⁺ T cells²⁸. The commitment of CD4⁺ T cells to one of the above lineages, depends on the signals received during the initial priming interaction with APCs, that include cytokines, co-stimulatory signals and signals depending on the duration of the interaction between the TCR and MHC-II:peptide complex²⁸. In response to viral infections, CD4⁺ T cells predominantly develop into Th1 cells that typically produce IFN- γ to promote antiviral and cell-mediated immunity, e.g. sustain CD8⁺ T cell response^{29,30}. However, CD4⁺ T cells are dispensable for virus control in mouse models of acute viral infections (LCMV Arm)³¹, although they improve the memory CD8⁺ T cell response²⁸.

During LCMV infection, CD4⁺ T cells also develop into Tfh cells that upregulate CXCR5 and downregulate CCR7. These cells move to the B cell zone to induce germinal center reactions that support B cell activation and antibody production some of which may neutralize LCMV³². To support B cell responses, CD40L expressed by Tfh cells interacts with CD40 expressed by B cells³². In addition, germinal center Tfh cells produce cytokines such as IL-4, IFN- γ or IL-17 to regulate class switching and thus the quality of the antibody response^{33, 34,35}.

1.5 Signalling pathways involved in CD8⁺ T cell activation

Naïve T cells are efficiently activated upon detection of a cognate MHC-peptide complex in the context of co-stimulation and signal 3 cytokines. Intracellular signalling events lead to profound changes in T cells via the activation of multiple signalling cascades such as calcium-calcineurin-nuclear factor of activated T cells (Ca²⁺-calcineurin-NFAT), RasGRP-1 (rat sarcoma guanyl releasing protein) – Ras (rat sarcoma) – ERK1/2 (extracellular signal-regulated protein kinase 1/2) – AP-1 and PKC θ - IKK (I κ B Kinase) – NF- κ B among many others. Thereby, they induce the activation and nuclear translocation of downstream targets, such as NFAT (nuclear factor of activated T cells), AP-1 or NF- κ B (**Fig. 3**). Activity of all three pathways is needed for IL-2 production.

TCR ligation activates cytosolic PTKs (protein-tyrosine kinases), such as SRC-family PTKs, Lck and Fyn and the ZAP-70 (zeta-chain-associated protein kinase)³⁶. Lck activation triggers phosphorylation of ITAMs present in CD3 chains, while phosphorylation of ITAMs in CD3 ζ recruit ZAP-70 via its Src homology 2 (SH2) domains³⁶. ZAP-70 phosphorylates the key adaptor proteins, LAT (linker for activation of T-cells family member), a transmembrane adaptor protein, and the cytosolic SLP-76 (SH2 containing leukocyte phosphoprotein of 76 kDa)³⁶ and activates PLC γ 1 (1-phosphatidylinositol 4,5-bisphosphate phosphodiesterase gamma), allowing cytosolic Ca²⁺ influx, NFAT activation and induction of the Ras/MAPK (mitogen-activated protein kinase) pathway.

AP-1 TFs are transcriptional effectors of growth factor/receptor tyrosine kinase (RTK) signalling and are activated by Ras/MAPK pathway³⁷. AP-1 is a homo- or heterodimeric complex that consists of members of the JUN, FOS, ATF (activating transcription factors) or MAF (musculoaponeurotic fibrosarcoma) proteins^{38,39}. AP-1 TFs bind to different sequence elements, distinct for each homo- or hetero-dimer combination⁴⁰. For instance, while c-Jun and c-Fos family member positively regulate cellular proliferation, JunB negatively regulates

proliferation⁴⁰. Therefore, the AP-1 complex can have multiple functions, depending on its composition.

Ca²⁺ influx activates calcineurin, a protein phosphatase that dephosphorylates NFAT, allowing nuclear translocation of NFAT³⁶. Nuclear NFAT, in ternary complexes with AP-1 transcription factors (Jun/Fos), can induce expression of genes related to T cell activation, e.g. IL-2, IL-3, Fas-ligand (FasL) and others^{36,41}. In the absence of diacylglycerol (DAG)-derived signals, and consequently in the absence of AP-1, Ca²⁺-calcineurin-NFAT pathway induces T cell anergy³⁶. Anergic T cells are unable to initiate a productive response to restimulation⁴².

PLC γ activates PKC θ (protein kinase C theta) through additional signalling molecules such as DAG. PKC θ phosphorylates the adaptor proteins CARMA1 (caspase recruitment domain-containing membrane-associated guanylate kinase protein 1), Bcl10 and MALT1 (mucosa-associated lymphoid tissue lymphoma translocation protein), which form a trimolecular CBM (CARMA1/Bcl10/MALT1) complex³⁶. The association of Bcl10 with MALT1 results in the phosphorylation of I κ B (Inhibitor of nuclear factor kappa B), which leads to its degradation. This allows translocation of NF- κ B into the nucleus³⁶. NF- κ B regulates gene expression essential for T cell activation, survival, homeostasis and effector functions³⁶. NF- κ B activation following PKC θ downstream signalling promotes IL-2 production²¹. Additionally, proper NF- κ B activation is necessary to preserve Eomes (eomesodermin) expression and to maintain the fitness of memory cells following the clearance of an acute infection⁴³.

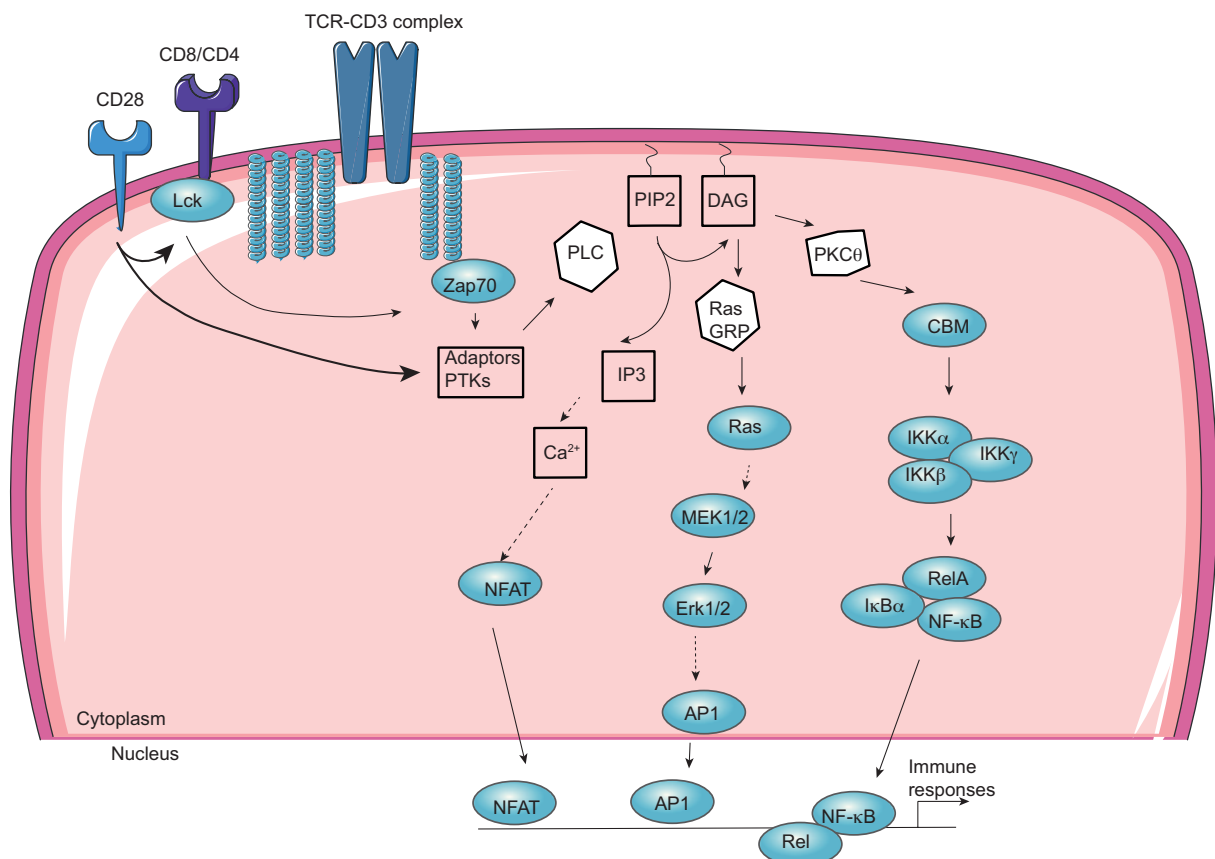


Figure 3: Schematic illustration of TCR signalling. TCR, CD8 and CD28 engagement induces via Lck and Zap70 phosphorylation and activation that leads via adaptor protein-tyrosine kinases to PLC- γ activation that induces multiple downstream cascades, such as Ca²⁺-calcineurin-NFAT, RasGRP1-Ras-ERK1/2 - AP-1 and PKC θ -IKK-NF- κ B among many others. These signalling cascades lead to the activation and subsequent nuclear translocation of the transcription factors NFAT, AP-1 and NF- κ B that induce pleiotropic effects, such as transcription, translation and subsequent production of various cytokines and other effector molecules³⁶. Figure adapted from Gorentla, B.K. and Zhong, X.-P., *J Clin Cell Immunol*, 2012³⁶.

1.6 CD8⁺ T cell differentiation during acute infection

The population of antigen-specific CD8⁺ T cells arising from naïve T cells in response to infections is heterogeneous. At the peak of the immune response, two main populations of cells have been distinguished. Most cells are terminally differentiated short-lived effector cells (SLEC) that are characterized by high KLRG1 (killer-cell lectin like receptor G1), low CD127 (IL7Ra) expression and cytolytic activity⁴⁴. Most SLEC undergo apoptosis once the pathogen is cleared. Memory precursor effector cells (MPEC) are characterized by low KLRG1 and high CD127 (IL7ra) expression. MPEC cells are more likely to survive and differentiate into memory cells. However, these fates are not mutually exclusive since many MPEC cells undergo apoptosis, while some SLEC cells can survive long-term^{45,46}. As MPEC express Granzyme B (GzmB) and have lytic activity, they would need to undergo de-differentiation (i.e. lose lytic capacity) to form central memory⁴⁷.

Bifurcation of antigen-specific CD8⁺ T cells into MPEC and SLEC was suggested to occur during the first cell division, based on the unequal inheritance of cellular components (asymmetric division) (**Fig. 4**). Daughter cells developed proximal to the APC, which formed an immunological synapse with the APC, had increased granularity, low levels of CD62L and higher levels of CD69, CD25 and CD44⁴⁸. The daughter cell distal to the synapse exhibited greater expression of CD62L protein and *Il7ra* mRNA, markers of MPECs⁴⁸.

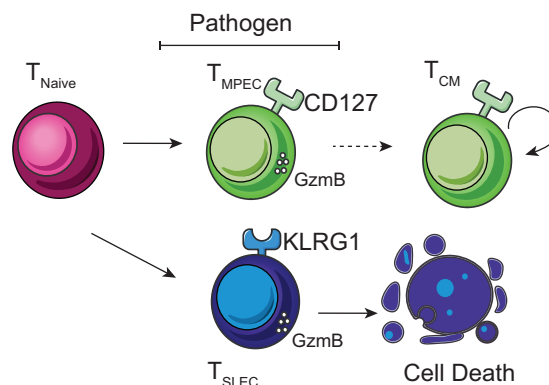


Figure 4: Bifurcative model of CD8⁺ T cell differentiation. Activation of naïve cells leads to asymmetric cell division into memory-precursor effector cells (MPECs, CD127⁺) and short-lived effector cells (SLECs, KLRG1⁺) that have both cytolytic activity (GzmB). While most MPECs remain after antigen-clearance and differentiate into self-renewing long-lived central memory (T_{CM}) without cytolytic activity, most SLECs undergo contraction after pathogen elimination. Figure adapted from¹⁵.

After clearance of the pathogen, most virus-specific CD8⁺ T cells die but a small fraction (5-10%) survives long-term⁴⁹. The maintenance of the memory CD8⁺ T cell pool in the absence of antigen is due to cytokine-driven (IL-7 and IL-15) homeostasis⁵⁰.

The key function of immunological memory is the protection against re-infection. This is ensured in part by an increased number of antigen-specific T cells compared to the naïve T cell pool⁵¹. Additionally, memory cells respond faster to antigen re-encounter than naïve cells⁵².

The population of memory CD8⁺ T cells is heterogeneous with specific functions and characteristics for each subtype. Central memory (T_{CM}) cells are characterized by the expression of CD62L and C-C chemokine receptor 7 (CCR7)¹⁵. These cells lack lytic function, are found in secondary lymphoid organs and can recirculate¹⁵. They have the ability to mount a complete immune response upon restimulation. In contrast, effector-memory (T_{EM}) cells lack CD62L and CCR7, they can recirculate but cannot home to lymph nodes¹⁵. In response to

antigen re-encounter, T_{EM} cells have limited proliferative capacity but rapidly produce antiviral cytokines and have immediate cytolytic activity^{15,53}. Finally, immune surveillance within non-hematopoietic tissues is mediated by tissue resident memory T cells (T_{RM}). T_{RM} cells express surface integrins CD103 and CD49a⁵⁴. They do not re-circulate, and in response to antigen re-encounter they have very limited proliferative capacity but rapidly produce antiviral cytokines and have immediate cytolytic function⁵⁴.

More recently it was shown that T_{CM} cells quantitatively derive from a rare population of cells that is present during the effector phase of the primary response (**Fig. 5**)⁵⁵. These central memory precursor (T_{pCM}) cells are defined by the expression of the TF T cell factor 1 (Tcf1; encoded by the *Tcf7* gene) and by markers expressed by T_{CM} cells such as Ccr7 and CD62L and the production of IL-2⁵⁵. Additionally, these *Tcf7*⁺ cells fail to kill due to low expression of GzmB, GzmA and Perforin⁵⁵.

Tcf7⁺ T_{pCM} cells do not only quantitatively yield, T_{CM} cells, they already have all the functions associated with T_{CM} cells i.e. efficient recall expansion as well as self-renewal and differentiation capacity⁵⁵. Indeed, upon restimulation *Tcf7*⁺ T_{pCM} differentiate into *Tcf7*⁻ effector T cells (T_{EFF}) that express KLRG1 and Cx3cr1 and lytic effector molecules, such as granzymes-A, -B and -C, as well as perforin⁵⁶. This new study suggests that naïve cells first differentiate into T_{pCM} . Their further stimulation induces differentiation into effector cells, while absence of further stimulation yields central memory without passing through a lytic phase. The apparent discrepancy to the classical model (shown above) is explained by the fact that T_{pCM} represent only about 10% of MPEC.

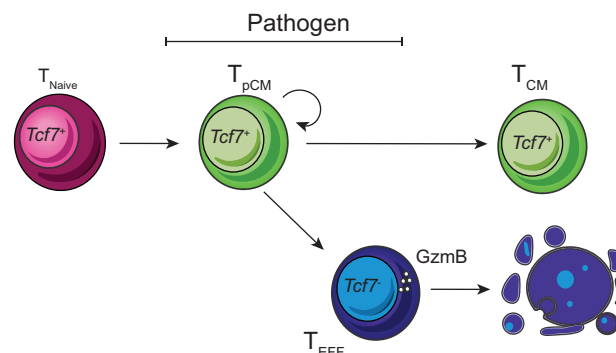


Figure 5: Central memory $CD8^+$ T cells derive from *Tcf7*⁺ cells without passing through effector differentiation. Antigen-specific naïve $CD8^+$ T cells (T_{Naive}) develop into *Tcf7*⁺ memory-precursor $CD8^+$ cells (T_{pCM}). Effector-phase *Tcf7*⁺ $CD8^+$ T (T_{EFF}) cells do not undergo cytolytic differentiation and already have key properties of central memory cells, including stemness. After clearing the infection, T_{pCM} remain and form central memory T_{CM} , whereas T_{EFF} undergo apoptosis. Figure adapted from⁵⁵.

1.6.1 Transcription factors involved in effector and memory differentiation

TFs promoting effector differentiation comprise *Id2*, *Tbx21* (encoding T-bet), *Zeb2*, *Prdm1* (encoding Blimp1)⁵⁷. These TFs are highly upregulated during effector differentiation and promote the expression of *Prf1*, *Gzma*, *Gzmb* that are essential for cytotoxicity of $CD8^+$ T_{EFF} cells. *Prdm1* is induced in T cells by IL-2 and other cytokines, but leads to the repression of *Il2* gene transcription and therefore seems to serve as a negative feedback loop⁵⁸. *Id2* (inhibitor of DNA binding 2) expression is necessary for T_{EFF} differentiation and maintenance, since loss of *Id2* impairs SLEC differentiation and reduces their survival⁵⁹.

The TFs FoxO1, Tcf1, Stat3, Id3 and Myb are essential to promote the development and function of memory cells and to counteract effector differentiation⁶⁰. TFs Tcf1, Bcl6, Id3,

Eomes and Stat3 define T_{CM} , while T_{EM} express T-bet, Blimp1, Id2 and Stat4⁶¹. T_{RM} express reduced levels of TFs Klf2, Eomes, T-bet and Tcf1, but high levels of Hobit and Blimp1⁶¹. $CD8^+$ T cells lacking Myb undergo increased apoptosis already during the initial phase of the primary immune response⁶⁰. These $CD8^+$ T cells are more differentiated and have a decreased number of memory precursor $CD62L^+KLRG1^-CD8^+$ T cells⁶⁰. This implies that Myb restrains $CD8^+$ T cell differentiation⁶⁰. Myb is a positive regulator of the pro-survival Bcl-2/Bcl-xL factors⁶², potentially ensuring the survival of T_{PCM} cells.

Tcf1 was originally identified as a nuclear effector of the canonical Wnt/ β -catenin signalling pathway⁶³. Consistent with that Tcf1 contains a N-terminal β -catenin binding domain⁶⁴. It also includes a C-terminal high mobility group (HMG) DNA-binding domain and a central domain, which can bind co-repressors and seems to have histone deacetylase (HDAC) activity. Tcf1 is expressed at high levels in naive $CD8^+$ T cells, is downregulated in effector T cells and expressed in memory cells. Tcf1 is dispensable for the effector response to infection and the generation of T_{PCM} ⁵⁵, but is essential for T_{PCM} stemness. That seems to be mediated by a set of Tcf1-dependent stemness genes, which includes *Klf4*, *Smad1*, *Elovl6* and *Plxdc2*⁵⁵. Tcf1 is also essential for the generation of T_{CM} cells, which is in part mediated by the maintenance of the TF Eomes^{65,66}.

1.7 The $CD8^+$ T cell response in chronic viral infection

While an effector $CD8^+$ T cell response is normally able to clear viral infection, this does not occur in certain viral infections. In this case, a $CD8^+$ T cell response co-exists with viral replication (**Fig. 6**). Even though, an effector response is initiated, virus-specific T cells gradually lose their functionality during the course of such a chronic infection. This was first shown during persistent LCMV infections in mice^{67,68} and was rapidly extended to other model systems and persistent infections in humans, such as HIV, hepatitis B virus (HBV) and HCV.

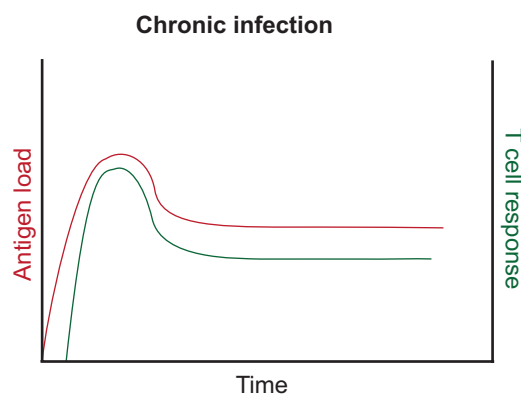


Figure 6: T cell response during chronic infection. During chronic infection, T cell responses are generated and maintained but fail to clear the pathogen. $CD8^+$ T cell responses are necessary to restrict the viral replication. Figure adapted from¹⁴.

The chronicity of LCMV infection depends mainly on the viral load, since low dose LCMV cl13, LCMV Docile (Doc) infection results in acute resolve infection, while high viral doses leads to chronic infection⁶⁹. The chronic LCMV cl13 strain was derived from the LCMV Arm strain, which causes acute resolved infection. LCMV Arm and cl13 differ by 3 amino acids, F260L of the viral glycoprotein (gp, GP260), N176D of the glycoprotein (GP176) and substitution of K1079Q of the viral polymerase gene L⁷⁰. None of these differences impact the main epitopes used for T cell recognition⁷⁰. However, the K1079Q change enhances the viral RNA replication

in plasmacytoid DCs and therefore the viral load in the early phase of the infection⁷⁰. The increased viral replication of LCMV cl13 increases the chronicity by inducing CD8⁺ T cell exhaustion⁷⁰.

Chronic viral infections drive a continuous antiviral T cell response, leading to continuous T cell activation over a long period^{14,71}. As a result, the phenotype of virus-specific CD8⁺ T cells is altered and their functionality is reduced, whereby cells lose functionality in a hierarchical manner (**Fig. 7**). First, they lose the ability to produce IL-2, their proliferative capacity and *ex vivo* killing^{71,72}. Next, they lose the ability to produce TNF, IFN- γ and β -chemokines^{71,72}. The final stage may be the deletion of virus-specific CD8⁺ T cells⁶³. A hallmark of chronically stimulated CD8⁺ T cells is the expression of the inhibitory receptors such as PD-1 (programmed cell death protein 1), Tim3 (T-cell immunoglobulin and mucin domain-containing protein 3) and Lag3 (lymphocyte-activation gene 3), 2B4 (CD244) and CD160⁷³. The extent of the co-expression of inhibitory receptors correlates with the severity of the functional impairment⁷¹. The phenotype of chronically activated CD8⁺ T cells is collectively referred to as T cell "exhaustion". CD8⁺ T cells expressing PD-1 levels also exist in other chronic infections, such as SIV and HCV.

A key feature of chronic viral infections is the persistent exposure of T cells to antigen, whereby high antigen load and long duration of antigen exposure lead to more severe T cell exhaustion⁶³. The reduced function of CD8⁺ T cells is due in part to two main factors, by extrinsic negative regulatory pathways (such as signalling via the immunoregulatory cytokines IL-10⁷⁴ or TGF- β ⁷⁵) and cell-intrinsic negative regulatory pathways (signalling by inhibitory receptors such as PD-1, Lag3 and others)⁷¹. Blockade of IL-10 or IL-10^{-/-} mice are able to clear LCMV cl13 infection. IL-10 blockade mainly seems to improve DC function and thus have an indirect effect on CD8⁺ T cells. However, more recently it was shown that IL-10 reduces the sensitivity of the TCR, which suggests a direct effect of IL-10 on CD8⁺ T cell TCR signal inhibition⁷⁴. On the other hand, PD-1 blockade leads to CD8⁺ T cell proliferation and improves their effector functions, which transiently increases viral control but does not lead to viral clearance^{76,77,78}. Thus, both extrinsic and intrinsic pathways significantly contribute to CD8⁺ T cell dysfunction.

Even though exhausted CD8⁺ T cells are functionally impaired compared to T_{EFF} cells, they are not inert and still have residual functions. Depletion of CD8⁺ T cells during the chronic phase of simian immunodeficiency virus (SIV) infection increases viremia and progression to AIDS^{79,80}. Further, the efficiency of the immune response against viruses, which harbour T cell epitope mutations, decreases over time⁸¹. Therefore, exhausted CD8⁺ T cells are important to contain viral replication⁸².

The evolutionary driver of T cell exhaustion seems to be the protection of the host against excessive immunopathology⁸². Thereby, the host tissue is protected from severe immunopathology while limited pathogen still occurs.

Early studies compared the gene expression profiles of virus-specific CD8⁺ effector and memory cells with that of CD8⁺ T cells from chronic infection. Exhausted CD8⁺ T cells are more similar to T_{EFF} than T_M cells with very low CD62L and CD127 mRNA levels⁸³. Additionally, chronically stimulated CD8⁺ T cells differ from T_{EFF} by increased expression of inhibitory receptors, and reduced KLRG1 expression⁸³. Chronically stimulated CD8⁺ T cells are distinct from anergic CD8⁺ T cells, since anergy-associated genes are not enriched in T_{EX} cells⁸³. Chronically stimulated CD8⁺ T cells also differ distinctly from senescent cells, since the former express low levels of CD44 or KLRG1, but high levels of inhibitory receptors (PD-1, Lag3), which is not the case in senescent cells⁸².

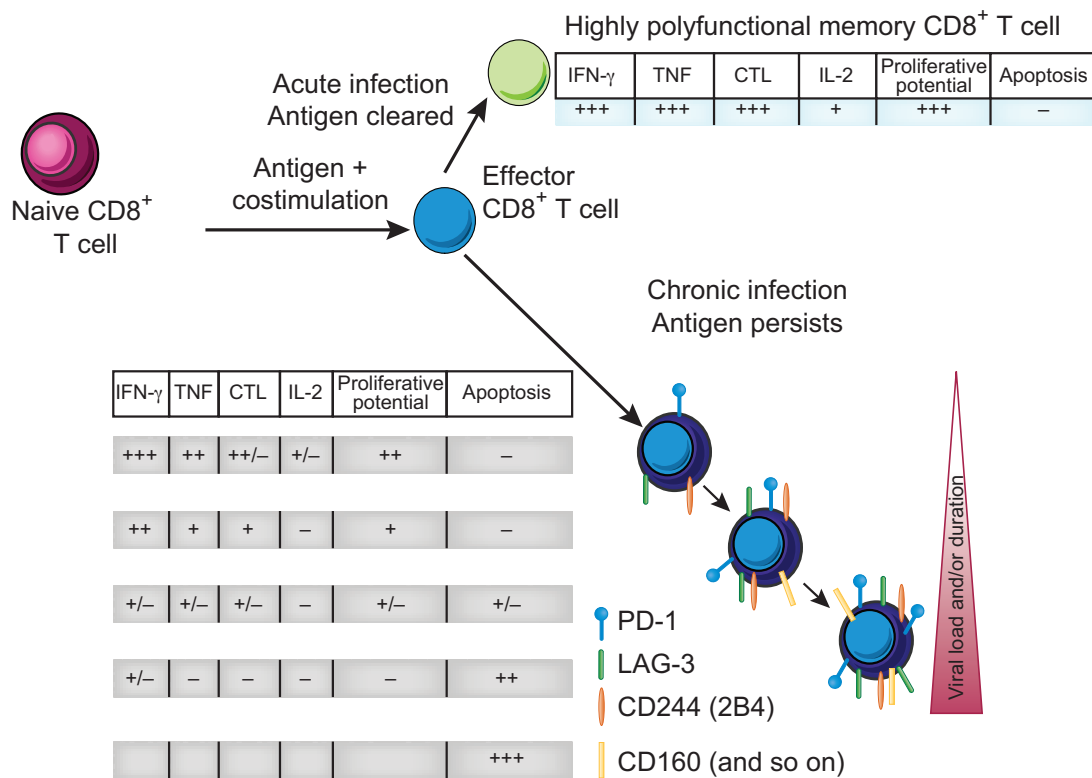


Figure 7: Hierarchical T cell exhaustion during chronic virus infection. During initial infection, naïve T cells are primed by antigen, costimulation and cytokines and differentiate into antigen-specific effector T cells. Acute infection leads to antigen clearance and allows maintenance of highly polyfunctional memory T cells that coproduce several cytokines (such as IFN- γ , TNF and IL-2) and have cytolytic and proliferative capacity. These memory CD8 T cells have an immense survival capacity and are maintained long term without antigen. In chronic virus infection antigen persists after the effector phase, inducing progressive T cell dysfunction, by losing effector functions in a hierarchical manner. Simultaneously the T cell dysfunction is accompanied by progressively increased expression of inhibitory receptors. The severity of T cell exhaustion is correlated with high viral load and expression of inhibitory receptors. The activity of each property is presented on a scale from high (+++) to low (-), CTL indicates cytotoxic potential. Figure adapted from⁷¹.

Exhausted CD8⁺ T cells differ from anergic and senescent cells. Exhaustion is induced by persistent overstimulation of TCR. Anergy is based on TCR stimulation in absence of co-stimulation⁸². Senescence develops based on repetitive re-stimulations following productive priming, leading to a limited cell replication at later time points⁸². All three dysfunctional T cell responses have a low proliferative capacity⁸². Furthermore, the gene expression profiles of exhausted, anergic and senescent cells are distinct. Nonetheless, exhausted and anergic cells overlaps functionally, since both have reduced proliferative capacity and effector functions⁸². In chronic LCMV infection, blockade of the interaction of inhibitory receptor PD-1 to its ligand PD-L1, so called immune checkpoint blockade, results in a proliferative burst of virus-specific CD8⁺ T cells, improved cytokine secretion and viral clearance in the presence of CD4 help⁷⁸. Even in the absence of CD4 help, CD8⁺ T cells expand in response to checkpoint blockade, proliferate more and produce more IFN- γ compared to controls⁷⁸. Simultaneous blockade of multiple inhibitory receptors, as for example Lag3 or Tim3 in combination with PD-1 further improves expansion, compared to individual checkpoint blockade⁸². Additional to LCMV, heterogenous CD8⁺ T cell populations with varying PD-1 levels also exist in other chronic infections, as in simian immunodeficiency virus (SIV) and HCV. In SIV infection, the SIV tetramer⁺ CD8⁺ T cells expressed the highest level of PD-1 among the PD-1⁺ CD8⁺ T cells found in the non-lymphoid tissues⁸⁴. Also, HCV-specific CD8⁺ T cells from the liver express

high levels of PD-1⁸⁵. However, in both HCV and SIV circulating antigen-specific CD8⁺ T cells with reduced expression of PD-1 are found in PBMCs. Therefore, the data obtained in mice showing increased expansion of antigen-specific CD8⁺ T cells in response to PD-1 blockade could have direct relevance to human chronic viral infections.

The observation of increased expansion in response to PD-1:PD-L1 blockade were difficult to reconcile with the terminal differentiation of chronically activated T cells. Moreover, if chronically activated T cells were indeed terminal differentiated it was not clear how the response was maintained long-term.

1.8 CD4⁺ T cell response in chronic infection.

The abundance of Th1 CD4⁺ T cells that produce IFN- γ and TNF are similar in the early phases of acute and chronic LCMV infections. However after the first week of infection, the frequency of Th1 CD4⁺ T cells decreases and these cells produce less cytokine⁸⁶. The loss of Th1 cells is due to type I IFN induced PD-L1 and IL-10 expression by suppressive DCs⁸⁷. Indeed, inhibiting PD-L1 and IL-10 restores the Th1 response and enhances the CD8⁺ T cell response⁸⁷. The loss of Th1 cells in chronic LCMV infection is accompanied by a gain of Tfh cells, which are characterized by CXCR5 and Bcl6 expression and IL-21 secretion²⁸. Similar augmentations of the Tfh and decreases in Th1 cells were observed in HIV, SIV and HCV infections^{88,89,90,91}. Possible functions of Tfh in chronic infections include the reduction of Th1-driven immunopathology²⁸. In addition, Tfh are a source for IL-21 that improves CD8⁺ T cell dependent cytokine production²⁸. The main function of Tfh is to provide B cell help by supporting antibody class-switching and the production of high-affinity antibody responses. Indeed, viremia in chronic LCMV infection is eventually cleared by neutralizing antibodies.

1.9 Memory-like CD8⁺ T cells sustain the immune response in chronic infection

Recent work has identified so called “memory-like” T cells (T_{ML}) (or “stem-like” or “progenitor exhausted”) CD8⁺ T cells that are necessary to sustain the CD8⁺ T cell response to chronic viral infections^{57,92}. T_{ML} cells are also essential for the proliferative burst in response to checkpoint blockade⁵⁷.

T_{ML} cells display features of central memory cells⁵⁷. They are defined by the expression of the transcription factor Tcf1, which is critical to maintain protective immunity after resolution of acute infections (**Fig. 8**)^{65,93}. Furthermore, T_{ML} cells express additional factors expressed by central memory cells, such as IL7Ra, CD62L, CCR7 and Id3⁵⁷. Thus, Tcf1⁺ T_{ML} cells have the ability to receive IL-7 signals, which could in part explain their maintenance^{44,57}. T_{ML} cells further express Ly108 (encoded by *Slamf6*) and were independently identified based on the expression of CXCR5⁹², whose expression overlaps considerably but not entirely with that of Tcf1. Like T_{PCM} and T_{CM}, T_{ML} cells retain some capacity to produce IL-2 and to expand in response to re-stimulation. T_{ML} cells also express certain inhibitory receptors such as PD-1⁵⁷ and Lag3 but not Tim3. Finally, T_{ML} cells lack an effector signature⁵⁷. Indeed, T_{ML} cells express only low levels of TF T-bet (encoded by *Tbx21*) or Blimp-1, similar to T_{CM}⁵⁷. Tcf1⁺ T_{ML} cells are relatively quiescent based on the expression of cell-division-related genes (*Mki67*, *Ccnb1*, *Plk1*, *Aurkb*)⁵⁷.

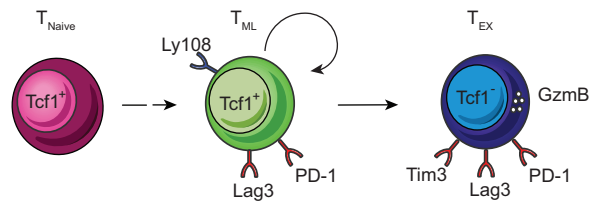


Figure 8: Memory-like CD8⁺ T cells (T_{ML}) sustain the immune response in chronic viral infection. A virus-specific CD8⁺ T cell subset sustains the immune response during chronic viral infection, so called memory-like CD8⁺ T cells (T_{ML}). Thereby, they have characteristics of stemness, which implies they are able to self-renew, they maintain their proliferative capacity and they produce more differentiated progeny, terminal differentiated exhausted T_{EX} cells. However, concurrently T_{ML} cells also express high levels of inhibitory receptors, such as programmed cell death protein 1 (PD-1) and lymphocyte activation gene (Lag3). Besides Tcf1, T_{ML} cells can also be defined by the surface marker Ly108. Terminally differentiated T_{EX} are negative for Tcf1, but express effector markers, such as GzmB and some additional inhibitory receptors that are absent in T_{ML} cells, such as T cell immunoglobulin and mucin domain-containing protein 3 (Tim3). Figure created according to the model suggested from⁵⁷.

Most importantly, T_{ML} cells have stemness, i.e. the ability to expand upon re-challenge, and to self-renew or to differentiate into more differentiated cells (so called T_{EX}) that acquire lytic capacity but have more limited proliferative capacity. Notably, the recall response of T_{ML} cells is considerably lower than that of T_{CM} cells⁹⁴.

Additionally, T_{ML} cells are enriched in genes related to type I IFN signalling⁹⁵, which are excessively induced early after chronic viral infection and drive T cell exhaustion^{96,97}. Type I IFN appears to maintain Tcf1⁺ T_{ML} cells in a cell-intrinsic manner, by suppressing their differentiation⁹⁵. T_{EX} cells lack Tcf1 and other memory markers, express additional inhibitory receptors (such as Tim3) and upregulate effector features such as the expression of granzyme B (GzmB) and KLRG1⁵⁷. Additionally, T_{EX} cells have no proliferative capacity in contrast to T_{ML} cells⁵⁷.

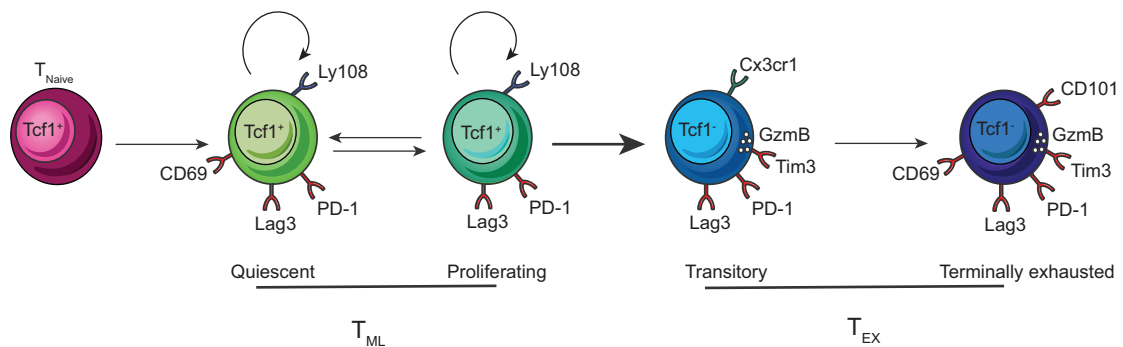


Figure 9: Populations of T_{ML} and T_{EX} cells during chronic infections. Naïve cells (T_{Naive}) differentiate into antigen-specific CD8⁺ T cells during chronic infection are a heterogeneous population defined by the expression of several TFs and surface receptors. Memory-like (T_{ML}) cells have the ability to self-renew and express Tcf1 and Ly108. Additionally, they express markers of exhaustion, such as Lag3 and PD-1 but not Tim3. Some T_{ML} cells express CD69, which indicates a more quiescent state, while T_{ML} cells lacking CD69 proliferate more. The two T_{ML} populations are dynamic and interchangeable. T_{ML} cells give rise to progenitor cells, so called exhausted effector (T_{EX}) cells that lack Tcf1 and Ly108 expression, but express Tim3 and express GzmB. T_{EX} cells can be separated into cycling (Cx3cr1) and less exhausted transitory cells that are essential for residual virus control and terminally exhausted cells that express CD69 and CD101. Figure created according to the model suggested from^{57,98,99}.

Recently, additional heterogeneity was described to exist among T_{ML} and T_{EX} cells (**Fig. 9**). CD69 expression was found to divide the T_{ML} population into quiescent CD69⁺ that are preferentially in the white pulp of the spleen and circulating CD69⁻ cells that are preferentially located in the red pulp of the spleen⁹⁹. Therefore, CD69 expression appears to correlate with

the known residency of memory-like in the splenic white pulp¹⁰⁰. CD69⁺ progenitor 1 cells express the TFs *Tcf7*, *Myb*, *Il7r* and *Sell* as well as *Cxcr5*, *Icos* and *Cd28*⁹⁹. These TFs were also expressed by the CD69⁻ progenitor 2 subset but at lower levels⁹⁹. It appears that these two populations are interconvertible and able to differentiate into *Tcf7*⁺ T_{EX} cells⁹⁹.

“Transitory exhausted” CD8⁺ T cells are the first cells downstream of T_{ML} cells. These cells lack *Tcf1* but express *Tim3* and *Cx3cr1*⁹⁸. These transitory *Cx3cr1*⁺ cells express effector molecules, such as *KLRG1*, *T-bet*, *Zeb2* and *GzmB* and are essential for residual virus control⁹⁸. *Cx3cr1*⁺ transitory cells differentiate into terminally exhausted cells, which is marked by high expression of *Pdcd1* and *Lag3*, expression of *CD101* and *CD69*, and relative lack of *Cx3cr1*, *GzmB* and *T-bet*⁹⁸.

Similar to murine CD8⁺ T cells, subpopulations of less differentiated *Tcf1*⁺*CD127*⁺*PD-1*⁺ and more differentiated *Tcf1*⁻*CD127*⁻*PD-1*⁺ cells were identified among in human HCV-specific CD8⁺ T cells¹⁰¹. The latter disappear after the control of viral infection based on direct-acting antiviral therapy¹⁰¹. Therefore, *Tcf1*⁺ T_{ML} like cells seem to sustain the CD8⁺ T cell response to human chronic viral infections.

1.9.1 Transcription factors involved in T_{ML} and T_{EX} differentiation

T_{EX} express TF that are associated with effector differentiation, such as *Id2*, *Tbx21* (encoding T-bet), *Prdm1*⁵⁷, and *Irf4*¹⁰². T_{ML} cells express TFs that promote memory differentiation, such as *Tcf1*, *Eomes*, *Id3* and *Bcl6*⁵⁷.

T-bet is critical for cytotoxic T lymphocytes (CTL) differentiation, since it induces expression of *Zeb2*. Both *Zeb2* and T-bet are needed for terminal effector differentiation and for repressing genes for central memory development¹⁰³. T-bet is downregulated in chronic, compared to acute infection¹⁰⁴. Enforced T-bet expression in CD8⁺ T cells responding to chronic infection reduces the expression of PD-1 and other inhibitory receptors and improves the persistence of T_{EX} cells¹⁰⁴. T_{EX} cells express high levels of the TCR-responsive TFs *Irf4* and *Batf*, whose expression correlates with high PD-1 expression¹⁰². Both, *Irf4* and *Batf* are required for the expansion and maintenance of T_{EX} cells since their deletion resulted in a dramatic loss of virus-specific T cells¹⁰². Additionally, *Irf4* and *Batf* promote T cell exhaustion by promoting the expression of inhibitory receptors, such as PD-1¹⁰². *BATF* expression seems necessary to establish a T_{EX} population¹⁰⁵.

Tcf1 expression by CD8⁺ T cells defines T_{ML} cells and is critical for the generation of T_{ML} cells⁵⁷. *Tcf1* antagonizes TF expression associated with effector function (e.g. T-bet), while positively regulating *Eomes* and *c-Myb* expression¹⁰⁶. In chronic infection *Tcf1* seems to repress pro-exhaustion factors (e.g. *2B4*, *Lag3*), and to induce *Bcl6* in order to promote the memory-like fate⁹⁵.

BACH2 is transcriptionally and epigenetically active in stem-like CD8⁺ T cells, but not in T_{EX} cells¹⁰⁷. *BACH2*-deficient cells are impaired in the generation of T_{ML} cells, whereas *BACH2* overexpression enforced generation of T_{ML} that expressed less PD-1 and the chronic stimulation TF *Tox*¹⁰⁵.

The calcium/calcineurin-regulated TF NFATs are involved in T cell activation, T cell anergy and T cell exhaustion. During T cell activation a balanced ratio of NFAT:AP-1 fosters the expression of genes involved effector function. Indeed, CD8⁺ T cells lacking NFAT expand poorly and do not acquire effector functions including cytokine production¹⁰⁸. In contrast to acute infection, NFAT translocation in chronic LCMV infection is impaired, and this correlated with impaired cytokine expression¹⁰⁹. The forced expression of an NFAT1 variant that cannot associate with

AP-1 attenuates the expression of effector genes and induces expression of inhibitory receptors, such as PD-1, Lag3 and Tim3⁶³.

Chronic LCMV infection reportedly reduces AP-1 expression⁸³. Thus the NFAT:AP-1 ratio is thought to shift towards higher, and thus potentially partnerless, NFAT expression⁶³ and consequently the induction of exhaustion genes, including TOX, TOX2 and NR4A family members^{110,111} (see below).

Irf4 and NFAT form a positive feedback circuit, since NFAT is necessary to induce Irf4 expression during chronic infection and contributes to increased expression of Irf4 and Batf¹⁰². NFAT further induces the expression of the secondary TFs such as NR4A and Tox¹¹⁰. The NR4A family consists of 3 members, *NR4A1* (encoding Nur77), *NR4A2* and *NR4A3* that are induced in response to TCR signalling. In CD8⁺ T cells, Nur77 is expressed within one day after LCMV cl13 infection, but is no longer expressed on day 3 post infection¹¹². *Nr4a2* mRNA is up-regulated in exhausted compared to effector cells in chronic LCMV infection¹¹⁰. Triple knockout Nr4a chimeric antigen receptor (CAR) T cells express less PD-1 and Tim3 and produce more TNF- α and IFN- γ ¹¹³. Already single knock-out of NR4A1 in CD8⁺ T cells results in increased IFN- γ and TNF- α and reduced PD-1 and Tim3 expression¹¹⁴. Enforced expression of Nr4a1 down-regulates effector genes such as, *Ii2*, *Ifn γ* , *Gzmb* in CD4⁺ T cells¹¹⁴. Nr4a1 is recruited to AP-1 binding sites, preventing the activation of effector-genes¹¹⁴.

Tox is the first TF associated selectively with chronically stimulated CD8⁺ T cells. Tox is transiently expressed in acute infections, but only at very low levels, however, it is continuously expressed in chronically stimulated cells¹¹⁵. Tox expression is positively correlated with the expression of inhibitory receptors (e.g. PD-1, Lag3), but negatively correlated with KLRG1 expression^{115,116}. Calcium signalling and NFAT2 are required to induce Tox, but are dispensable to sustain Tox expression¹¹⁵. Tox deficiency results in reduced expression of *Pdcd1* and *Cd160* as well as genes associated with T_{ML} population, such as *Myb*, *Cxcr5*, *Lef1*, *Slamf6* and *Tcf7*¹¹⁵. At the same time TOX deficiency upregulated genes involved in effector differentiation, including, *Klrg1*, *Gzma*, *Gzmb*, *Cx3cr1*, *Zeb2* and *Prf1*¹¹⁵. During chronic LCMV infection, Tox deficiency leads to a decrease of T_{ML} cells and a defect in T_{EX} generation¹¹⁷. Enforced Tox expression induces exhaustion related genes (e.g. PD-1 at low levels) in the absence of chronic stimulation⁹⁴. Finally, once Tox dependent, exhaustion associated changes are acquired, they are maintained through Tox independent mechanisms¹¹⁶. Tox thus seems to have a dual role, on one hand promoting the typical dysfunctional phenotype, but on the other hand supporting long-term survival and maintenance of virus-specific T cell populations during chronic infection^{116,117}.

1.9.2 Metabolism of CD8⁺ T cells during chronic virus infection

Upon acute viral infection, activated T cells undergo metabolic reprogramming. The cells switch from quiescent IL-7 dependent¹¹⁸ mitochondrial oxidative phosphorylation (OXPHOS) to glycolysis and glutaminolysis in effector cells^{119,118}. The metabolic change is thought to occur through TCR and CD28-dependent PI3K and Akt-mediated mammalian target of rapamycin (mTOR) signalling^{118,119}. These signals induce the expression of the glucose transporter (GLUT)1¹¹⁸. Increased glucose uptake triggers glycolytic flux to produce pyruvate and synthesize adenosine triphosphate (ATP) to meet the increasing energy demands¹¹⁸.

T_M cells mainly depend on to fatty acid oxidation¹¹⁸. Reduced dependence of T_M on glycolysis is due to increased expression of FOXO1, while the dependence on fatty acid oxidation is mediated by tumour necrosis factor receptor-associated factors (TRAF)6 signalling¹¹⁸. In

addition, IL-15 signalling activates mitochondrial biogenesis and thereby increases mitochondrial density in T_M cells¹¹⁸. Consequently T_M have a greater ability to produce ATP than naïve cells, which allows faster proliferation and cytokine production upon restimulation¹²⁰.

In T_{EX} cells, glycolysis and mitochondrial metabolism are repressed compared to T_{EFF} cells¹²¹. Despite their metabolic impairment, chronically activated CD8⁺ T cells exhibit an increased mTOR activity, compared to T_{EFF} cells, which reflects the increased cellular need for glycolysis and OXPHOS¹²¹. However, chronically activated CD8⁺ T cells fail to meet their energetic demand, due to impaired glucose uptake, which seems partially regulated by PD-1 engagement¹²¹. The metabolic dysregulation of early T_{EX} cells alters their metabolic phenotype and skews them to mitochondrial depolarization and high reactive oxygen species (ROS) production¹²¹. Whether absence of PD-1 results in metabolic changes in T_{ML} cells remains to be determined.

1.10 Importance and function of PD-1 in chronic infections

A hallmark of chronically activated CD8⁺ T cells is the continuous expression of co-inhibitory receptors, such as PD-1, Lag3, Tim3, CTLA4 and others²⁴. The expression of co-inhibitory molecules follows activation of T cells, suggesting a tidal model of co-signalling¹²². For example, CTLA4 expression is induced following T cell activation and terminates T cell responses by competing with CD28 for binding to CD80 or CD86 that are expressed by APC. Additionally, CTLA4 recruits phosphatases to the immunological synapse to dephosphorylate key signalling molecules and to disrupt positive signalling²⁴.

The inhibitory effects of PD-1 are mediated by engagement with its ligands PD-L1 and PD-L2. PD-L1 (CD274 or B7.H1) is expressed on T cells, NK cells, macrophages, myeloid dendritic cells, B cells, epithelial cells, vascular endothelial cells and tumour cells¹²³. PD-L1 expression can also be induced by IFN- γ ¹²⁴. PD-L2 (CD273 or B7.DC) is expressed by APCs, such as macrophages and dendritic cells, and its expression can be induced on a variety of cells by T helper cell 2 (Th2)-associated cytokines¹²³.

The cytoplasmic domain of PD-1 contains an immunoreceptor tyrosine based inhibitory motif (ITIM) and an immunoreceptor tyrosine-based switch motif (ITSM)¹²⁵. The switch motif might be the mediator of the PD-1 inhibitory signalling activity by recruiting phosphatases containing Src homology 2 (SH2) domains, such as SHP1 and SHP2¹²⁵. Indeed, the combined absence of SHP1 and SHP2 but not the absence of either phosphatase alone, impairs inhibitory signalling. PD-1 engagement mediates the dephosphorylation of CD28¹²⁴. In addition, PD-1 mediated dephosphorylation of CD3 ζ , zeta-chain-associated protein kinase-70 (ZAP-70) and PI3K has also been reported^{126,127}. Consequently, PD-1 impairs TCR and CD28 signalling and downstream pathways such as NFAT, AP-1 and NF- κ B (**Fig. 10**)³⁶. In addition to impairing co-stimulation, glycolysis and amino acid metabolism are reduced^{128,123}. Thereby, metabolic alterations might change the course of T cells differentiation¹²³.

PD-1 expression is induced transiently after T cell activation in an antigen and NFAT-dependent fashion¹²⁹. Persistent TCR stimulation leads to constitutive PD-1 expression during chronic infections^{130,131}. The *Pdcd1* locus is highly methylated in naïve CD8⁺ T cells. Methylation of a *Pdcd1* promoter-proximal regulatory region is lost upon CD8⁺ T cell activation. This region is re-methylated and PD-1 expression returns to baseline in memory cells¹³². This is mediated by a lysine-specific demethylase 1 (LSD1), which is recruited to the

Pdcd1 locus by Blimp-1¹³². During chronic stimulation, LSD1 is not recruited, despite Blimp-1 binding and PD-1 expression remains high¹³².

PD-1 is transiently expressed by CD8⁺ T cells during acute infections. PD-1 blockade during the first three days does not change the abundance of antigen-specific cells, but increases the frequency of memory precursor cells¹²⁹.

Blockade of the inhibitory PD-1/PD-L1 interaction during established chronic infection, bleads to a proliferative response of PD-1⁺ T cells, improves cytokine expression, lytic activity and enhances viral clearance¹²⁹. This has been referred to as T cell “reinvigoration”⁷⁸. However, the beneficial effects of PD-1 blockade are transient and several weeks after treatment has ended the transcriptional profiles of treated and untreated cells are similar¹³³.

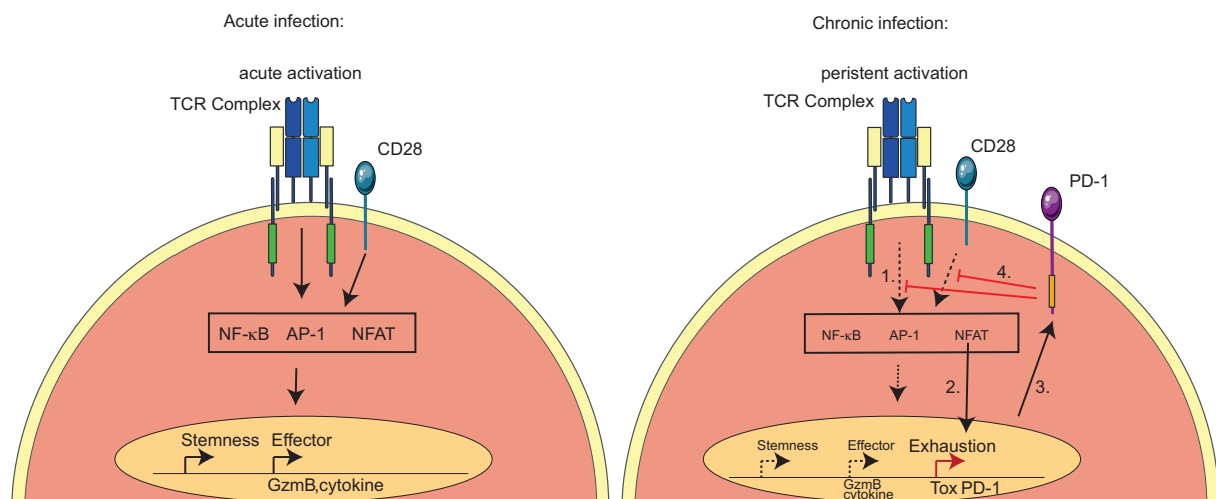


Figure 10: During chronic infection PD-1 signal inhibits the TCR signalling and CD28 co-stimulation pathways. In acute infection, TCR and CD28 receptor get engaged and activate downstream signalling via NFAT, A-1 and NF-κB and leads to the activation of stemness or effector genes (GzmB, cytokines). In chronic infection, NFAT leads to the expression of exhaustion signature and upregulates PD-1 expression. PD-1 signalling inhibits TCR:pMHC and CD28 co-stimulation. The intracellular part of the PD-1 receptor recruit’s phosphatases that dephosphorylate Zap70 and thereby suppresses NFAT, AP-1 and NF-κB, which leads to the inhibition of multiple T-cell activation pathways. Thereby, depending on the cell type, stemness or effector genes are downregulated. Persistent antigen-stimulation during chronic infection leads to the expression of inhibitory and exhaustion genes, such as *Pdcd1* and *Tox*. Figure adapted from Odorizzi P.M. and Wherry, E.J. 2012, J Immunol¹³⁴ according to the model suggested from¹²⁴.

The effects of PD-1 blockade depends on the time of LCMV cl13 infection¹³⁵. PD-1 blockade during the chronic phase of infection (d23-37) leads to an expansion of antigen-specific CD8⁺ cells and improved viral clearance. Blockade during the subacute phase (d8-d22) promotes persistent viremia via lymphoid organ damage mediated by CD8⁺ T cells¹³⁵. PD-1:PD-L1 blockade started at the time of infection leads to the death of mice (d8), recapitulating the results obtained in PD-1 deficient mice^{78,135,136}. Death depended on the production of type-I IFNs, since IFNAR blockade rescued the mice¹³⁵. Similarly, PD-1-deficiency results in severe immunopathology and death of the mice following chronic LCMV infection^{78,136}. Therefore, PD-1 dependent suppression of the CD8⁺ T cell response appears to be an immune mechanism to limit tissue damage¹³⁷.

Similar to the infection of PD-1 ko mice, adoptive transfer of naive virus specific CD8⁺ T cells lacking PD-1 followed by LCMV cl13 infection is lethal to recipient mice above a certain T cell dose. Recipient mice survive when a low T cell dose is transferred. In this case, PD-1-deficient (PD-1 ko) CD8⁺ T cells are more abundant than WT CD8⁺ T cells, yet they express higher levels of inhibitory receptors, such as Lag3, Tim3, 2B4 (CD244), and produce less cytokines compared

to WT cells¹³⁸. This indicates that PD-1-deficient CD8⁺ T cells are more “exhausted” than WT cells¹³⁸. At very late stages of the chronic infection (>d200), however, PD-1 ko CD8⁺ T cells appeared reduced compared to WT cells¹³⁸.

Finally, it has been shown that the proliferative burst of chronically stimulated CD8⁺ T cells in response to PD-1 blockade derives from T_{ML} cells^{92,57}. However, the role of PD-1 for the generation, the maintenance and the function of T_{ML} cells has not been addressed directly.

Aim of this study

Continuous expression of the co-inhibitory receptor PD-1 is a hallmark of chronically stimulated CD8⁺ T cells. Adoptive transfer of virus specific CD8⁺ T cells lacking PD-1 followed by LCMV cl13 infection is lethal to recipient mice above a certain dose. Recipient mice survive when a low dose of cells is transferred. In this case, PD-1-deficient (PD-1 ko) CD8⁺ T cells are more abundant than wild-type (WT), yet they express higher levels of inhibitory receptors, such as Lag3, Tim3, 2B4 (CD244), and express less cytokines compared to WT cells. This indicates that PD-1-deficient CD8⁺ T cells are more “exhausted” than WT cells¹³⁸. Further, PD-1 blockade during chronic viral infection leads to T cell expansion, increased effector functions and reduced pathogen load^{78,139,140}. This improvement, which is often referred to as T cell reinvigoration, seems to be transient¹³³.

More recent work has revealed that exhausted CD8⁺ T cells are heterogenous and that the production of terminally differentiated exhausted cells (T_{EX}) is maintained by a population of memory-like (T_{ML}) progenitor cells^{57,92}. T_{ML} cells were found to have stem cell-like properties, as they can expand and self-renew or differentiate exhausted cells in response restimulation. Indeed, it has been shown that T_{ML} cells mediate the proliferative burst in response to PD-1 blockade³. As the earlier studies determined the impact of PD-1 deficiency on the entire population of chronically stimulated CD8⁺ T cells, the aim of this thesis was to address the role of PD-1 expression on the generation, the maintenance and stemness of T_{ML} cells.

It has been reported that CD8⁺ T cells lacking PD-1 expand better than wild-type cells during the acute phase of a chronic infection, are maintained equally during the chronic phase but are reduced at very late stages of the chronic infection¹³⁸. Since the response to chronic infection is driven by T_{ML} cells, we hypothesized that PD-1 ko T_{ML} cells may eventually lose their stemness and thus that PD-1 was required to preserve the stemness of T_{ML} cells.

2. Materials and Methods

2.1 Mouse strain information

Mice used in this study were bred in the animal facility of the Department of Oncology, at the University of Lausanne. H2D^b P14 TCR transgenic mice, specific for the LCMV gp33-41 epitope (gp33), were provided by H.P. Pircher (Freiburg, Germany)¹⁴¹, V β 5¹⁴² TCR transgenic mice were provided by P. Fink (Seattle, USA) and PD-1 ko P14 TCR transgenic mice provided by G. Guarda (Bellinzona, Switzerland). *Tcf7*^{GFP} 57 and *Tcf7*^{DTR-GFP} 143 mice have been described. *Tcf7*^{GFP} P14 TCR transgenic mice were crossed with PD-1 ko P14 TCR transgenic mice.

Tcf7^{GFP} P14 (CD45.2⁺ or CD45.1/2⁺), *Tcf7*^{DTR-GFP} (CD45.2⁺), PD-1 ko P14 (CD45.2⁺), PD-1 ko *Tcf7*^{GFP} P14 (CD45.2⁺) and V β 5 (CD45.1⁺) mice were obtained by breeding.

Both male and female mice from 6 weeks of age were used in experiments, whereby donors and recipients of adoptive T cell transfers were sex matched. Animal experiments were performed in accordance with protocols approved by the veterinary authorities of the Canton de Vaud.

2.2 Antibodies

2.2.1 Flow Cytometry

Antibodies for flow cytometry

Specificity/Fluorochrome	Source	Clone/Identifier
AnnexinV – apoptosis Detection Kit - APC	eBioscience	Cat. # 88-8007-72
Anti-Active Casp3	BD Pharming	Cat#: ab13847 RRID: AB 559565
Anti-Human Granzyme B – PE-Text red	Life Technologies	Clone: GB11
Anti-Mouse CD8 α – APC, APC-eF780 or BV 650, AF700, BV785	eBioscience / BioLegend / In house	Clone: 53.6.7
Anti-Mouse CD45.1 – BV 785, Pacific Blue or AF647	BioLegend / In house	Clone A20.1
Anti-Mouse CD45.2 – PerCP-Cy5.5, APC-eFlour750, BV 650, PEF610 AF680	eBioscience / BioLegend	Clone: 104 Clone: Ali4A2
Anti-Mouse CD62L –BV 711, PE	eBioscience / BioLegend / In house	Clone: Mel14
Anti-Mouse CD69 – BV421, FITC	BD Biosciences	Clone: H1.2F3
Anti-Mouse CD127 – APC or PE	eBioscience / In house	Clone A7R34
Anti-Mouse c-Fos	Cell Signaling Technology	Clone: 9F6
Anti-Mouse c-Jun	Cell Signaling Technology	Clone: 60A8
Anti-Mouse Cx3cr1 – BV711 or BV650	BioLegend	Clone: SA011F11
Anti-Mouse IFN- γ – PerCPCy5.5	eBioscience	Clone: XMG1.2
Anti-Mouse IL-2 – APC	eBioscience	Clone JES6-5H4
Anti-Mouse Ki67 – FITC	BD Biosciences	RRID:AB_396302
Anti-Mouse KLRG1 – PE Cy7 or BV 421	eBiosciences / BioLegend	Clone: 2F1
Anti-Mouse Lag3 (CD223) – PE or PerCPCy5.5	eBioscience	Clone: C9B7W
Anti-Mouse Ly108 – APC, PE Biotin	BioLegend/ eBioscience	Clone: 330-AJ

		Clone: 13G3-19D
Anti-Mouse PD-1 (CD279) - PECy7, BV711	BioLegend	Clone: RMP1-30 Clone: 29F.1A12
Anti-Mouse Tim3 (CD366) – APC, BV785, PE	BioLegend/BioLegend/ eBioscience	Clone: RMT3-23
Anti-Mouse TNF α – PE Cy7	eBioscience / BioLegend	Clone: MP6-XT22
Anti-Mouse/human TCF1 Rabbit monoclonal antibody	Cell Signaling Technology	Clone: C63D9
Anti-Mouse V α 2	BD Pharming	Clone: B20.1
CellROX [®] Deep Red Reagent	Molecular probes, Life Technologies	Cat #: C10422
F(ab') ₂ -Donkey anti-Rabbit IgG (H+L) - PE	eBioscience	RRID:AB_1210761
Goat Anti-Rabbit IgG (H+L) - AF647	Molecular Probes (Invitrogen)	RRID:AB_141663
Isotype Granzyme B – mouse IgG1 – PE-Tx red	LifeTechnologies	Cat. # MG117
MitoTracker [®] Deep Red	ThermoFisher	Cat. # M22426
MitoTracker [®] Green	ThermoFisher	Cat. # M7514
Phospho-c-Fos (Ser32) AlexaFluor647	Cell Signaling Technology	Clone: D82C12
Phospho-c-Jun (Ser73) PE	Cell Signaling Technology	Clone: D47G9
Streptavidin conjugate – FITC	eBioscience	
Streptavidin conjugate – PE-Cy7	eBioscience	
24G2 supernatant (Fc block)		In house

2.2.2 *In vivo* blocking antibodies

Specificity/Fluorochrome	Source	Clone
Anti-mouse-PD-1	BioXCell	RPM1.14
Anti-mouse-PD-L1 antibody	BioXCell	B7-H1;10F.9G2
IgG2a Isotype control	BioXCell	2A3
IgG2b Isotype control	BioXCell	LTF2

2.3 Lentivirus and Retrovirus constructs

Recombinant DNA list

Plasmid name	Source	Identifier/Target sequence
pCL-Eco	Addgene	Addgene: 12371
pCMV-dR8.74	D. Trono, EPFL	Addgene: 22036
pMD2.G	D. Trono, EPFL	Addgene: 12259
pLV[shRNA]-mCherry-U6>Scramble_shRNA	VectorBuilder	CCTAAGGTTAAGTCGCCCTCG
pLV[shRNA]-mCherry-U6>mTcf7[shRNA#1]	VectorBuilder	GCCACAAGTCTAAACAATAAT
pLV[shRNA]-mCherry-U6>mKlf4[shRNA#1]	VectorBuilder	CATGTTCTAACAGCCTAAATG
pLV[shRNA]-mCherry-U6>mKlf4[shRNA#2]	VectorBuilder	AGTTGGACCCAGTATACATTC
LV_U6-mMyb_shRNA#1_hpgk_mcherry	VectorBuilder	TGTCGCATTGCATGTTAATAT
LV_U6-mMyb_shRNA#3_hpgk_mcherry	VectorBuilder	CAACAGCGAATATCCCTATTA

IRES2-Cherry (MSCV-IRES2- Cherry)	VectorBuilder	Insert IRES2/Cherry sequential PCR from #242 and #690 into #573 EcoRI/ClaI
pMSCV[Exp]-mKlf4:IRES:mCherry	VectorBuilder	VectorBuilder: VB201028-1154xta
pMSCV[Exp]-mMyb[NM_001198914.1]:IRES:mRFP1	VectorBuilder	VectorBuilder: VB191004-1013chp

2.4 Primers for qPCR

Oligonucleotides list

Gene name	Primer sequence
mTcf7 Fw	TGCTGAGTGCACACTCAAGG
mTcf7 Re	TGCGGGCCAGTTCATAGTA
mKlf4 Fw	GTGCCCCGACTAACCGTTG
mKlf4 Re	GTCGTTGAACTCCTCGGTCT
mb2m Fw	AGACTGATACATACGCCTGCAG
mb2m Re	GCAGGTTCAAATGAATCTTCAG
cMyb Fw	AGACCCCGACACAGCATCTA
cMyb Re	CAGCAGCCCATCGTAGTCAT

2.5 Chemicals

Reagent or Resource	Source	Identifier
Brefeldin A	BioLegend	Cat# 420601
MitoTracker® Deep Red FM	ThermoFisher Scientific	Cat# M22426
MitoTracker® Green FM	ThermoFisher Scientific	Cat# M7514
Trizol	Life Technologies	Cat# 15596026
DAPI (4',6-diamidino-2-phenylindol, Dihydrochloride)	MolecularProbes, ThermoFisher	Cat# D-1306
7AAD Viability Staining Solution	BioLegend	Cat# 420404

2.6 Cell culture

Medium	Supplements	Supplier
DMEM (Dulbecco's Modified Eagle's Medium) 4500 mg/L glucose	10% FCS, 1% penicillin/streptomycin	GIBCO® Invitrogen GmbH, Germany
HBSS (Hanks' Balanced Salt solution) -CaCl ₂ -MgCl ₂		GIBCO® Invitrogen GmbH, Germany
RPMI 1640 10% (Roswell Park Memorial Institute) Medium, liquid with GlutaMAX™ I	10% FCS, 1% penicillin/streptomycin	GIBCO® Invitrogen GmbH, Germany
RPMI 1640 10% (Roswell Park Memorial Institute) Medium, liquid with GlutaMAX™ I	10% FCS, 1% Penicillin/Streptomycin 1% Heps 0.2% Glutamine 0.1% β-mercaptoethanol	GIBCO® Invitrogen GmbH, Germany
Probenicid 250mM dissolved in HBSS		Molecular probes®, Invitrogen detection technologies

2.7 Buffers and Solutions

Name	Composition	Source
Ammonium-Chloride-Potassium (ACK) buffer		In house
FACS buffer	PBS, 2% FCS	In house
Stem cell buffer		In house
4% PFA	In ddH ₂ O	In house

2.8 Chemicals, Peptides, recombinant Proteins and Commercial assays

Reagent or Resource	Source	Identifier
Annexin V -APC Apoptosis Detection Kit	eBioscience	RRID:AB_2575165 Cat#
BD Cytofix	BD Bioscience	Cat# 554655
BD PERM buffer III	BD Bioscience	Cat# 558050
FoxP3/Transcription factor staining buffer set	eBiosciences	Cat# 00-5523
Dynabeads Mouse T-Activator CD3/CD28	ThermoFisher Scientific	Cat# 11452D
Intracellular Fix & Perm Buffer set	eBiosciences	Cat# 88-8824
KAPA SYBR FAST qPCR Kit Master Mix	Kapabiosystems	Cat# KR0389
Lipofectamine™ 2000 Transfection Reagent	ThermoFisher Scientific	Cat# 11668019
Mouse CD8 ⁺ T cell enrichment kit	StemCell Technologies	Cat# 19853
NEBNext High-Fidelity 2X PCR Master Mix	New England Biolabs	Cat# M0541
Phosphate Buffered Saline (PBS)	In house	
Peptide: LCMV glycoprotein amino acids 33-41 (gp33) (KAVYNFATM)	TC Metrix	N/A
Polybrene	Sigma-Aldrich	Cat# TR-1003-G
Recombinant human IL-2	Glaxo IMB, Genève, Switzerland	gift from N. Rufer
SuperScript III First-Strand Synthesis System	ThermoFisher Scientific	Cat# 18080051
TaqMan™ Fast Universal PCR Master Mix (2X), no AmpErase™ UNG	ThermoFisher Scientific	Cat# 4352042
TaqMan™ MicroRNA Reverse Transcription Kit	ThermoFisher Scientific	Cat# 4366596
Trizol	Life Technologies	Cat# 15596026
TurboFect Transfection Reagent	Thermo Scientific	Cat# R0531
Zombie Aqua Fixable Viability kit	Biolegend	Cat# 423101

2.9 LCMV infections, LCMV epitopes and viral titers

For chronic viral infections, mice were infected intravenously (i.v.) with 2×10^6 plaque forming units (PFU) LCMV clone 13 (cl13). For re-call responses, mice were infected intraperitoneally (i.p.) with 2×10^5 PFU LCMV 53b Armstrong (Arm).

The CD8⁺ T cell response to LCMV of H-2^b mice (e.g. C57BL/6) is directed against epitopes located in the nucleoprotein (np) or glycoprotein (gp) i.e. np396-404 (FYPYNGYFI), gp33-41/43 (KAVYNFATC/GI) and gp276-286 (SGVENPGGYCL) that are restricted by H-D^b ¹⁴⁴ or gp34-42 that is restricted by H-2K^b ¹⁴⁵. In acute LCMV infection, np396-404 is the immunodominant

epitope, and after clearance the dominance of the epitopes declines as followed from np396 to gp33 to gp34 to gp276⁷². LCMV Arm and cl13 differ by 3 amino acids, none of which impact the above epitopes⁷⁰. Nevertheless, the epitope dominance during chronic infections is altered compared to acute infection. During chronic LCMV infection H-2D^b/np396-404 and H-2K^b/gp34-42 specific CD8⁺ T cells are strongly reduced⁷². On the other hand, H-2D^b/gp276-286 cells are strongly expanded during chronic viral infection.

To determine viral titers, kidneys from LCMV-infected mice were frozen at -80°C. Diluted samples were used to infect Vero cells, and viral titers were determined by a LCMV focus-forming assay as described elsewhere¹⁴⁶. LCMV Plaque Forming Units (PFU) were calculated per gram of kidney.

2.10 Adoptive T cell transfer

Single cell suspension was obtained, by mashing the spleen through a 40 µm nylon strainer (BD Falcon). Red blood cell lysis was performed with a hypotonic ammonium-chloride-potassium (ACK) buffer for 2' at room temperature (RT) and was stopped by addition of complete DMEM medium. CD8⁺ T cells were purified using a mouse CD8⁺ T cell enrichment kit (StemCell Technologies). Purified P14 cells (CD45.2 or CD45.1/2) were adoptively transferred i.v. into naïve Vβ5 (CD45.1) mice one day prior to infection (d-1). For primary responses, 250 or 500 PD-1 ko P14 cells in contrast to 500 or 5000 WT P14 cells were transferred, into individual host. Additionally, PD-1 ko P14 (CD45.2) and WT P14 (CD45.1/2) were transferred into the same host (Vβ5, CD45.1) with a ratio of either 1:1 or 1:5 PD-1 ko to WT cells with a total number of 500 transferred cells.

For secondary transfer experiments ~10⁴ flow sorted Ly108^{hi}Tim3⁻ or *Tcf7*^{GFP^{hi}} P14 cells were transferred either individually or as a mix of ~10⁴ flow sorted *Tcf7*^{GFP^{hi}} WT and PD-1 ko cells. All experiments involving flow sorted cells, cell transfer and infection were performed on the same day (d0).

2.11 Plasmids, virus production and T cell transduction

Retroviral (RV) constructs and the RV packaging construct (pCL-Eco) were obtained from Addgene, as indicated in Table 3.3. The RV Myb or Klf4 OE construct was obtained from VectorBuilder (Table 3.3).

Lentivirus (LV) U6-shRNA hPGK-mCherry knockdown constructs were synthesized by VectorBuilder, while 2nd generation packaging constructs (pCMV-dR8-74 and pMD2-G) were obtained from D. Trono (EPFL).

For RV production, 293T cells (passage number <10) were transiently transfected with Klf4 RV or ctrl RV and pCL-Eco packaging plasmid using TurboFectTM Transfection Reagent (ThermoFisher). For LV production, 293T cells were transiently transfected with knockdown and 2nd generation packaging plasmids (pCMV-dR8.74 and pMD2.G) using lipofectamine 2000 (ThermoFisher) in the absence of antibiotics. 48h after transfection, RV and LV culture supernatants were collected, filtered (0.45 µM Millex) and either used directly to transduce activated CD8⁺ T cells or stored at -80°C.

For LV or RV transduction, CD8⁺ T cells were purified from the spleen of naïve P14 *Tcf7*^{GFP} or *Tcf7*^{DTR-GFP} mice, as described above. The *Tcf7*^{DTR-GFP} reporter was used for shRNA and RV overexpression (OE) experiments, because the *Tcf7*^{GFP} reporter expresses mCherry in addition to GFP, resulting in high background mCherry signal.

Purified cells were activated for 24 h *in vitro* with Dynabeads Mouse T-Activator CD3/CD28 (ThermoFisher) (1:1 cell:beads ratio) in the presence of recombinant human IL-2 (50 ng/mL) (gift from N. Rufer, CHUV) before the addition of viral supernatant.

LV and RV transductions were performed with polybrene (4 µg/mL) (Sigma) during spin infection (1800 rpm for 90 min at 30°C). The cells were subsequently cultured overnight at 37°C. The next morning, 3x10⁴ transduced P14 cells were transferred i.v. into Vβ5 (CD45.1) mice that had been infected with LCMV cl13 one day earlier. Additionally, P14 cells were kept in culture for 48h to determine the transduction efficiency.

2.12 Tissue preparation and cell suspension

Spleens were mashed through a 40 µM nylon cell strainer to obtain cell suspensions and followed by red blood cell lysis using ACK buffer.

Peripheral blood was collected in 1.5 mL Eppendorf tubes containing 15 µl of 0.5M EDTA. Lysis of red blood cells with ACK buffer was performed to obtain Peripheral blood mononuclear cells (PBMCs) that were subsequently washed with FACS buffer.

2.13 Flow cytometry and cell sorting

Surface staining was performed using mAb diluted appropriately in PBS supplemented with 2% FCS for 20' at 4°C. Cells were washed twice and subsequently secondary Ab were added together with Zombie Aqua Fixable Viability kit (BioLegend), diluted in PBS, for 10' at 4°C, to exclude dead cells.

Cells were stained on the surface first and were subsequently fixed for intranuclear staining cells using eBioscience™ FoxP3 transcription factor staining buffer set (eBioscience: cat # 00-5523). For fixation and permeabilization Perm diluent and Concentrate were diluted 3:1 and cells were incubated for 45' at 4°C. Intranuclear antibodies were diluted, accordingly, in 1x Permeabilization Buffer (Perm buffer) and incubated for 1h at 4°C. Cells were washed twice with 1x Perm buffer before subsequent incubation with secondary Abs diluted in 1x Perm buffer for 15' at 4°C.

For cell cycle analysis cells were stained on the surface and subsequently intracellularly as described for intranuclear staining. Together with the intranuclear Abs, Ki67 or its isotype IgG1 FITC were diluted accordingly in 1x Perm buffer and incubated for 1h at 4°C. After washing, DAPI (2 µg/mL) diluted in 1x Perm buffer was added for 10' at 4°C.

To detect intracellular activated Casp3, splenocytes were incubated for 4h at 37°C and subsequently stained on the surface, fixed and permeabilized (Intracellular Fixation & Permeabilization Buffer Set, eBioscience kit: Cat # 88-8824) for 45' at 4°C and subsequently stained intracellularly with primary Casp3 antibody diluted in 1x Perm buffer, for 1h at 4°C. The secondary antibody was added following washing for 15' diluted in 1x Perm buffer.

To detect cytokine production, splenocytes were re-stimulated *in vitro* with 1 µM LCMV gp33-41 (gp33) peptide for 5h at 37°C. Brefeldin A (5 µg/mL) was added after 30' of incubation until the end. Cells were stained on the surface, followed by intracellular fixation and permeabilization (Intracellular Fixation & Permeabilization Buffer Set, eBioscience kit: Cat # 88-8824). Intracellular mAbs were diluted accordingly in 1x Perm buffer.

Splenocytes were cultured for 4h at 37°C without growth factors to perform apoptosis assays. The cells were stained on the surface, and subsequently with Annexin V-APC Apoptosis Detection Kit (eBioscience), following the manufacturers protocol. 7-AAD was added 10' prior to acquisition at the flow cytometer.

To analyse phosphorylated Fos and Jun, splenocytes were stimulated *in vitro* with 1 μ M LCMV gp33 peptide for 1h at 37°C. Zombie Aqua Fixable Viability kit (BioLegend) diluted in PBS was added for 5' at 4°C. Cells were fixed subsequently with BD Cytokix (BD Bioscience, Cat # 554655) solution for 20' on ice. Cells were washed with PBS containing 2% FCS. Fc-block was performed using 24G2 supernatant (25 μ l) for 5' at 4°C. 70 μ l of surface antibody-mix was added on top for 20'. Cells were washed once in PBS containing 2% FCS and subsequently permeabilized in BD Perm buffer III (BD Bioscience, cat # 558050) for 30' on ice. Cells were washed once in PBS. Thereafter, antibodies for Fos, phosphorylated-Fos, Jun, phosphorylated-Jun, diluted in PBS, were added for 30' in the dark at RT. After a washing step with PBS, secondary antibodies diluted in PBS were added for 15' in the dark at RT. Thereafter, cells were washed in PBS and then resuspended in PBS containing 2% FCS for acquisition at the flow cytometer.

Cellular ROS production was determined using CellROX[®] Deep Red Reagent (LifeTechnologies, cat # C10422). Therefore, the cells were first stained on the surface and then incubated in HBSS containing CellROX[®] Deep Red Reagent (5 μ M) and Probenecid prediluted in HBSS (2.5 mM) for 30' at 37°C. Subsequently, cells were washed in PBS and then incubated in Zombie Aqua Fixable Viability kit (BioLegend) diluted in PBS 10' at 4°C. Finally, cells were resuspended in PBS containing 2% FCS for acquisition at the flow cytometer and acquired within 1-2h after staining.

Mitochondrial potential was analysed using MitoTracker[®] Deep Red (10 nM) and MitoTracker[®] Green (100 nM). First, cells were incubated in DMEM complete medium containing MitoTracker[®] Deep Red and MitoTracker[®] Green for 15' at 37°C. Thereafter, cells were washed with PBS containing 2% FCS and stained for cell surface markers. Cells were acquired within 1h after staining at the flow cytometer.

Non-fixed cells were analysed the same day. Flow cytometry acquisition of cells was performed on LSR-II or Fortessa flow cytometers (BD). Data were analysed with FlowJo (TreeStar).

For cell sorting, CD8⁺ P14 cells (CD45.2 or CD45.1/2) were enriched with the mouse CD8⁺ T cell enrichment kit (StemCell Technologies) and then stained for CD45.1 (V β 5 host) and CD45.2 (P14). Ly108⁺Tim3⁻ and Ly108⁻Tim3⁺ or *Tcf7*^{GFP^{hi} and *Tcf7*^{GFP⁻ cells were flow sorted on either FACSAriaIII (BD) or FACSAriaIIU (BD) flow cytometer. The purity of sorted cells was greater than 99%, assessed by post-sort analysis.}}

2.14 RT-qPCR analysis

For the detection of *Tcf7*, *c-Myb* and *Klf4*, naive, d8 or d36 Ly108^{hi} or *Tcf7*^{GFP^{hi} (T_{ML}) and d8 or d36 Ly108⁻ or *Tcf7*^{GFP⁻ (T_{EX}) cells were flow sorted and lysed with Trizol LS (Life Technologies) and RNA was extracted using Direct-zolTM RNA MiniPrep kit (Zymo Research). cDNA was synthesized with the SuperScript III First-Strand Synthesis System (ThermoFisher Scientific). KAPA SYBR FAST qPCR Kit master Mix (Kapabiosystems) was used to perform real-time quantitative PCR on a LightCycler 480 Instrument (Roche), using the primers indicated in **Table 2.4**. Gene expression was quantified relative to mouse *b2m*.}}

2.15 RNA-Seq analysis

CD8⁺ enriched WT or PD-1 ko P14 cells were flow-sorted according to CD8⁺CD62L⁺ to obtain cellular RNA or for transfer into V β 5 hosts (CD45.1), according to CD62L⁺ that were infected with LCMV cl13 the following day. V β 5 hosts that had obtained WT P14 cells were bled at d19

to determine which mice received α PD-L1 (200 μ g B7-H1; clone 10F.9G2) checkpoint blockade at d24, d28 and d32. Thirty-six days after infection CD8⁺ T cells were enriched and splenic Ly108⁺Tim3⁻ and Ly108⁻Tim3⁺ P14 cells from WT and PD-1 ko mice were flow-sorted. Sorted cells were lysed and stored in Trizol before extraction of total cellular RNA using the Direct-zol™ RNA MiniPrep kit (Zymo Research).

RNA quality was assessed on a Fragment Analyzer (Agilent Technologies) and all RNAs had an RQN \geq 8.7. From 50 ng total RNA, mRNA was isolated with the NEBNext Poly(A) mRNA Magnetic Isolation Module. RNA-seq libraries were then prepared from the mRNA using the NEBNext Ultra II Directional RNA Library Prep Kit for Illumina (New England Biolabs, Massachusetts, USA). Libraries were quantified by a fluorimetric method, and their quality assessed on a Fragment Analyzer (Agilent Technologies). Cluster generation was performed with the resulting libraries using Illumina HiSeq 3000/4000 SR Cluster Kit reagents. Libraries were sequenced on the Illumina HiSeq 4000 with HiSeq 3000/4000 SBS Kit reagents for 150 cycles. Sequencing data were demultiplexed with the bcl2fastq Conversion Software (v. 2.20, Illumina; San Diego, California, USA).

Purity-filtered reads were trimmed to remove adapters and low-quality bases with Cutadapt (v. 1.8,¹⁴⁷). Reads matching to ribosomal RNA sequences were removed with fastq_screen (v. 0.11.1). The remaining reads were further filtered to remove low complexity reads with reaper (v. 15-065,¹⁴⁸). Reads were aligned against the *Mus musculus* (GRCm38.92) genome using STAR (v. 2.5.3a,¹⁴⁹). The number of read counts per gene locus was summarized with htseq-count (v. 0.9.1,¹⁵⁰) using the *Mus musculus* (GRCm38.92) gene annotation. Quality of the RNA-seq data alignment was assessed using RSeQC (v. 2.3.7,¹⁵¹).

Differential gene expression analysis was performed using R (v. 3.5.3)¹⁵². Genes were filtered to retain only the ones detected at 1 count per million (cpm) in at least 1 sample, yielding 13,303 retained genes. Normalization factors were calculated using the weighted trimmed mean of M-values (TMM) method implemented in the edgeR package (v. 3.24.3)¹⁵³. Gene counts were next transformed to $\log_2(\text{cpm})$ and the mean-variance modeling was performed using the voom function implemented in the limma package (v. 3.38.3)^{154,155}. A linear model was fitted for each gene, and moderated t-statistics were computed using the lmFit and eBayes functions of the limma package¹⁵⁶. Genes differentially expressed between pairwise comparisons were considered significant at adjusted p-value <0.05 after Benjamini-Hochberg (BH) adjustment¹⁵⁷.

Gene set enrichment analysis (GSEA) was performed using the clusterProfiler package (v. 4.0.4¹⁵⁸) in R v. 4.1.0, against the Hallmark and the Pathway Interaction Database (PID)¹⁵⁹ gene sets available on the Molecular Signatures Database (MSigDB, v.7.4¹⁶⁰). The genes were sorted according to their t-statistic and analysed for enrichment using the GSEA function of the clusterProfiler package, with a seed set to 1234 and a minimum p-value boundary of 1e-50. Enriched gene sets were considered significant at adjusted p-value <0.05 after BH adjustment.

2.16 Data analysis

Fold-expansion of CD8⁺ P14 T cells was determined relative to an estimated 10% of engraftment of the transferred cells¹⁶¹.

All statistical analyses were performed using the latest version of GraphPad Prism between 8.0 and 9.1.2 (GraphPad Software). Statistical significance was achieved when p values were < 0.05 with a 95% confidence level (*=p <0.05 , **=p <0.01 , ***=p <0.001 , ****=p <0.001) as indicated with asterisks in the figures; p >0.5 was considered non-significant (ns). Data are

depicted in mean \pm SD. Non-paired *t* test (two-tailed, 95% confidence level) was used to compare 2 data sets. Paired *t* test (two-tailed, 95% confidence level) was used to compare paired values, e.g. WT and PD-1 ko values that were derived from the same host. ANOVA was used to compare >2 groups.

2.17 Figure creation

Figures were created with Adobe Illustrator 2020 and Smart SERVIER MEDICAL ART.

3. Results

3.1 Increased abundance of PD-1 ko T_{ML} cells in chronic LCMV infection

PD-1 expression dampens the expansion and modifies the differentiation of virus-specific CD8⁺ T cells responding to chronic virus infections⁷⁸. As the CD8⁺ T cell response to chronic virus infections is maintained by memory-like (T_{ML}) CD8⁺ T cells we wanted to gain insights into how PD-1 expression affected the phenotype and/or the function of T_{ML} cells. *Pdcd1* knock out mice (referred to as PD-1 ko) were crossed with P14 transgenic mice, in which all CD8⁺ T cells express a T cell receptor (TCR) specific for the LCMV epitope gp33-41. Purified WT and PD-1 ko cells (CD45.2⁺) were transferred into Vβ5 mice (CD45.1⁺) before infection with LCMV clone 13 (cl13) strain, which causes chronic viral infection (**Fig. 11 A**). Vβ5 mice are transgenic for the TCR β-chain of the ovalbumin-specific OT-1 TCR¹⁴². Consequently, the TCR repertoire of Vβ5 mice is skewed towards ovalbumin recognition and responds poorly or not at all to LCMV. This results in long-term chronic infection of Vβ5 mice, similar to CD4 T cell-depleted mice, and reduces immunopathology associated with chronic LCMV infection.

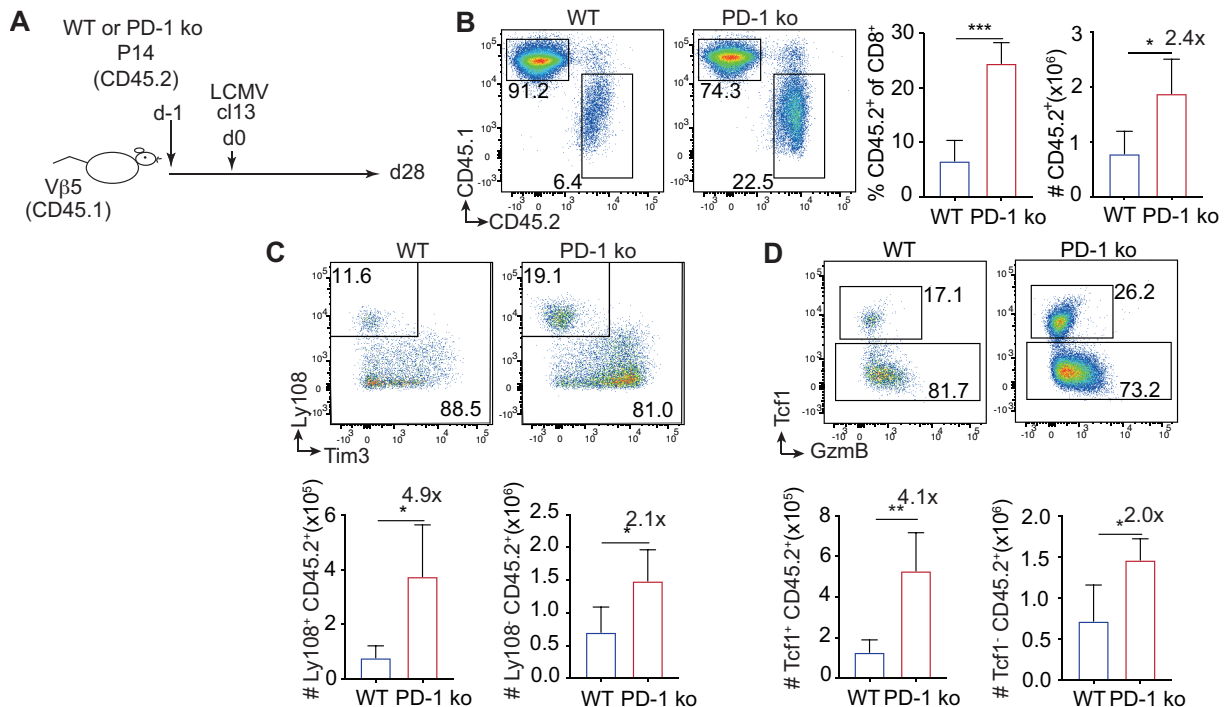


Figure 11: Increased abundance of PD-1 ko T_{ML} cells in chronic LCMV infection.

A) Scheme of the experimental design. 500 WT or PD-1 ko P14 cells (CD45.2) were injected intravenously (i.v.) into Vβ5 mice (CD45.1), which were then infected with LCMV cl13 and analysed 28 days later. **B**) Representative dot plots depict WT (CD45.2, blue bar) and PD-1 ko (CD45.2, red bar) P14 cells among splenic CD8⁺ T cells. Bar graphs show the percentage and absolute number of P14 cells in recipient spleen. **C**) Representative dot plots depict CD8⁺ P14 memory-like Ly108⁺ T_{ML} and exhausted Ly108⁻ T_{EX} cells. Bar graphs show total numbers of Ly108⁺ T_{ML} and Ly108⁻ T_{EX} cells. **D**) Representative dot plots depict CD8⁺ P14 memory-like Tcf1⁺ T_{ML} and exhausted Tcf1⁻ T_{EX} cells. Bar graphs show total numbers of Tcf1⁺ T_{ML} and Tcf1⁻ T_{EX} cells.

B-D) Data are derived from 4-5 mice per group and are representative of n=4 independent experiments. (blue: WT, red: PD-1 ko, grey: host). Bar graphs show the mean percentage (±SD). Two-tailed t-test was performed to determine significant differences (*p<0.05, **p<0.01, ***p<0.001, ns=not significant p>0.5).

At day 28 post infection (d28 p.i.) with LCMV cl13, PD-1 ko P14 cells (CD45.2⁺) were 2.4-fold more abundant than WT P14 cells (**Fig. 11 B**). P14 cells were then separated into memory-like (T_{ML}) cells (Tcf1⁺GzmB⁻ or Ly108⁺Tim3⁻) and exhausted (T_{EX}) cells (Tcf1⁻GzmB⁺ or Ly108⁻Tim3⁺). PD-1 ko T_{ML} cells, based both on Ly108 or Tcf1 expression, were 4.1 and 4.9-fold more

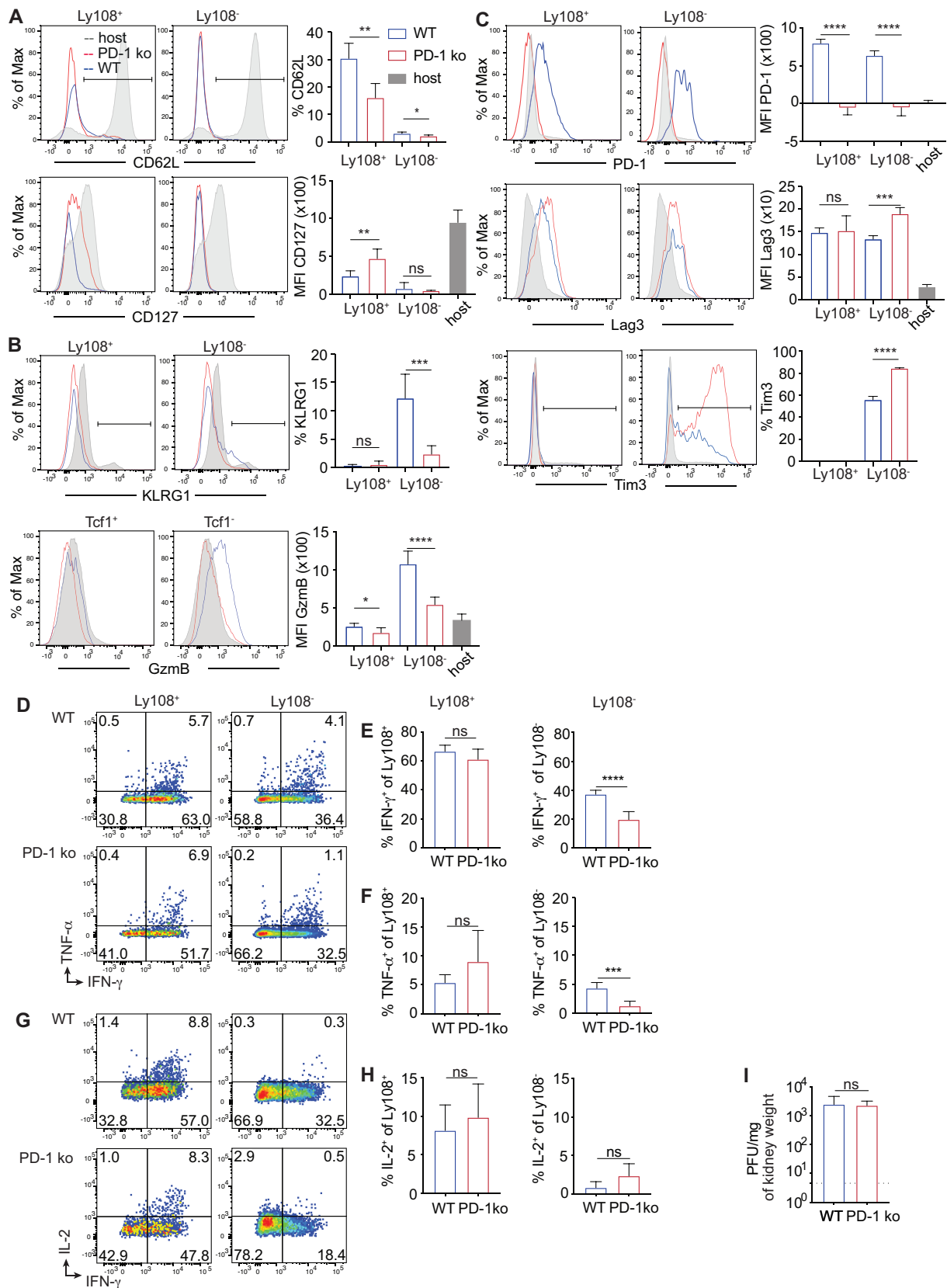


Figure 12: Similar phenotype and functionality of WT and PD-1 ko T_{ML} cells.

Phenotypic analysis of WT and PD-1 ko T_{ML} and T_{EX} cells at d28 p.i.. **A**) Representative histograms depict CD127 and CD62L expression on WT (blue) and PD-1 ko (red) Ly108⁺ T_{ML} and exhausted Ly108⁻ T_{EX} cells compared to host CD8⁺ T cells (grey fill). The bar graph shows the geometric mean fluorescence intensity (MFI) of CD127 and the frequency of CD62L expression on WT and PD-1 ko T_{ML} and T_{EX} cells. **B**) Representative histograms depict KLRG1 and GzmB expression by WT (blue) and PD-1 ko (red) Ly108⁺ or Tcf1⁺ T_{ML} cells and by exhausted Ly108⁻ or Tcf1⁻ T_{EX} cells.

Tcf1⁺ T_{EX} cells compared to host CD8⁺ T cells (grey fill). The bar graph shows the MFI of GzmB or the frequency of KLRG1 expression on WT and PD-1 ko T_{ML} and T_{EX} cells. **C)** Representative histograms show Lag3, PD-1 and Tim3 expression by WT (blue) and PD-1 ko (red) Ly108⁺ T_{ML} cells and by exhausted Ly108⁻ T_{EX} cells compared to host CD8⁺ T cells (grey fill). The bar graph shows the MFI of PD-1 and Lag3 or the frequency of Tim3 expression on WT and PD-1 ko T_{ML} and T_{EX} cells.

D-H) To analyse cytokine production, splenocytes were stimulated *in vitro* with gp33-peptide for 5h in the presence of Brefeldine A (BFA) for the last 4.5h. Gated Ly108⁺ and Ly108⁻ cells were analysed for IFN- γ and TNF- α and IL-2 expression. **D)** Representative dot plots depict IFN- γ vs TNF- α expression by WT or PD-1 ko Ly108⁺ or Ly108⁻ cells. **E-F)** Bar graphs show percentage of T_{ML} and T_{EX} cells expressing IFN- γ (**E**) or TNF- α (**F**). **G)** Representative dot plots depict IL-2 expression by T_{ML} and T_{EX} cells. **H)** Bar graphs show percentage of T_{ML} and T_{EX} cells expressing IL-2. **I)** Plaque forming units (PFU) per mg of kidney weight from V β 5 mice that obtained WT (blue) or PD-1 ko (red) P14 cells.

A-C) Data are derived from 4-5 mice per group and are representative of n=3 independent experiments. (blue: WT, red: PD-1 ko, grey: host). **E-H)** Data are derived from 4-5 mice per group and are representative of n=3 independent experiments. **I)** Data are derived from 4-5 mice per group and are representative of n=7 independent experiments.

(A-I) Bar graphs show the mean percentage (\pm SD). Two-tailed t-test was performed to determine significant differences (*p<0.05, **p<0.01, ***p<0.001, ns=not significant p>0.5).

abundant than WT cells (**Fig. 11 C,D**). PD-1 ko T_{EX} cells were 2-fold more abundant. Thus, PD-1 ko T_{ML} cells were significantly expanded compared to WT.

The analysis of memory markers revealed reduced expression of CD62L but increased expression of CD127 (*IL7Ra*) by PD-1 ko compared to WT T_{ML} cells. As expected from T_{ML} cells, effector markers were not expressed when T_{ML} cells lacked PD-1 (**Fig. 12 A,B**). Furthermore, production of IFN- γ , TNF- α and IL-2, following *in vitro* LCMV gp33-41 peptide re-stimulation, was not different between WT and PD-1 ko T_{ML} cells (**Fig. 12 D-H**). Finally, as expected PD-1 protein was absent from PD-1 ko cells. Lag3 expression was equal in WT and PD-1 ko T_{ML} cells. On the other hand, PD-1 ko T_{EX} cells expressed significantly more Lag3 and Tim3 but less of the effector markers KLRG1 and GzmB. PD-1 ko T_{EX} cells also produced significantly less IFN- γ and TNF- α than WT T_{EX} cells (**Fig. 12 B,C,E,F**). Thus, the increased exhaustion previously observed in total PD-1 ko CD8⁺ T cells¹³⁸ derived from T_{EX} cells and was not observed in T_{ML}. Despite the above differences, LCMV titers were not different in hosts receiving WT or PD-1 ko P14 cells (**Fig. 12 I**), suggesting that the phenotypic and functional differences observed above were independent of the infectious or inflammatory environment.

3.2 Impaired stemness of PD-1 ko T_{ML} cells from chronic LCMV infection

A hallmark of T_{ML} cells is their stemness, i.e. their ability to expand and self-renew or differentiate in response to restimulation. To compare the stemness of WT and PD-1 ko T_{ML} cells, equal numbers of T_{ML} cells (defined by their expression of Ly108 and lack of Tim3) were flow sorted and transferred into V β 5 hosts that were infected with LCMV Armstrong (Arm) strain, which causes acute resolved infection (**Fig. 13 A**).

The analysis of V β 5 mice at d8 p.i. revealed that PD-1 ko T_{ML} cells yielded 2.8-fold less P14 cells than WT T_{ML} cells (**Fig. 13 B**). Both WT and PD-1 ko T_{ML} cells yielded differentiated Tcf1⁻GzmB⁺ as well as Tcf1⁺GzmB⁻ P14 cells. The number of secondary PD-1 ko Tcf1⁺GzmB⁻ cells was significantly reduced (5.7-fold) compared to WT (**Fig. 13 C**). On the other hand, the generation of secondary PD-1 ko Tcf1⁻GzmB⁺ cells was only reduced 2.6-fold compared to WT.

PD-1 ko T_{ML}-derived Ly108⁺ cells expressed similar CD127 but less KLRG1 and GzmB (**Fig. 13 D-F**). WT and PD-1 ko T_{EX}-derived Ly108⁻ cells expressed similar levels of all three markers.

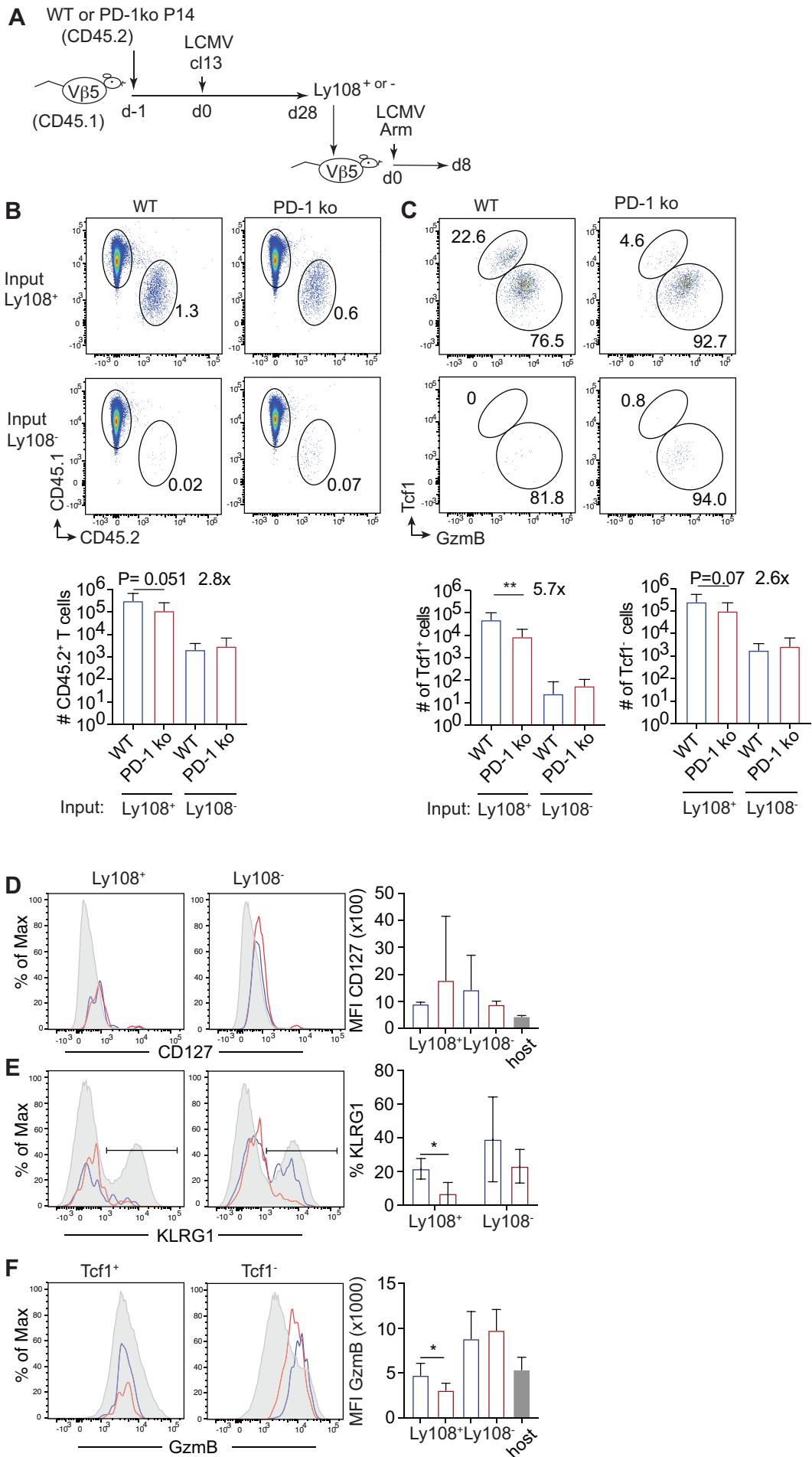


Figure 13: Reduced recall expansion capacity of PD-1 ko T_{ML} cells.

A) Schematic representation the experimental approach. At d-1 5000 naïve WT or 500 naïve PD-1 ko P14 cells (CD45.2⁺) were transferred into Vβ5 mice (CD45.1⁺). At d0 mice were infected with LCMV cl13. At d27/d28 mice were sacrificed and Ly108⁺ T_{ML} and Ly108⁻ T_{EX} (CD45.2⁺) cells were flow sorted. 8-10⁴ T_{ML} or T_{EX} cells were transferred i.v. into new Vβ5 hosts that were infected with LCMV Arm (i.p.). Secondary recipients were analysed 8 days later.

B) Representative dot plots show WT or PD-1 ko P14 cells (CD45.2) derived from transferred T_{ML} or T_{EX} cells. The bar graphs show the total number of WT (blue bars) or PD-1 ko P14 cells (red bars). **C)** Representative dot plots show Tcf1 versus Granzyme B expression by gated P14 cells. The bar graphs show the number of secondary Tcf1⁺ or Tcf1⁻ P14 cells. **D-F)** Representative histograms depict CD127 (**D**), KLRG1 (**E**) and GzmB (**F**) expression by WT (blue) and PD-1 ko (red) Ly108⁺ T_{ML} cells and by exhausted Ly108⁻ T_{EX} cells compared to host CD8⁺ T cells (grey fill). The bar graph shows the MFI of CD127 (**D**), frequency of KLRG1⁺ (**E**) and the MFI of GzmB (**F**).

A-C) Data are from n=14 mice per group and are compiled of n=3 independent experiments.

D-F) Data are derived from 4-5 mice per group and are representative of n=2 independent experiments. (blue: WT, red: PD-1 ko, grey: host).

A-F) Bar graphs show the mean percentage (±SD). Two-tailed t-test was performed to determine significant differences (*p<0.05, **p<0.01, ***p<0.001, ns=not significant p>0.5).

This was in contrast to d28 of the primary response, where PD-1 ko T_{EX} cells expressed significantly lower KLRG1 and GzmB (**Fig. 11 F-H**).

Recall stimulation of PD-1 ko T_{EX} cells yielded very low numbers of P14 cells, only showing survival after re-transfer instead of expansion, comparable in number to WT T_{EX} cells. Thus, the deficient recall expansion of T_{EX} cells was not due to PD-1 mediated inhibition. We concluded that PD-1 ko T_{ML} cells had significantly impaired stemness, whereby the self-renewal capacity was particularly affected. Therefore, our data suggested that PD-1 expression was necessary to preserve stemness.

3.3 Increased abundance of PD-1 ko T_{ML} cells in a competitive situation

To rule out the possibility that the differences between PD-1 ko vs WT cells was due to the unequal input and/or a distinct inflammatory environment we repeated the above experiments using a 1:1 mix of WT and PD-1 ko P14 cells. We further introduced a *Tcf7*^{GFP} reporter allele, in order identify T_{ML} using *Tcf7* expression^{57,55}. Purified WT (CD45.1/2⁺) and PD-1 ko (CD45.2⁺) *Tcf7*^{GFP} P14 cells were mixed 1:1 and transferred into Vβ5 hosts (CD45.1⁺) that were subsequently infected with LCMV cl13 (**Fig. 14 A**).

Despite the equal input (**Fig. 14 B**), at d28 p.i., PD-1 ko P14 cells were >15-fold more abundant than WT cells (**Fig. 14 C**). Similarly, PD-1 ko cells were significantly more abundant among both *Tcf7*^{GFP+} T_{ML} (30-fold) and *Tcf7*^{GFP-} T_{EX} cells (11-fold) (**Fig. 14 E**). Thus, PD-1 ko T_{ML} cells were considerably more competitive than WT cells.

PD-1 ko T_{ML} cells expressed less CD62L, CD127, and TNF-α but comparable IFN-γ and IL-2 and Lag3 relative to WT T_{ML} cells (**Fig. 15 E-I**). On the other hand, PD-1 ko T_{EX} cells expressed less KLRG1, GzmB, IFN-γ and TNF-α and more Lag3 and Tim3 compared to their WT counterparts (**Fig. 15 B,C,I**). Thus, in agreement with the results of the individual transfers, PD-1 ko T_{EX} cells were also more exhausted in a mixed environment.

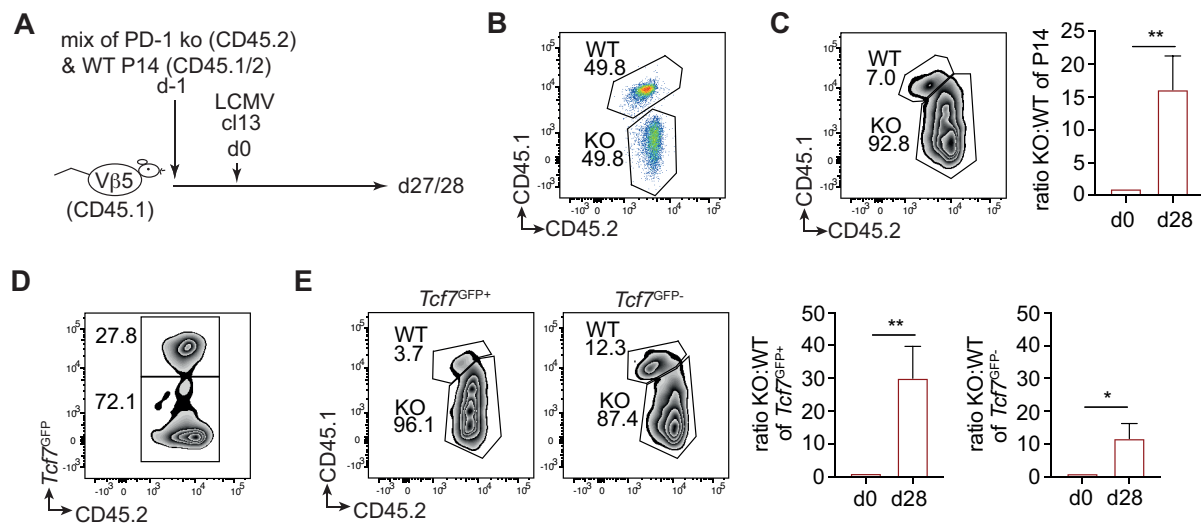


Figure 14: Increased expansion of PD-1 ko T_{ML} cells in a competitive environment.

A) Schematic representation of mixed transfer. 250 PD-1 ko (CD45.2) and WT $Tcf7^{GFP+}$ P14 (CD45.1/2) cells were transferred into Vβ5 (CD45.1) mice and were infected i.v. with LCMV cl13 on the subsequent day. P14 cells among splenocytes were analysed during the chronic phase of infection (d27/28). **B)** Representative dot plot of WT and PD-1 ko ratio at d-1. **C)** CD8⁺ T cells were analysed for the abundance of WT and PD-1 ko P14 cells at d28 p.i.. Plot depicts representative example of WT and PD-1 ko P14 cells of $Tcf7^{GFP+}$ or $Tcf7^{GFP-}$ cells. Bar graph depicts the ratio of WT:PD-1 ko (KO) P14 cells comparing ratio at d0 and d8. **D)** Representative dot plots depicting $Tcf7^{GFP+}$ and $Tcf7^{GFP-}$ on the whole P14 population. **E)** Representative dot plots depict the distribution of WT and PD-1 ko populations was analysed among $Tcf7^{GFP+}$ or $Tcf7^{GFP-}$ cells. Bar graphs show the ratio of KO:WT P14 cells among $Tcf7^{GFP+}$ or $Tcf7^{GFP-}$ cells.

B-E) Data are derived from 4-5 mice and are representative of n=5 experiments. Paired t-test was performed to determine significant differences (* $p < 0.05$, ** $p < 0.01$, *** $p < 0.001$, ns=not significant $p > 0.5$). (blue: WT, red: PD-1 ko).

While this study was underway Hudson *et al.* reported that Cx3cr1 expression separates $Tcf1^{-}$ cells into Cx3cr1⁺ transitory exhausted (high levels of GzmB, T-bet and Tim3) and Cx3cr1⁻ terminally exhausted cells (CD101⁺)⁹⁸. We observed that PD-1 ko P14 cells harbored a significantly smaller Ly108⁻Cx3cr1⁺ transitory exhausted and a significantly expanded terminally exhausted Ly108⁻Cx3cr1⁻ population (**Fig. 15 D**). PD-1 ko T_{ML} cells were thus phenotypically similar but more competitive than WT T_{ML} cells in a mixed environment.

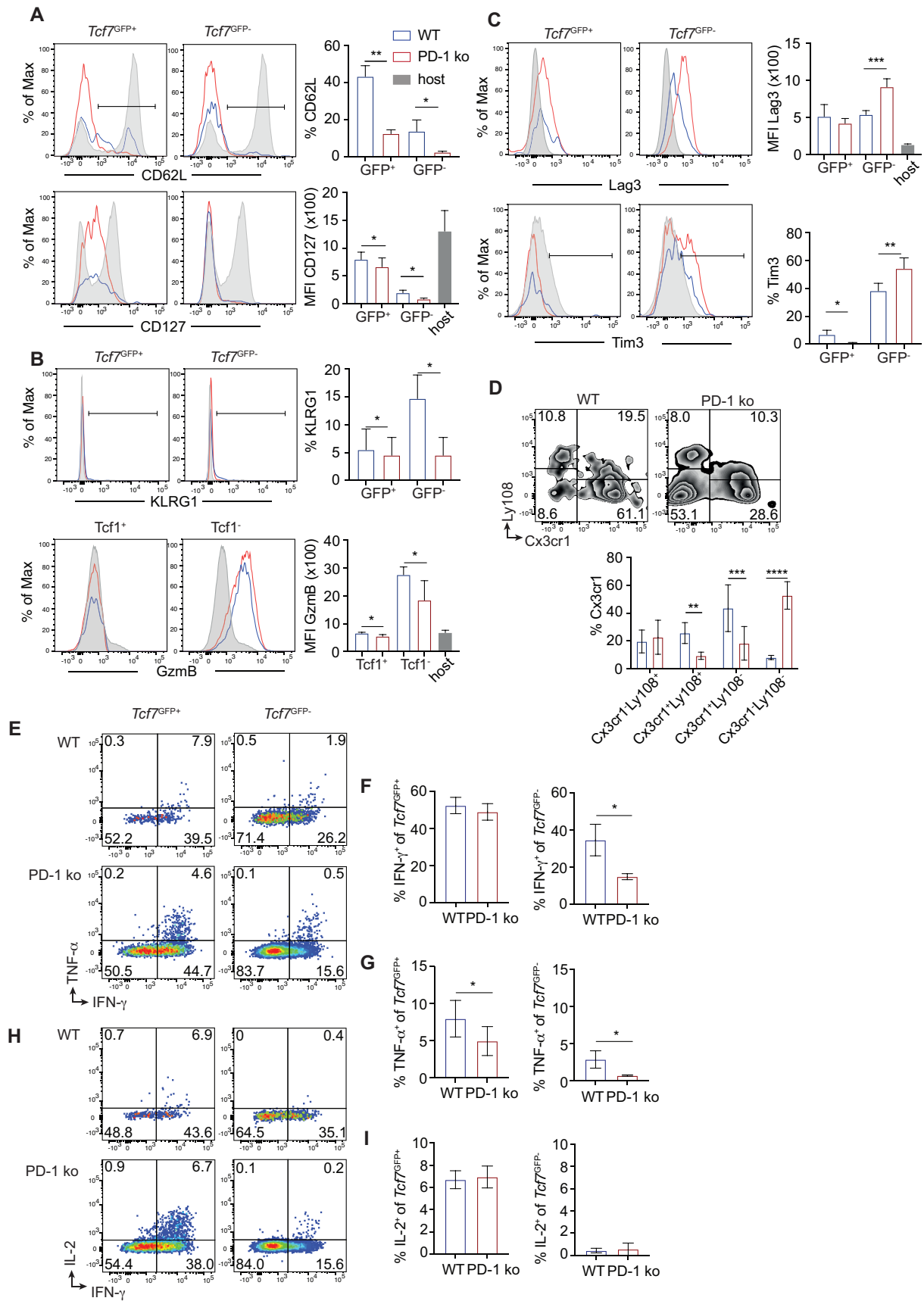


Figure 15: PD-1 ko T_{ML} cells are phenotypically similar to WT T_{ML} in a competitive environment.

Phenotypic analysis of WT and PD-1 ko T_{ML} and T_{EX} cells in mixed transfer at d28 p.i. using **A**) Representative histograms depict CD127 and CD62L expression by WT (blue) and PD-1 ko (red) $Tcf7^{GFP+}$ T_{ML} or $Tcf7^{GFP-}$ T_{EX} cells compared to host CD8⁺ T cells (grey fill). The bar graphs show MFI of CD127 staining or the frequency of CD62L

expression by WT and PD-1 ko T_{ML} and T_{EX} cells. **B)** Representative histograms depict KLRG1 and GzmB expression on WT (blue) and PD-1 ko (red) $Tcf7^{GFP+}$ or $Tcf1^+$ T_{ML} and exhausted $Tcf7^{GFP-}$ or $Tcf1^-$ T_{EX} cells compared to host $CD8^+$ T cells (grey fill). The bar graph shows the MFI of GzmB or the frequency of KLRG1 expression on WT and PD-1 ko T_{ML} and T_{EX} cells. **C)** Representative histograms show Lag3, PD-1 and Tim3 expression on WT (blue) and PD-1 ko (red) $Ly108^+$ (T_{ML}) and exhausted $Ly108^-$ T_{EX} cells compared to host $CD8^+$ T cells (grey fill). The bar graph shows the MFI of PD-1 and Lag3 or the frequency of Tim3 expression on WT and PD-1 ko T_{ML} and T_{EX} cells. **D)** Distribution of WT or PD-1 ko P14 cells was analysed among $Ly108$ and $Cx3cr1$ cells. Bar graphs show the frequency of WT and PD-1 ko population among $Cx3cr1^-Ly108^+$, $Cx3cr1^+Ly108^+$, $Cx3cr1^+Ly108^-$, $Cx3cr1^-Ly108^-$ populations (blue: WT, red PD-1 ko).

E-I) To analyse cytokine production, splenocytes were stimulated *in vitro* with gp33-peptide for 5h in the presence of Brefeldin A (BFA) for the last 4.5h. Gated $Tcf7^{GFP+}$ and $Tcf7^{GFP-}$ cells were analysed for IFN- γ and TNF- α and IL-2 expression. **E)** Representative dot plots depict IFN- γ vs TNF- α expression upon mixed transfer of WT or PD-1 ko $Tcf7^{GFP+}$ or $Tcf7^{GFP-}$ cells. **E-G)** Bar graphs show mean percentage (\pm SD) of T_{ML} and T_{EX} cells expressing IFN- γ (**F**), TNF- α (**G**). **H)** Representative dot plots depict IL-2 expression among T_{ML} and T_{EX} cells upon mixed transfer. **I)** Bar graphs show mean percentage (\pm SD) of T_{ML} and T_{EX} cells expressing IL-2.

A-D) Bar graphs show the mean percentage (\pm SD). Two Way ANOVA with uncorrected Fisher's LSD was performed to determine significant differences between WT and PD-1 ko populations. Data are derived from 4-5 mice per group and are representative of n=5 independent experiments.

E-I) Data are derived from 4-5 mice and are representative of n=2 independent experiments. Paired t-test was performed to determine significant differences (* $p < 0.05$, ** $p < 0.01$, *** $p < 0.001$, ns=not significant $p > 0.5$). (blue: WT, red: PD-1 ko).

3.4 Impaired stemness of PD-1 ko T_{ML} cells in a competitive situation

We further tested the stemness of PD-1 ko vs WT T_{ML} cells that derived from a competitive environment. To this end, the mix of PD-1 ko and WT T_{ML} cells was flow sorted, based on $Tcf7^{GFP+}$ expression, and transferred into new hosts that were infected with LCMV Arm and either treated with isotype or α PD-1 (**Fig. 16 A**). As indicated in the representative plots, the skew towards PD-1 ko T_{ML} cells, which was 54-fold at input (d28) (**Fig. 16 B**), was reduced to 18-fold after the recall response (d28+8 -iso) (**Fig. 16 C**). Similar skews were observed among secondary $Tcf7^{GFP+}$ and $Tcf7^{GFP-}$ cells (**Fig. 16 D,E -iso**). This showed that the recall response and thus the stemness of PD-1 ko T_{ML} cells was reduced approximately 3-fold compared to WT T_{ML} cells, similar to the individual transfers.

In order to compile values from independent experiments, the KO:WT ratio after recall at d28+8 was calculated relative the KO:WT ratio at d28 (input). This showed that the KO:WT ratio, which was 1.0 at input (d28), was reduced approximately 3.2-fold after recall (**Fig. 16 B,C -iso**). Secondary $Tcf7^{GFP+}$ and $Tcf7^{GFP-}$ cells showed similar skews against PD-1 ko cells (**Fig. 16 D,E -iso**).

We further tested whether the effect was underestimated since PD-1 inhibited WT but not PD-1 ko T_{ML} cells during the recall response. When the mixed recall response was performed in the presence of blocking PD-1 antibody, the skew towards PD-1 ko T_{ML} cells (54-fold, calculated based on the ratio of WT to PD-1 ko cells at Input) was reduced to 4.9-fold, compared to 18-fold in the presence of an isotype control Ab (**Fig. 16 C - α PD-1**). Similar values were observed among secondary $Tcf7^{GFP+}$ and $Tcf7^{GFP-}$ cells (**Fig. 16 D,E - α PD-1**). The normalized values combined from 2 independent experiments confirmed the >7-fold reduced stemness of PD-1 ko T_{ML} cells when PD-1 on WT cells was blocked (**Fig. 16 C-E**). These experiments confirmed that the stemness of chronic phase PD-1 ko T_{ML} cells was reduced compared to WT T_{ML} cells.

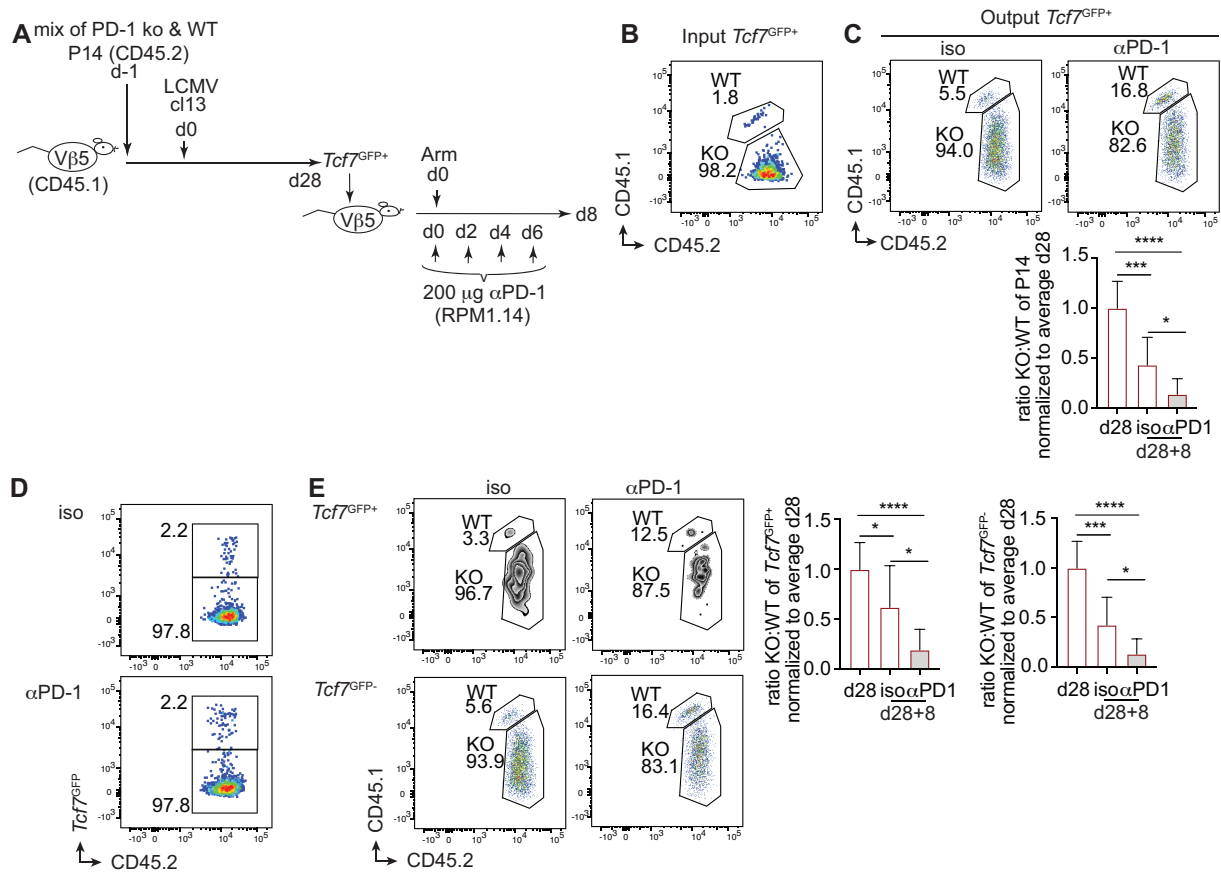


Figure 16: Impaired stemness of PD-1 ko compared to WT T_{ML} cells.

A) Schematic representation of mixed retransfer of WT or PD-1 ko $Tcf7^{GFP+}$ T_{ML} cells. At d-1 500 naïve WT (CD45.1/2) and naïve PD-1 ko (CD45.2) P14 cells were mixed 1:1 (or 4:1 in repeat experiment) and transferred into Vβ5 mice (CD45.1). At d0 mice were infected with LCMV cl13. At d28, 10^4 $Tcf7^{GFP+}$ cells containing a mix of WT and PD-1 ko T_{ML} cells were sorted and transferred into new hosts (Vβ5). Mice were infected the same day with LCMV Arm and treated with 200 μg of anti-PD-1 (αPD-1) or isotype control Ab every two days until sacrifice at d8 post re-transfer. **B)** Representative dot plot of WT and PD-1 ko cells after sort at d28. **C)** Representative dot plot depicting the ratio of WT and PD-1 ko P14 cells after recall (d28+8) in the presence of anti-PD-1 or control Ab. Bar graphs show the ratio of KO vs WT P14 cells at d28+8 compared to the ratio at d28 (=1.0). **D)** Representative dot plots depicting $Tcf7^{GFP+}$ and $Tcf7^{GFP-}$ P14 populations at d28+8. **E)** Representative dot plots depicting the ratio of WT and PD-1 ko P14 cells among $Tcf7^{GFP+}$ and $Tcf7^{GFP-}$ cells at d28+8. Bar graphs show the ratio of KO vs WT P14 cells at d28+8 (isotype or anti-PD-1 treatment) compared to the input ratio at d28 (=1.0). **B-E)** Dot plots are representative from n=10 mice derived from n=2 independent experiments. Bar graphs show the mean ratios (±SD). One-way ANOVA or Mixed-effect analysis with Tukey's correction was performed to determine statistically significant differences (*p<0.05, **p<0.01, ***p<0.001, ns=not significant p>0.5).

3.5 Increased abundance of PD-1 ko T_{ML} during the acute phase of chronic infection

Since PD-1 ko T_{ML} cells were significantly more abundant than WT T_{ML} cells during the chronic phase, we compared the presence of T_{ML} cells during the acute phase of LCMV cl13 infection. As before, WT or PD-1 ko P14 cells were transferred into naïve Vβ5 hosts that were infected with LCMV cl13. At d8 p.i., both the fraction and the total number of PD-1 ko P14 cells was significantly greater than WT (6-fold) (**Fig. 17 A**), as expected from Odorizzi *et al.*¹³⁸. The fraction and total number of PD-1 ko T_{ML} and T_{EX} cells were comparably increased (**Fig. 17 B,C**). The increase at d8 (6-fold) was higher than that observed at d28, which had been 4-fold and 2-fold for T_{ML} and T_{EX}, respectively.

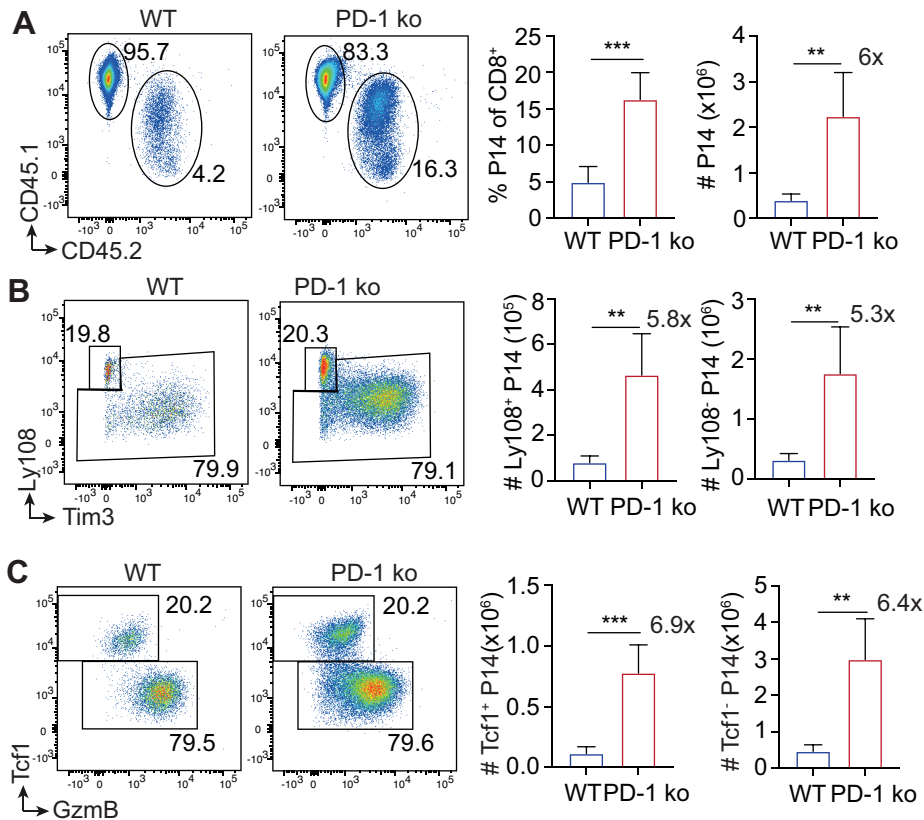


Figure 17: Increased primary expansion of acute phase PD-1 ko T_{ML} and T_{EX} cells.

A-C) At d-1, 500 naïve WT or naïve PD-1 ko P14 cells (CD45.2) were transferred into $\nu\beta 5$ mice (CD45.1). At d0 mice were infected with LCMV cl13. **A)** Representative dot plots show WT or PD-1 ko P14 cells (CD45.2) at d8 p.i.. The bar graphs show the mean number of WT (blue bars) or PD-1 ko P14 cells (red bars). **B)** Representative plots show $Ly108^+$ T_{ML} versus $Ly108^-$ T_{EX} expression. The bar graphs show the mean number of T_{ML} and T_{EX} cells. **C)** Representative dot plots show $Tcf1^+$ T_{ML} and exhausted $Tcf1^-$ T_{EX} cells. Bar graphs show total numbers of $Tcf1^+$ T_{ML} and $Tcf1^-$ T_{EX} cells.

A-C) Data are derived from 4-5 mice per group and are representative of n=3 independent experiments. (blue: WT, Red: PD-1 ko, grey: host). Bar graphs show the mean percentage (\pm SD). Two-tailed t-test was performed to determine significant differences (* $p < 0.05$, ** $p < 0.01$, *** $p < 0.001$, ns=not significant $p > 0.5$).

Thus, PD-1 ko T_{ML} cells initially expanded more potently than WT but were then maintained less efficiently and differentiation into T_{EX} appeared to occur less efficiently.

At d8 p.i. fewer PD-1 ko T_{ML} cells expressed CD62L, which was similarly observed at d28 (**Fig. 18 A**). On the other hand, CD127 expression by T_{ML} cells was similar to WT at d8, but was increased on PD-1 ko T_{ML} cells at d28 (**Fig. 12 C**). While cytokine expression ($IFN-\gamma$, $TNF-\alpha$ and $IL-2$) was similar at d8, PD-1 ko T_{ML} expressed higher Lag3 levels than WT at d8 but not at d28 (**Fig. 18 C-H**).

WT and PD-1 ko T_{EX} cells comparably expressed KLRG1 at d8 while KLRG1 was reduced on PD-1 ko T_{EX} cells at d28 p.i.. Gzmb, $IFN-\gamma$ and $TNF-\alpha$ expression by PD-1 ko T_{EX} cells were already reduced while Lag3 expression was increased at d8 p.i., similar to d28 p.i. (**Fig. 18**). In summary, PD-1 ko T_{ML} cells had expanded significantly more than WT during the acute phase of the infection but did not show major phenotypic differences to WT T_{ML} cells. On the other hand, d8 T_{EX} cells already showed evidence of increased exhaustion, similar to d28. LCMV titers were not different in hosts receiving WT or PD-1 ko P14 cells at d8 p.i. (**Fig. 18 I**), suggesting that the observed differences were independent of the infectious or inflammatory environment.

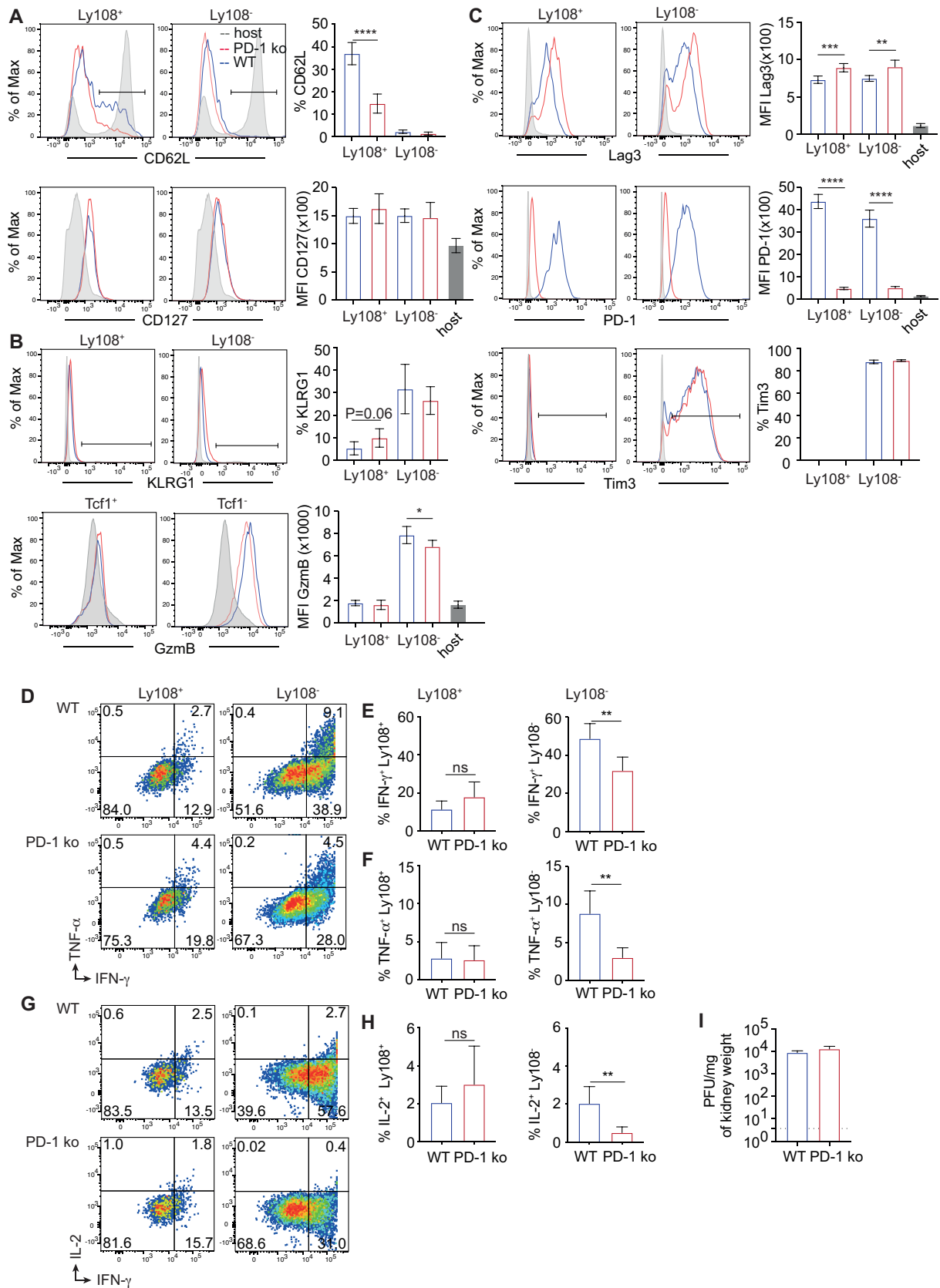


Figure 18: Similar phenotype and functionality of acute phase WT and PD-1 ko T_{ML} cells.

A) Representative histograms depict CD62L and CD127 expression by WT (blue) and PD-1 ko (red) Ly108⁺ (T_{ML}) and exhausted Ly108⁻ T_{EX} cells compared to host CD8⁺ T cells (grey fill) at d8 p.i.. The bar graph shows the MFI of CD127 expression and frequency of CD62L⁺ WT and PD-1 ko T_{ML} and T_{EX} cells. **B)** Representative histograms depict

KLRG1 and GzmB expression by WT (blue) and PD-1 ko (red) Ly108⁺ or Tcf1⁺ T_{ML} and exhausted Ly108⁻ or Tcf1⁻ T_{EX} cells compared to host CD8⁺ T cells (grey fill). The bar graph shows the MFI of GzmB or the frequency of KLRG1 expression on WT and PD-1 ko T_{ML} and T_{EX} cells. **C)** Representative histograms show Lag3, PD-1 and Tim3 expression on WT (blue) and PD-1 ko (red) Ly108⁺ T_{ML} and Ly108⁻ T_{EX} cells compared to host CD8⁺ T cells (grey fill). The bar graph shows the MFI of PD-1 and Lag3 expression or the frequency of Tim3 expression on WT and PD-1 ko T_{ML} and T_{EX} cells.

D-H) Splenocytes were stimulated *in vitro* with gp33-peptide. Gated Ly108⁺ and Ly108⁻ P14 cells were analysed for IFN- γ , TNF- α and IL-2 expression, depicted on representative dot plots. Bar graphs show mean percentage of T_{ML} and T_{EX} cells expressing IFN- γ (**E**), TNF- α (**F**) or IL-2 (**H**). **I)** Viral titers in the kidney of V β 5 mice that have received WT or PD-1 ko P14 cells (PFU/mg of LCMV cl13 of kidney weight) at d8 p.i..

A-I) Data are derived from 4-5 mice per group and are representative of n=3 independent experiments. (blue: WT, red: PD-1 ko). Bar graphs show the mean percentage (\pm SD). Two-tailed t-test was performed to determine significant differences (*p<0.05, **p<0.01, ***p<0.001, ns=not significant p>0.5)

3.6 Increased stemness of PD-1 ko T_{ML} cells present at the acute phase of chronic infection

Since we observed reduced stemness of PD-1 ko T_{ML} cells present at the chronic phase of infection, we determined whether this defect was already present at the acute phase of the infection. Therefore, Ly108⁺ WT and PD-1 ko T_{ML} cells were flow sorted at d8 p.i. and transferred into new V β 5 hosts that were infected with LCMV Arm (**Fig. 19 A**).

At d8+8 p.i., P14 cells derived from PD-1 ko T_{ML} cells were 9-fold more abundant than those derived from WT T_{ML} cells (**Fig. 19 B,C**). Similarly, PD-1 ko T_{ML} cells yielded 8.5-fold more secondary Tcf1⁺GzmB⁻ cells and 9.5-fold more Tcf1⁻GzmB⁺ cells than WT T_{ML} cells. These data showed that acute phase PD-1 ko T_{ML} cells had increased stemness compared to the corresponding WT cells, in sharp contrast to d28 PD-1 ko T_{ML} cells, whose stemness was reduced.

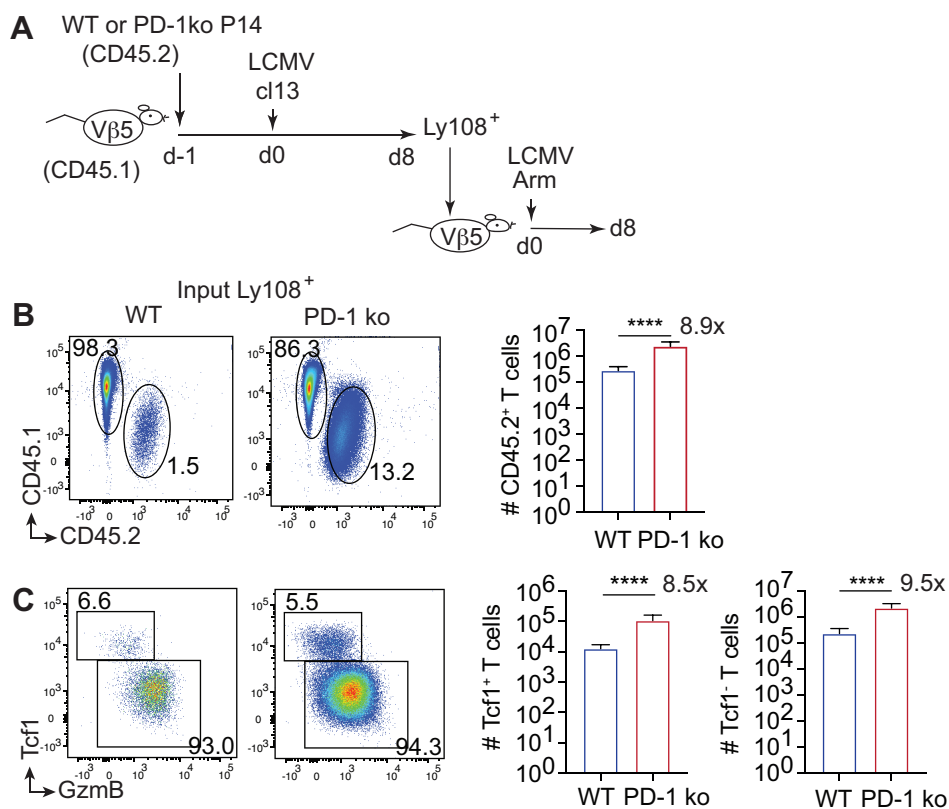


Figure 19: Superior stemness of acute phase PD-1 ko T_{ML} cells.

A) At d-1, 500 naïve WT or naïve PD-1 ko P14 cells (CD45.2) were transferred into V β 5 mice (CD45.1). At d0 mice were infected with LCMV cl13. At d8 mice were sacrificed and CD8⁺ T cells were purified and Ly108⁺ T_{ML} (CD45.2⁺) cells were flow sorted. 10⁴ T_{ML} cells were transferred i.v. into new V β 5 hosts that were infected with LCMV Arm. Secondary recipients were analysed 8 days later. **B)** Representative dot plots depict WT and PD-1 ko P14 populations at d8+8. The bar graphs show the mean number of WT (blue bars) or PD-1 ko P14 cells (red bars). **C)** Representative dot plots depict the secondary Tcf1⁺ and Tcf1⁻ populations at d8+8. The bar graphs show the mean number of secondary WT and PD-1 ko Tcf1⁺ and Tcf1⁻ cells. **B-C)** Data are from n=10 mice per group and are combined of n=2 independent experiments. Bar graphs show the mean number (\pm SD). Two-tailed t-test was performed to determine statistically significant differences (*p<0.05, **p<0.01, ***p<0.001, ns=not significant p>0.5).

3.7 Increased expansion of acute phase PD-1 ko T_{ML} cells in mixed transfers

To rule out the possibility that the difference between PD-1 ko and WT cells was due to a distinct environment, we repeated the above experiments using a 1:1 mix of WT and PD-1 ko P14 cells. Purified WT and PD-1 ko Tcf7^{GFP+} P14 cells were mixed in equal proportions and transferred into the same V β 5 hosts that were then infected with LCMV cl13 (**Fig. 20 A**). At d8 p.i., the ratio of PD-1 ko to WT P14 cells was skewed 3.7-fold in favour of PD1 ko cells (**Fig. 20 B**). Tcf7^{GFP+} (4-fold) and Tcf7^{GFP-} cells (3.7-fold) were similarly skewed in favour of PD1 ko cells (**Fig. 20 C,D**).

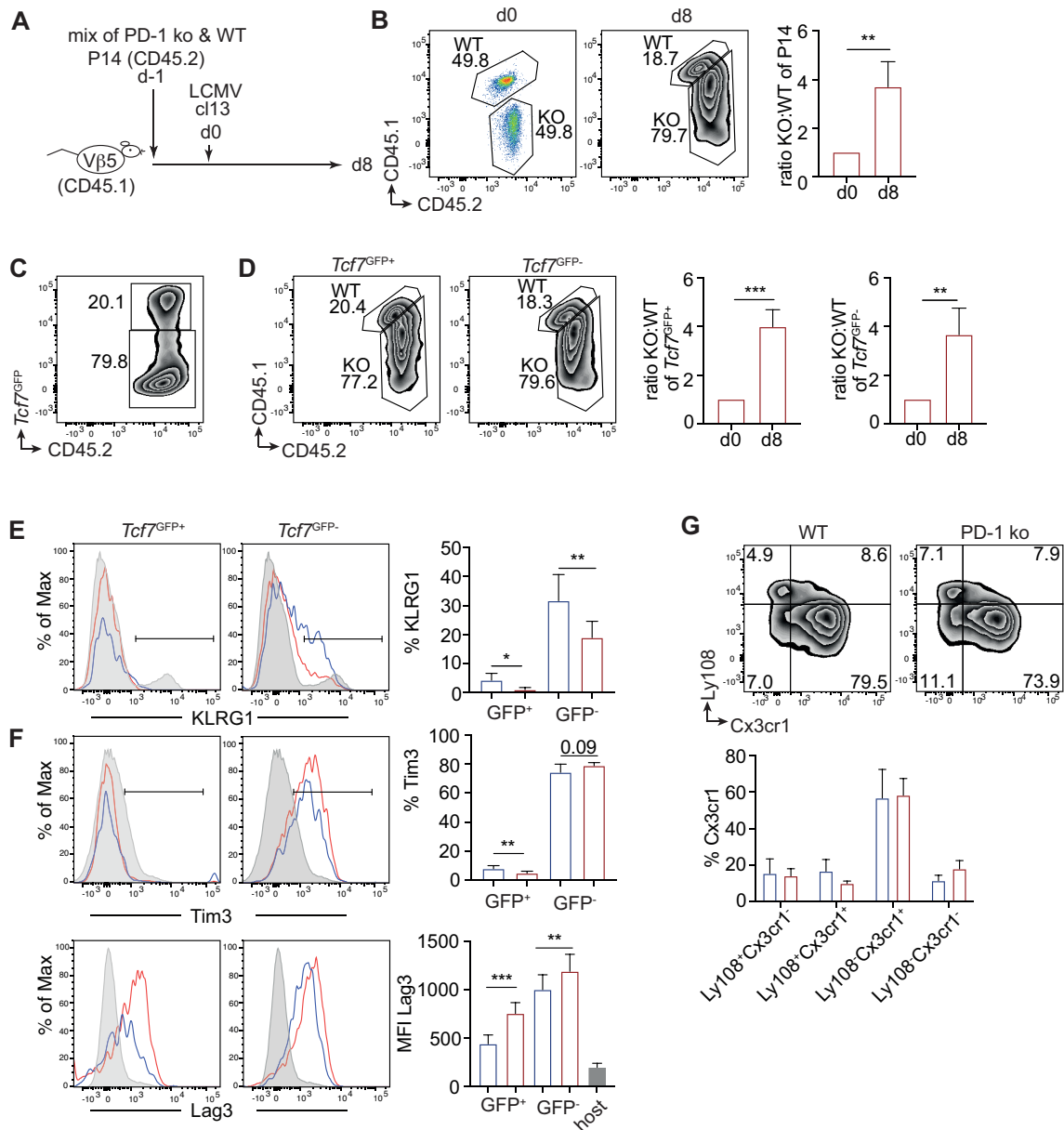


Figure 20: Increased expansion of PD-1 ko T_{ML} cells in a mixed environment.

A) Schematic representation of the experiment. At d-1, 250 WT (CD45.1/2⁺) and 250 PD-1 ko (CD45.2⁺) *Tcf7*^{GFP+} cells were mixed and co-injected i.v. in Vβ5 (CD45.1⁺) mice. Subsequently, at d0 mice were infected with LCMV cl13 and expansion of P14 cells was analysed 8 days later. **B**) Representative dot plots depicting the ratio of WT and PD-1 ko P14 cells at d0 (input) and at d8 p.i. The bar graph shows the ratio of KO vs WT P14 cells at d0 and d8. **C**) Representative dot plot depicting *Tcf7*^{GFP+} P14 cells at d8. **D**) Representative dot plots depicting the ratio of PD-1 ko vs WT cells among gated *Tcf7*^{GFP+} and *Tcf7*^{GFP-} cells. **E**) Representative histograms depict KLRG1 expression by WT (blue) and PD-1 ko (red) Ly108⁺ T_{ML} and Ly108⁻ T_{EX} cells compared to host CD8⁺ T cells (grey fill). The bar graph shows the frequency of KLRG1 expression among WT and PD-1 ko T_{ML} and T_{EX} cells. **F**) Representative histograms show Lag3 and Tim3 expression by WT (blue) and PD-1 ko (red) Ly108⁺ T_{ML} and Ly108⁻ T_{EX} cells compared to host CD8⁺ T cells (grey fill). The bar graph shows the MFI of Lag3 expression or the frequency of Tim3⁺ cells among WT and PD-1 ko T_{ML} and T_{EX} cells. **G**) Mean frequency (±SD) of Ly108 vs Cx3cr1 expression among WT (blue) or PD-1 ko P14 cells (red).

B,D) Data shown are from n=5 mice (d8) and n=1 input mix (d0) and are representative of n=3 independent experiments. One sample t and Wilcoxon test was performed to determine statistically significant differences (*p<0.05, **p<0.01, ***p<0.001, ns=not significant p>0.5).

E-F) Data are derived from 4-5 mice and are representative of n=2 independent experiments. (blue: WT, red: PD-1 ko, grey: host). Bar graphs show the mean percentage (±SD). Paired t-test was performed to determine statistically significant differences (*p<0.05, **p<0.01, ***p<0.001, ns=not significant p>0.5).

G) Two Way ANOVA with uncorrected Fisher's LSD was performed to determine significant differences between WT and PD-1 ko populations. Data are derived from 4-5 mice and are representative of n=2 independent experiments.

Phenotypically, PD-1 ko *Tcf7^{GFP+}* cells expressed more Lag3 (**Fig. 20 E,F**). PD-1 ko *Tcf7^{GFP-}* cells expressed less KLRG1 and more Lag3 than WT. Further, WT and PD-1 ko T_{ML} cells showed similar Ly108 versus Cx3cr1 distribution (**Fig. 20 G**).

These data confirmed the increased initial expansion of PD-1 ko T_{ML} cells in response to chronic infection independent of environmental differences. They suggested that PD-1 limited the expansion of T_{ML} cells during the chronic phase of the infection. Notably the skew towards PD-1 ko cells at the acute phase (3.7-fold) was considerably less than at the chronic phase (54-fold), indicating that PD-1 ko T_{ML} cells out-competed WT cells during the chronic phase of the infection.

3.8 Comparable stemness of acute phase PD-1 ko and WT T_{ML} cells in mixed transfers

In order to determine the stemness of PD-1 ko T_{ML} cells, the mix of PD-1 ko and WT *Tcf7^{GFP+}* T_{ML} cells was flow sorted and transferred into new hosts that were infected with LCMV Arm and were treated with either anti-PD-1 or isotype (**Fig. 21 A**). The skew towards PD-1 ko T_{ML} cells, which was 3.5-fold at input (d8), was marginally reduced to 2.8-fold after the recall response (d8+8) (**Fig. 21 B,C** -iso). The skews were similar among secondary *Tcf7^{GFP+}* (3.6-fold) and *Tcf7^{GFP-}* cells (3.2-fold) (**Fig. 21 D,E** -iso). This showed that acute phase PD-1 ko T_{ML} and WT T_{ML} had comparable stemness.

We further tested whether the stemness of WT cells was underestimated due to PD-1-mediated inhibition during the recall response. Indeed, when the mixed recall response was performed in the presence of blocking PD-1 antibody, the output mix was skewed 2-fold in favor of PD-1 ko cells, compared to a 3.5-fold skew of the input mix (**Fig. 21 C** - α PD-1). Thus, when PD-1 was blocked, the stemness of acute phase PD-1 ko T_{ML} cells was modestly (about 2-fold) lower than that of WT T_{ML} cells (**Fig. 21 D,E** - α PD-1). Impaired stemness of PD-1 ko T_{ML} cells was thus mostly acquired during the chronic phase of infection. Thus, PD-1 expression maintained T_{ML} stemness in the face of continuous stimulation.

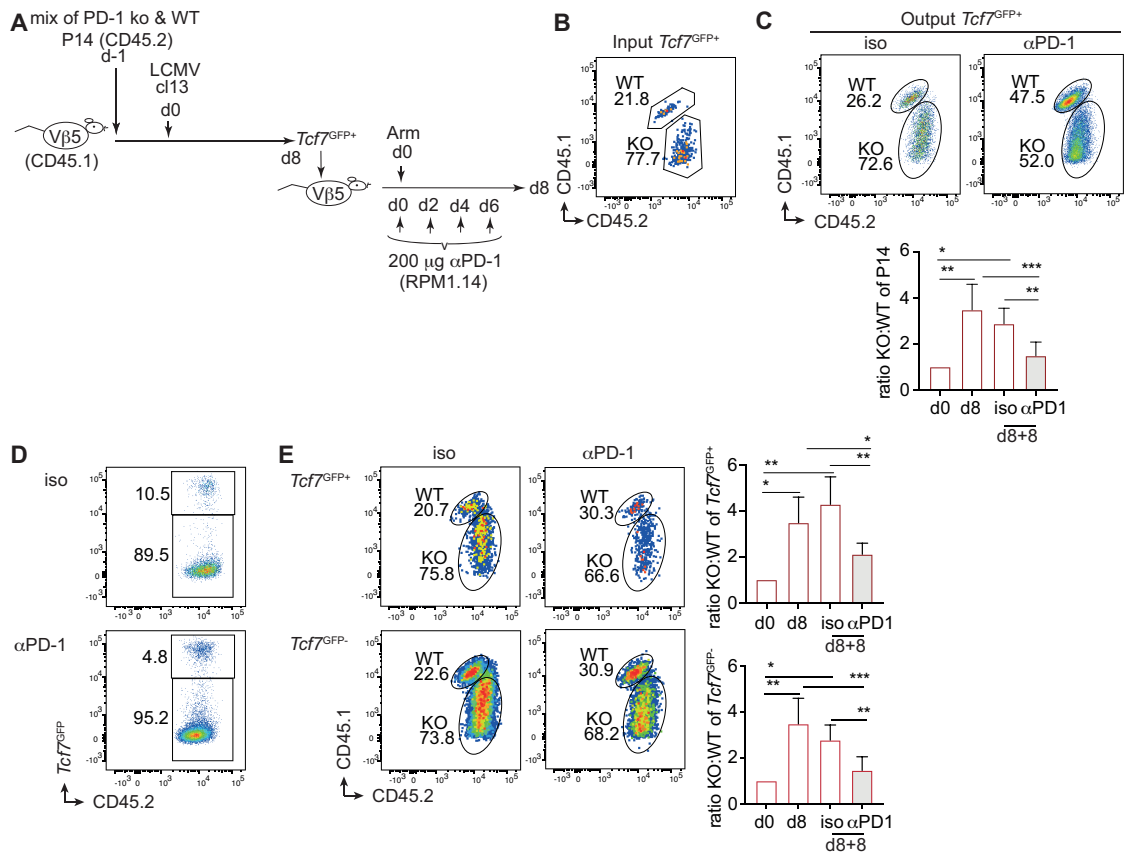


Figure 21: PD-1 ko and WT T_{ML} cells have comparable stemness in mixed transfers.

A) Schematic representation of mixed retransfer experiments. At d-1, naive WT (CD45.1/2⁺) and naive PD-1 ko (CD45.2⁺) P14 cells were mixed at a 1:1 ratio and transferred into Vβ5 mice (CD45.1⁺). At d0 mice were infected with LCMV cl13. At d8 p.i., 10⁴ total Tcf7^{GFP+} T_{ML} cells, containing a mix of WT and PD-1 ko cells, were sorted and re-transferred into new Vβ5 hosts. Secondary recipients were infected with LCMV Arm and treated with 200 μg of anti-PD-1 (αPD-1) (i.p.) or IgG2a (2A3) isotype control Ab, which was followed by 3 more injections every two days until sacrifice at d8 post re-transfer. **B**) Representative dot plot depicting the ratio of PD-1 ko to WT Tcf7^{GFP+} cells after the sort at d8 p.i.. **C**) Representative dot plot depicting the ratio of PD-1 ko to WT P14 cells at d8 after re-transfer (d8+8). Bar graph shows ratio of KO vs WT P14 cells at d0, d8 and d8+8 either isotype or αPD-1 treated. **D**) Representative dot plots depicting Tcf7^{GFP} expression among P14 cells at d8+8. **E**) Representative dot plots depicting the ratio of PD-1 ko to WT P14 cells among gated Tcf7^{GFP+} T_{ML} or Tcf7^{GFP-} T_{EX} cells at d8+8. Bar graphs show the ratio of KO vs WT P14 cells among gated Tcf7^{GFP+} T_{ML} or Tcf7^{GFP-} T_{EX} cells at d8+8 compared to d0 and d8.

B-E) Dot blots are from n=5 mice from a single experiment. Bar graphs show the means (±SD). One-way ANOVA or Mixed-effect analysis with Tukey's correction was performed to determine statistically significant differences (*p<0.05, **p<0.01, ***p<0.001, ns=not significant p>0.5).

3.9 PD-1:PD-L1 blockade reduces stemness of WT T_{ML} (in collaboration with Vijaykumar Chennupati)

In addition to the effects of PD-1-deficiency, we investigated whether PD-1-PD-L1 blockade during chronic infection impacted T_{ML} function. WT Tcf7^{GFP} P14 (CD45.2⁺) cells were transferred into Vβ5 (CD45.1⁺) hosts that were then infected with LCMV cl13 (**Fig. 22 A**). Recipients were treated with anti-PD-L1 or isotype control mAb starting at d20 p.i. five times, every four days. P14 cells were analysed four days after the last injection (d41 p.i.).

Anti-PD-L1 treatment significantly increased the abundance of P14 cells. Further, the abundance of $Tcf7^{GFP+}$ or $Tcf1^+$ (T_{ML}) cells and of $Tcf7^{GFP-}$ or $Tcf1^-$ (T_{EX}) cells were both increased (Fig. 22 B,C,D). These data were consistent with earlier data from Utzschneider *et al.*⁵⁷.

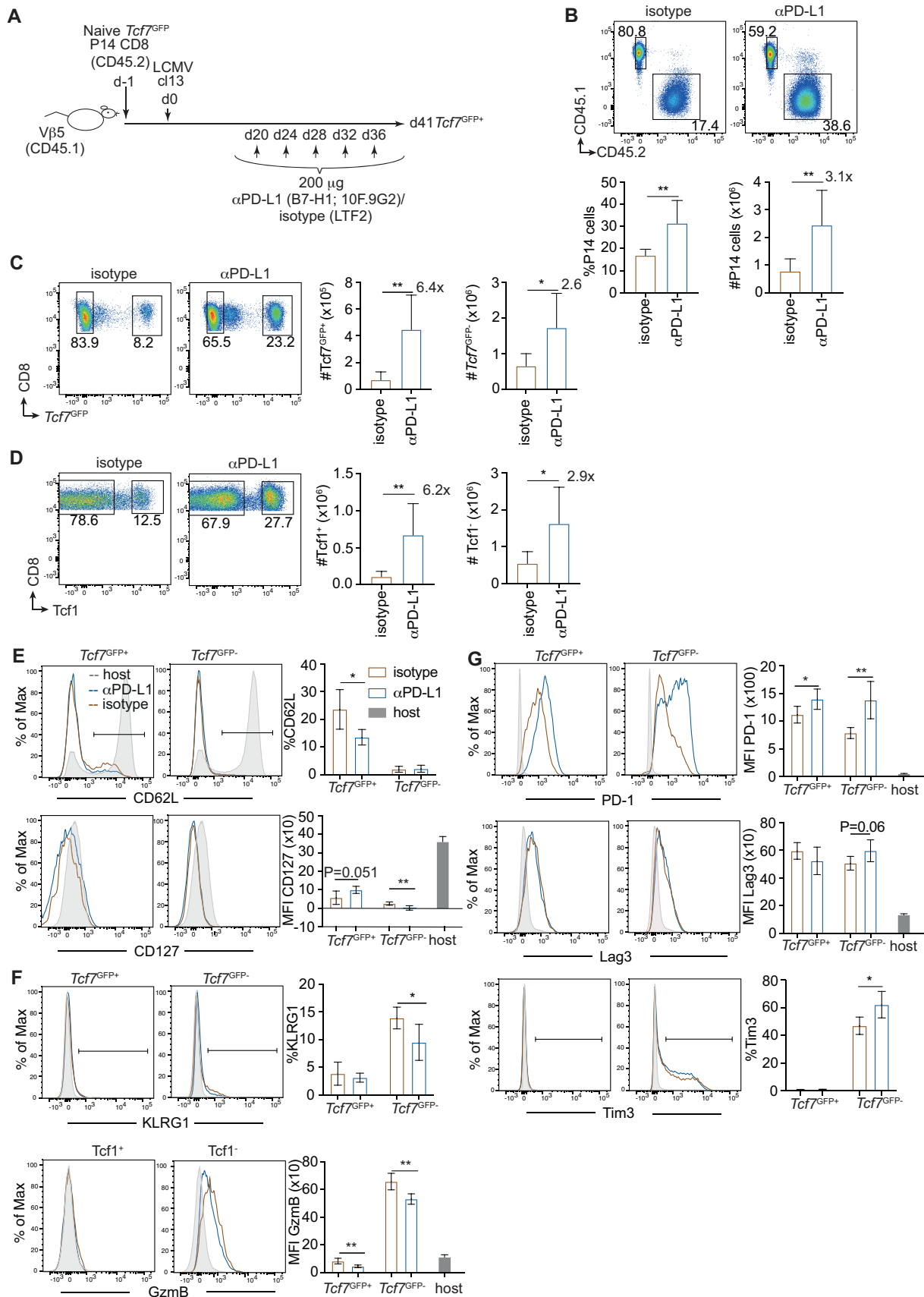


Figure 22: Anti-PD-L1 treatment expands T_{ML} cells.

A) Schematic representation of the experimental setup. At d-1, 10000 naïve WT *Tcf7^{GFP}* P14 cells (CD45.2⁺) were transferred into Vβ5 mice (CD45.1⁺). At d0 mice were infected with LCMV cl13. Mice were injected either 200 μg of anti-PD-L1 (αPD-L1;B7-H1; 10F.9G2) or isotype (LTF-2) starting at d20 until d36, every fourth day. At d41, mice were sacrificed, and cells were analysed by flow cytometry. **B)** Representative dot plots depict the analysis of gated P14 cells (CD45.2⁺) from isotype or anti-PD-L1 treated mice. **C)** Representative dot plots depict *Tcf7^{GFP+}* T_{ML} and *Tcf7^{GFP-}* T_{EX} cells in isotype and anti-PD-L1 treated mice. **D)** Representative dot plots depict Tcf1⁺ T_{ML} and Tcf1⁻ T_{EX} cells in isotype and αPD-L1 treated mice. **E)** Representative histograms depict CD127 and CD62L expression by *Tcf7^{GFP+}* T_{ML} and *Tcf7^{GFP-}* T_{EX} cells compared to host CD8⁺ T cells (grey fill). The bar graph shows the MFI of CD127 and frequency of CD62L⁺ cells among on WT and PD-1 ko T_{ML} and T_{EX} cells. **F)** Representative histograms depict KLRG1 and GzmB expression by *Tcf7^{GFP+}* or Tcf1⁺ T_{ML} and *Tcf7^{GFP-}* or Tcf1⁻GzmB⁺ T_{EX} cells compared to host CD8⁺ T cells (grey fill). The bar graph shows the MFI of GzmB or the frequency of KLRG1⁺ cells among WT and PD-1 ko T_{ML} and T_{EX} cells. **G)** Representative histograms show Lag3, PD-1 and Tim3 expression by *Tcf7^{GFP+}* T_{ML} and *Tcf7^{GFP-}* T_{EX} cells compared to host CD8⁺ T cells (grey fill). The bar graph shows the MFI of PD-1 and Lag3 or the frequency of Tim3⁺ cells among WT and PD-1 ko T_{ML} and T_{EX} cells.

B-D) Data are from n=5 mice per group and are representative of n=3 independent experiments, 2 experiments were performed by Dr. Vijaykumar Chennupati and one by myself. Bar graphs show the mean number (±SD). Two-tailed t-test was performed to determine statistically significant differences (*p<0.05, **p<0.01, ***p<0.001, ns=not significant p>0.5).

Fewer T_{ML} cells in anti-PD-L1 treated mice expressed CD62L, similar to PD-1 ko T_{ML} cells, whereas expression of CD127 was not significantly different (**Fig. 22 E**). In addition, PD-L1 blockade increased the expression of PD-1, but not Lag3 among T_{ML} cells (**Fig. 22 G**). Conversely, PD-L1 blockade increased the expression of both Tim3 and PD-1 and reduced GzmB and KLRG1 expression by T_{EX} cells (**Fig. 22 F,G**), similar to PD-1 ko T_{EX} cells. Four days after the last PD-L1 Ab treatment, IL-2 production by αPD-L1 treated T_{ML} was increased while INF-γ and TNF-α production by control and αPD-L1 treated T_{ML} or T_{EX} cells were not different (**Fig. 23 C,D,E**). Thus, the increased production of cytokines observed one or two days following the last anti-PD-L1 treatment⁷⁸ had mostly ceased 4 days after the last Ab injection. Therefore, besides cytokine production, anti-PD-L1 treatment and PD-1-deficiency resulted in overall similar phenotypic changes.

To analyse the effect of PD-L1 blockade on stemness, *Tcf7^{GFP+}* (T_{ML}) cells were flow sorted and transferred into new hosts (C57BL/6, CD45.1⁺) that were then infected with LCMV Arm. At d8 p.i., T_{ML} cells from anti-PD-L1 treated mice yielded 1.7-fold fewer P14 offspring than T_{ML} cells from controls. The production of secondary *Tcf7^{GFP+}* and *Tcf7^{GFP-}* cells were reduced 2.3-fold and 1.5-fold, respectively, when T_{ML} cells had been subjected to checkpoint blockade (**Fig. 23 F,G**). This suggested that even a temporary relieve of T_{ML} cells from inhibitory PD-1 signalling impaired their stemness.

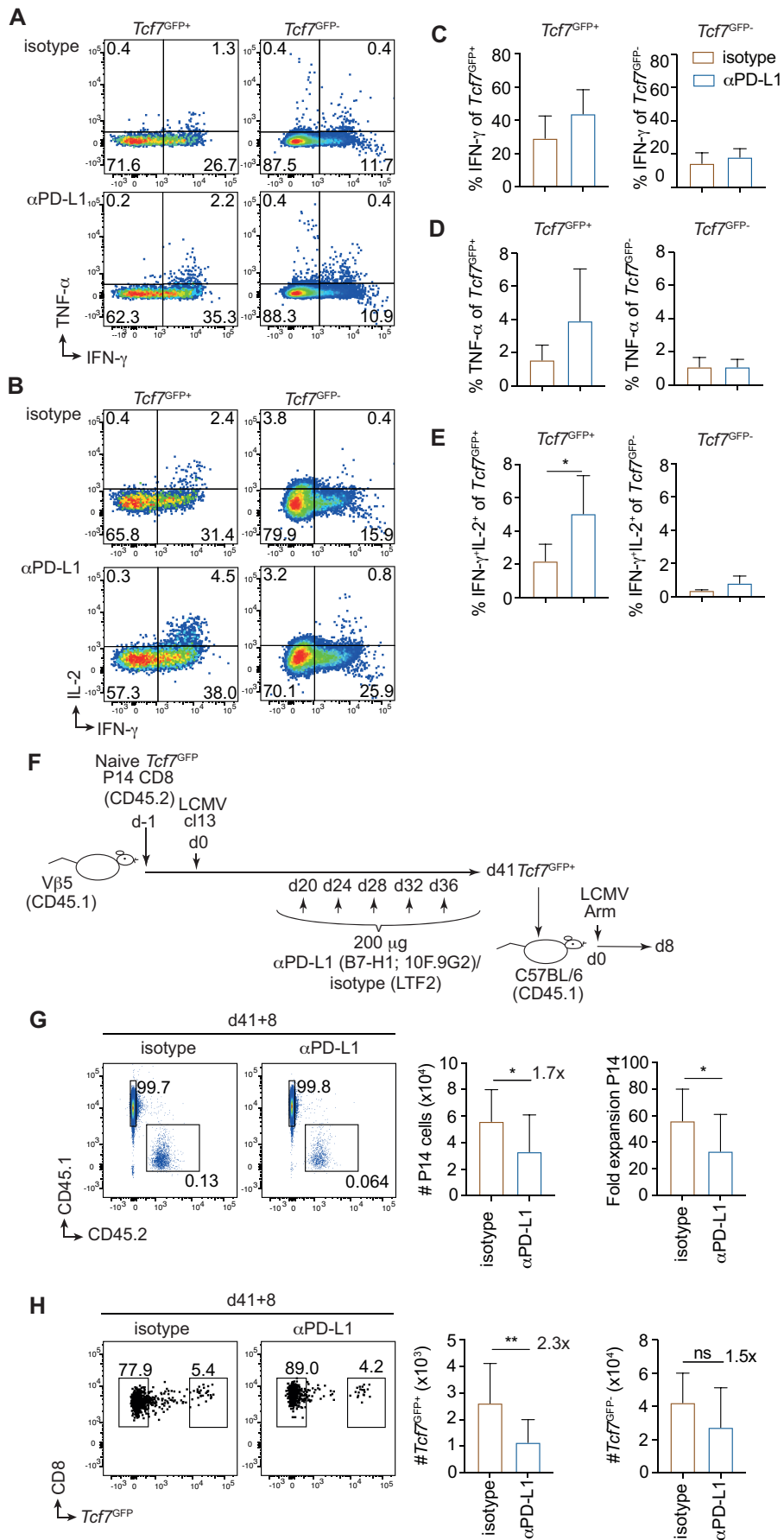


Figure 23: Impaired stemness of T_M from anti-PD-L1 treated mice.

Naïve WT (CD45.2) (10^4) were transferred into V β 5 mice (CD45.1). At d0 mice were infected with LCMV cl13. Mice were injected with α PD-L1 or isotype starting at d20 until d36, every fourth day with either 200 μ g of anti-PD-L1 (α PD-L1, B7-H1; 10F.9G2) or isotype (LTF-2). At d41, mice were sacrificed, and spleen cells were analysed. **A-E**) Splenocytes were stimulated *in vitro* with gp33-peptide. Gated $Tcf7^{GFP+}$ T_{ML} and $Tcf7^{GFP-}$ T_{EX} P14 cells were analysed for IFN- γ , TNF- α and IL-2 expression. Representative dot plots depict **(A)** TNF- α and IFN- γ and **(B)** IL-2 and IFN- γ expression among $Tcf7^{GFP+}$ T_{ML} and $Tcf7^{GFP-}$ T_{EX} P14 cells. **C-E**) Bar graphs depict the frequency of **(C)** IFN- γ^+ , **(D)** TNF- α^+ and **(E)** IL-2 $^+$ cells among $Tcf7^{GFP+}$ T_{ML} and $Tcf7^{GFP-}$ T_{EX} P14 cells.

F-H) At d41 p.i. $Tcf7^{GFP+}$ cells were flow sorted and transferred into new hosts (C57BL/6; CD45.1) that were infected with LCMV Arm. The recall response was analysed 8 days later (**d41+8**). **G**) Representative dot plots show P14 cells at d41+8. Bar graphs show the mean number (\pm SD) and the fold-expansion of $Tcf7^{GFP+}$ P14 cells from isotype and anti-PD-L1 treated mice. **H**) Representative dot plots show $Tcf7^{GFP+}$ T_{ML} and $Tcf7^{GFP-}$ T_{EX} cells among P14 cells at d41+8. Bar graphs show mean number (\pm SD) of $Tcf7^{GFP+}$ T_{ML} and $Tcf7^{GFP-}$ T_{EX} cells.

A-E) Data are derived from 5-7 mice per group and are representative of n=3 independent experiments, 2 experiments were performed by Dr. Vijaykumar Chennupati. Bar graphs show the mean percentage (\pm SD). Two-tailed t-test was performed to determine significant differences (* p <0.05, ** p <0.01, *** p <0.001, ns=not significant p >0.5).

G-H) Data are from n=10 isotype, n=15 mice aPD-L1 treatment that are compiled of n=2 independent experiments. Bar graphs show the mean number (\pm SD). Two-tailed t-test was performed to determine statistically significant differences (* p <0.05, ** p <0.01, *** p <0.001, ns=not significant p >0.5). The 2 compiled experiments were performed by Dr. Vijaykumar Chennupati. These 2 compiled experiments are representative of a third independent experiment performed by myself.

3.10 Chronic phase PD-1 ko T_{ML} cells have a greater propensity to undergo apoptosis

The impaired stemness of chronic phase PD-1 ko T_{ML} cells prompted us to investigate their cell cycle status and survival. To analyse the cell cycle status, gated $Tcf1^+$ or $Ly108^+$ cells were stained *ex vivo* for Ki67 and DAPI (DNA). (**Fig. 24 A-C**).

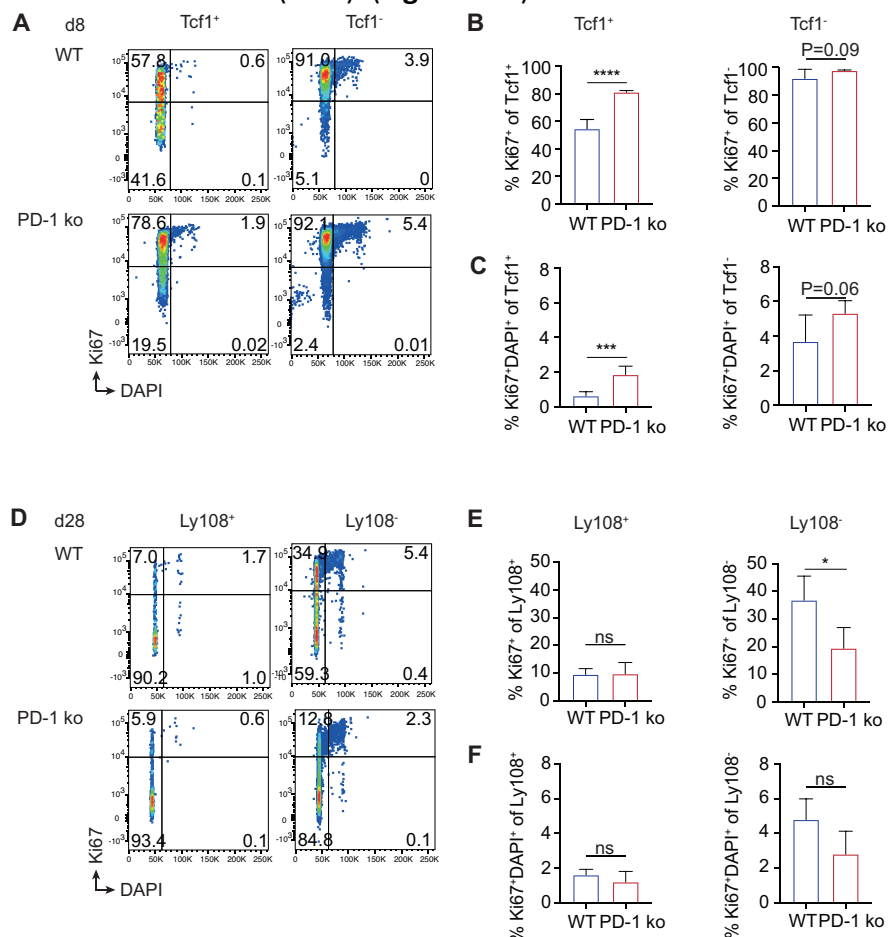


Figure 24: Increased cell cycling of acute phase PD-1 ko T_{ML} cells.

WT or PD-1 ko P14 cells (CD45.2⁺) (for d8 analysis, 500 cells each, for d28 analysis 5000 WT and 500 PD-1 ko P14 cells) were injected into Vβ5 mice (CD45.1⁺), which were then infected with LCMV cl13 and analysed at the indicated timepoints.

A, D) Representative Ki67 vs DAPI plots of WT and PD-1 ko T_{ML} and T_{EX} cells at **(A)** d8 and **(D)** d28 p.i. **B,C)** Bar graphs depict the fraction of Ki67⁺ and Ki67⁺DAPI⁺ cells among **(B)** Tcf1⁺ T_{ML} cells and **(C)** among Tcf1⁻ T_{EX} cells at d8. **D)** Representative plots of WT and PD-1 ko T_{ML} and T_{EX} cells at d28 p.i. (Ki67 vs DAPI). **E,F)** Bar graphs depict the fraction of Ki67⁺ and Ki67⁺DAPI⁺ cells among **(E)** Ly108⁺ T_{ML} cells and **(F)** among Ly108⁻ T_{EX} cells at d28 p.i..

A-C) Data derive from 4-5 mice per group and are representative of n=2 independent experiments (Blue: WT, red: PD-1 ko)

D-F) Data are derived from 4-5 mice per group and are representative of n=4 independent experiments. (Blue: WT, red: PD-1 ko).

B-F) Bar graphs show the mean percentage (±SD). Two-tailed t-test was performed to determine significant differences (*p<0.05, **p<0.01, ***p<0.001, ns=not significant p>0.5).

Ki67 protein is expressed during all phases of the cell cycle (G₁, S, G₂) except in quiescent cells (G₀)¹⁶². The fraction of acute phase Ki67⁺ PD-1 ko T_{ML} cells was increased compared to WT. A similar trend was observed among PD-1 ko T_{EX}. Similar data were obtained for Ki67⁺DAPI⁺ cells. To assess survival, splenocytes were cultured *in vitro* for 4h in the absence of growth factors before staining with AnnexinV and 7AAD. At d8 p.i. PD1 ko and WT T_{ML} cells included similar fractions of dead AnnexinV⁺7AAD⁺ cells (**Fig. 25 A,B**). The increased fraction of AnnexV⁺7AAD⁺ PD-1 ko T_{EX} cells seen in this experiment was not reproducible. Thus, increased cycling of PD-1 ko cells explained their increased abundance at d8.

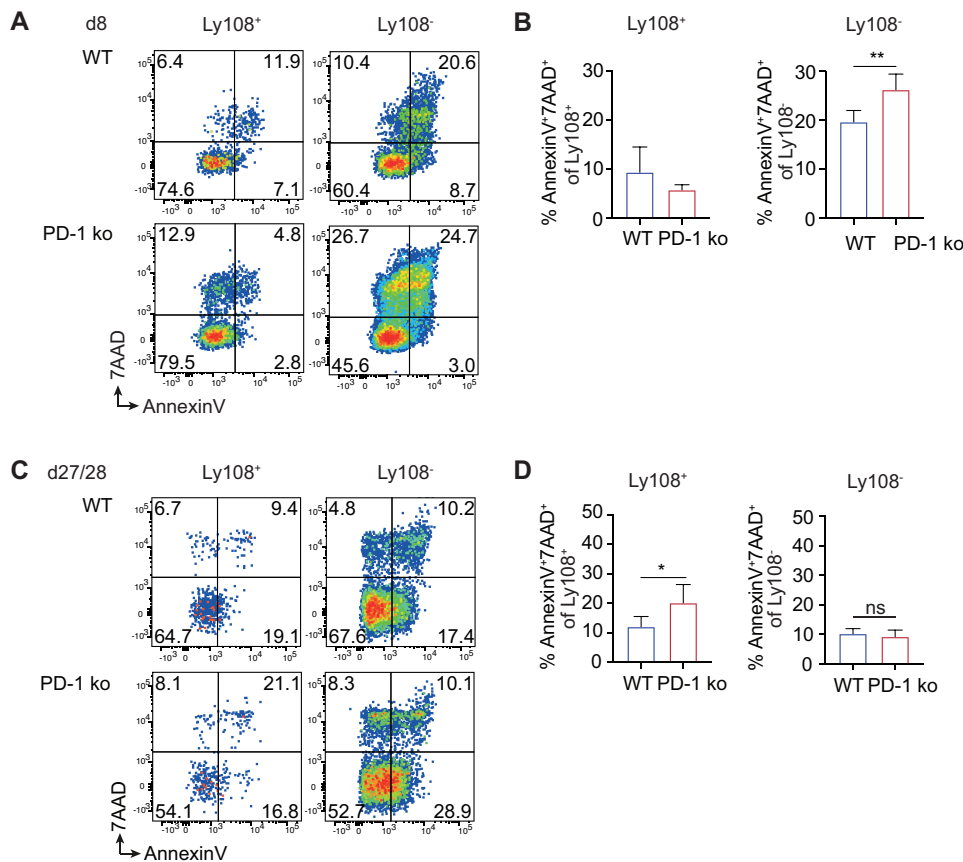


Figure 25: Increased apoptosis of chronic phase PD-1 ko T_{ML}.

Splenocytes were cultured for 4h at 37°C in the absence of growth factors. **A-D)** Representative dot plots depict 7AAD vs AnnexinV (AnnexV) expression by WT and PD-1 ko T_{ML} and T_{EX} cells **(A,B)** at d8 p.i. and **(C,D)** at d27/d28

p.i.. Bar graphs depict the frequency of AnnexinV⁺7AAD⁺ Ly108⁺ T_{ML} and Ly108⁻ T_{EX} cells at d8 (**B**) and d27/d28 (**D**).

A-B) Data are derived from 4-5 mice per group and are representative of n=2 independent experiments. **C-D**) Data are derived from 4-5 mice per group and are representative of n=4 independent experiments.

Bar graphs show the means (\pm SD). Two-tailed t-test was performed to determine significant differences (*p<0.05, **p<0.01, ***p<0.001, ns=not significant p>0.5).

There was no difference in the cycling between PD-1 ko and WT T_{ML} at d28, but the fraction of Ki67⁺ PD-1 ko T_{EX} was reduced compared to WT (**Fig. 24 D-F**). These findings might account for the decline of T_{EX} cells at the chronic phase. At d28 p.i. PD-1 ko T_{ML} cells included an increased fraction of AnnexinV⁺ 7AAD⁺ cells compared to WT (**Fig. 25 C,D**), whereas the PD-1 ko and WT T_{EX} cells included similar fractions of dead AnnexinV⁺7AAD⁺ cells. Thus, decreased survival correlated with the reduced stemness of chronic phase PD-1 ko T_{ML} cells.

3.11 Chronic phase PD-1 ko T_{ML} cells have an increased mitochondrial activity and cellular ROS content

Previous analysis of T cells responding to chronic infection suggested that PD-1 expression reduced mitochondrial fitness¹²¹, and increased ROS generation and ROS-driven apoptosis¹⁶³. Based on these findings we compared the mitochondrial mass and potential, as well as ROS production of PD-1 ko and WT T_{ML} cells. To determine mitochondrial mass and potential, cells were briefly cultured *in vitro* in the presence of MitoTracker[®] DeepRed (MDR) to measure mitochondrial potential and MitoTracker[®] Green (MG) to measure mitochondrial mass and subsequently stained for surface markers.

WT T_{ML} cells present at d8 and d28 showed increased mitochondrial membrane potential and mass compared to WT T_{EX} (**Fig. 26 A-G**). PD-1 ko T_{ML} or T_{EX} populations were not different at d8. In agreement with increased mitochondrial function at d28, cellular ROS levels were increased in PD-1 ko compared to WT T_{ML} cells (**Fig. 26 I,J**). Cellular ROS levels were also increased in PD-1 ko T_{EX}. In agreement with their similar mitochondrial activity, cellular ROS levels were not different at d8 (**Fig. 26 A-C,G,H**). The increased mitochondrial activity and ROS production in chronic phase PD-1 ko T_{ML} may contribute to reduced survival and stemness of these cells.

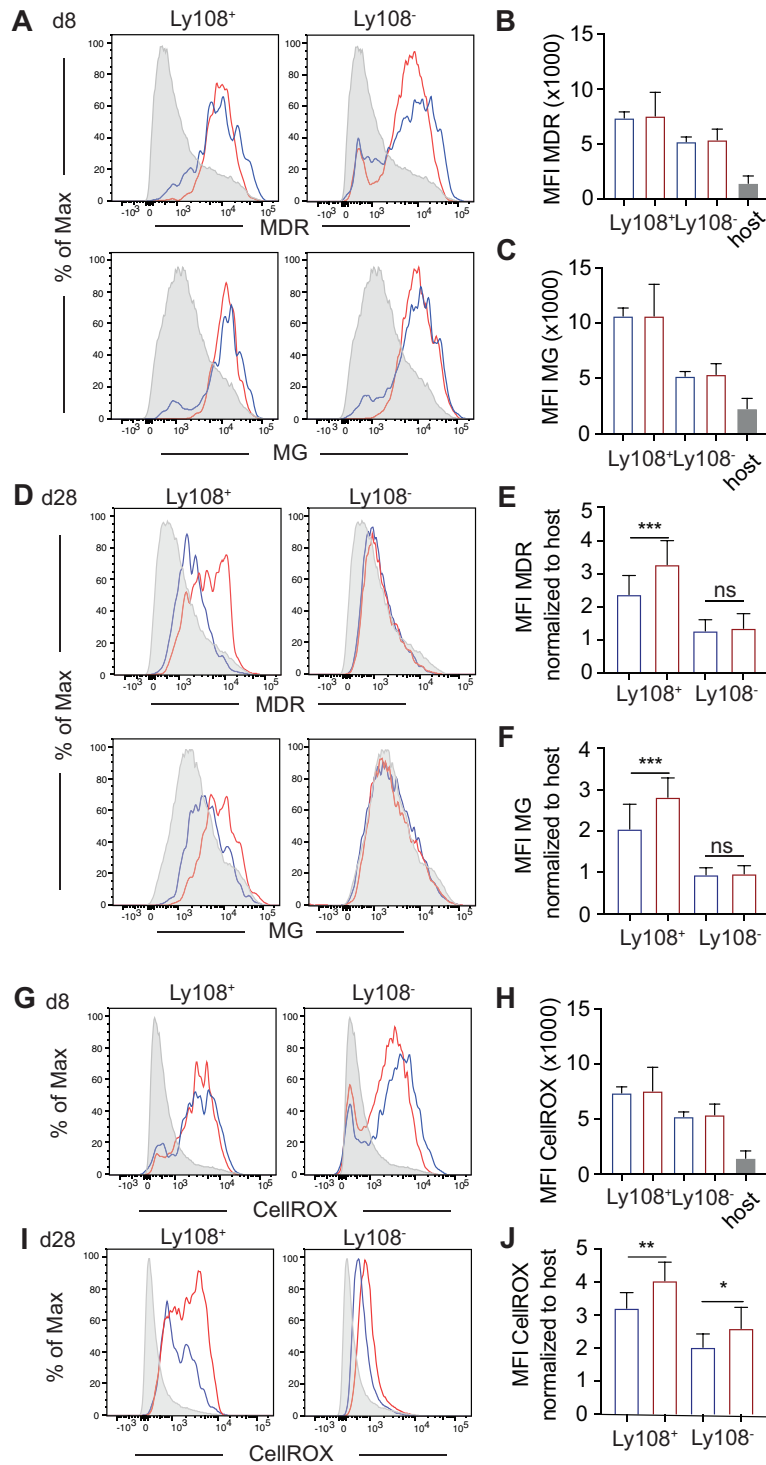


Figure 26: Increased mitochondrial activity and cellular ROS production by chronic phase PD-1 ko T_{ML} cells.

A-H) Splenocytes were cultured in the presence of fluorescent days MitoTracker® DeepRed (MDR) and MitoTracker® Green (MG) before staining. **A)** Representative histograms show mitochondrial mass (MG) and mitochondrial membrane potential (MDR) of WT (blue) and PD-1 ko (red) Ly108⁺ T_{ML} and Ly108⁻ T_{EX} at d8 p.i.. **B)** The bar graph shows MFI of MDR staining of WT (blue bars) or PD-1 ko (red bars) Ly108⁺ T_{ML} or Ly108⁻ T_{EX} cells at d8 p.i.. **C)** The bar graph shows the MFI ±SD of MG of WT (blue bars) or PD-1 ko T_{ML} (red bars) cells at d8 p.i.. **D)** Mitochondrial mass (MG) and mitochondrial membrane potential (MDR) of WT (blue) and PD-1 ko (red) Ly108⁺ T_{ML} and Ly108⁻ T_{EX} at d28 p.i.. **E)** The bar graph shows the MFI of MDR staining of WT (blue bars) or PD-1 ko (red bars) Ly108⁺ T_{ML} and Ly108⁻ T_{EX} cells at d28 normalized to the MDR signal from host cells. **F)** The bar graph shows the MFI of MG staining of WT (blue bars) or PD-1 ko (red bars) Ly108⁺ T_{ML} and Ly108⁻ T_{EX} cells normalized to MG signal in host cells at d28.

G-J) Splenocytes were stained and then cultured in HBSS in the presence of CellROX® Deep Red dye and probenecid for 30' at 37°C. **G-J)** CellROX® staining in WT (blue) and PD-1 ko (red) Ly108⁺ T_{ML} and Ly108⁻ T_{EX} cells at **(G,H)** d8 and **(I,J)** d28 p.i.

A-C, G-H) Data are derived from n=3-5 mice per group from one a single experiment. **D-F)** Data derive from n=15 mice per group and are compiled from n=3 independent experiments. **I,J)** Data derive from n=9 mice per group and compiled from n=2 independent experiments.

A-J) Bar graphs show the means (±SD). Two-tailed t-test was performed to determine significant differences between WT and PD-1 ko Ly108⁺ T_{ML} or WT and PD-1 ko Ly108⁻ cells (*p<0.05, **p<0.01, ***p<0.001, ns=not significant p>0.5).

3.12 Transcriptome analysis of WT and PD-1 ko T_{ML} cells (in collaboration with M. Charmoy & T. Wyss)

To identify differences between WT and PD-1 ko T_{ML} cells in an unbiased fashion we compared the transcriptome of these cells. To this end WT or PD-1 ko P14 cells (CD45.2⁺) were transferred into Vβ5 (CD45.1⁺) hosts that were subsequently infected with LCMV cl13. In addition, some mice receiving WT P14 cells were treated with anti-PD-L1, starting on d24 p.i. three times, every four days. Four days after the last Ab injection, at d36 p.i., Ly108⁺ (T_{ML}) and Ly108⁻ (T_{EX}) P14 cells were flow sorted and subjected to RNA-Seq analysis. The analysis further included naïve (CD62L⁺) WT and PD-1 ko P14 cells.

Principal component analysis (PCA) of the 13'303 expressed genes segregated T_{ML} and T_{EX} cells into two clearly separate clusters that were distinct from naïve CD8⁺ T cells (**Fig. 27 A**). Indeed, 5089 genes were differentially expressed between WT T_{ML} cells and WT T_{EX} cells (2397 genes were downregulated and 2692 were upregulated) (adjusted (adj.) p value <0.05). PD-1 ko T_{ML} cells and PD-1 ko T_{EX} cells differed by 4688 differentially expressed genes (DEG) (2281 were downregulated and 2407 were upregulated) (adj. p value <0.05). Anti-PD-L1 treated WT T_{ML} and T_{EX} cells differed by 4192 DEG (1895 downregulated and 2297 upregulated) (adj. p value <0.05).

WT, PD-1 ko and anti-PD-L1 treated T_{ML} cells clustered together. Indeed, only 430 genes were differentially expressed between WT and PD-1 ko T_{ML} cells (215 genes were downregulated and 215 were upregulated) (adj. p value <0.05), whereas anti-PD-L1 treated WT T_{ML} differed from WT T_{ML} cells by 759 DEG (380 genes were downregulated and 379 genes were upregulated) (adj. p value <0.05). In the comparison of PD-1 ko and anti-PD-L1 treated T_{ML} cells only 203 genes were differentially expressed (122 were downregulated and 81 were upregulated) (adj. p value <0.05).

Comparison of T_{EX} cells revealed larger differences. 1979 DEG between WT T_{EX} and PD-1 ko T_{EX} cells (1058 downregulated and 921 upregulated) (adj. p value <0.05). WT T_{EX} and anti-PD-L1 treated T_{EX} cells revealed 1020 DEG (481 were downregulated and 539 were upregulated) (adj. p value <0.05) while PD-1 ko T_{EX} and anti-PD-L1 treated T_{EX} cells differed by 457 genes (159 were downregulated and 298 were upregulated) (adj. p value <0.05).

These data confirmed that T_{ML} and T_{EX} were distinct and suggested that WT, PD-1 ko and anti-PD-L1 T_{ML} cells were relatively similar and that the different T_{EX} were more distinct.

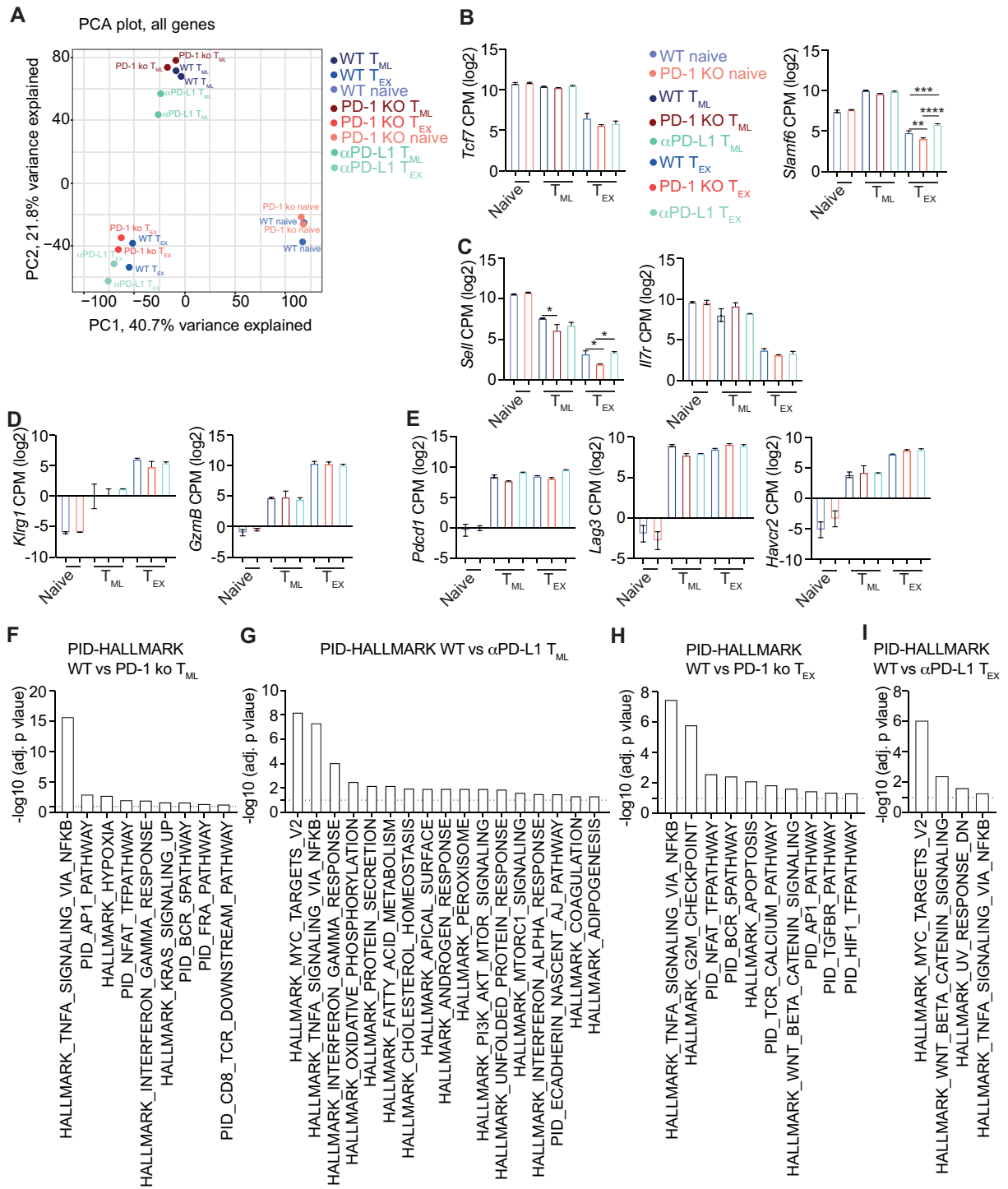


Figure 27: Transcriptome analysis reveals impaired downstream TCR signalling in PD-1 ko T_{ML} cells.

Vβ5 mice received 5000 WT or 500 PD-1 ko P14 CD8⁺ T cells before infection with LCMV cl13. Half of the mice that obtained WT cells were treated with anti-PD-L1 (αPD-L1; 200 μg) at d24, d28 and d32 p.i. All mice were analysed at d36 p.i.. Cells were enriched for CD8⁺ T cells and Ly108⁺ T_{ML} cells and Ly108⁻ T_{EX} cells were obtained by flow sorting. Total cellular RNA was subjected to RNA-Seq analysis. **A**) Principal Component Analysis (PCA) based on all genes expressed in naïve subsets (WT_naive; PD-1 ko_naive), Ly108⁺ T_{ML} subsets (WT T_{ML}, PD-1 ko T_{ML}, anti-PD-L1 treated T_{ML}), Ly108⁻ T_{EX} subsets (WT T_{EX}, PD-1 ko T_{EX}, anti-PD-L1 treated T_{EX}). **B-E**) Bar graphs depicting counts per million (CPM) (log₂) of genes (**B**) used to discriminate T_{ML} and T_{EX} populations (*Tcf7*, *Slamf6*) (**C**) genes associated with memory-formation (*Sell*, *Il7r*). (**D**) effector function (*Gzmb*, *Klrp1*) and (**E**) exhaustion (*Pdcd1*, *Lag3*, *Havcr2*). **F-I**) Gene set enrichment analysis (GSEA) using the pathway interaction database (PID) and Hallmark database. Bar graph depicting pathways enriched in WT T_{ML} vs PD-1 ko T_{ML} cells (**F**), WT T_{ML} vs anti-PD-L1 T_{ML} (**G**), WT T_{EX} vs PD-1 ko T_{EX} (**H**), WT T_{EX} vs anti-PD-L1 T_{EX} (**I**) (-log₁₀ of the adjusted p-value).

B-E) Data are derived from two replicates per population. Bar graphs show the mean percentage (\pm SD). One-way ANOVA was performed to determine significant differences between more than two groups ($*p<0.05$, $**p<0.01$, $***p<0.001$, ns=not significant $p>0.5$).

We first compared the gene expression data and the expression of selected markers used in flow cytometry analysis. As expected, the T_{ML} marker Ly108 (encoded by *Slamf6*) and the transcription factor Tcf1 (encoded by *Tcf7*) were highly expressed by WT and PD-1 ko T_{ML} but not T_{EX} cells (**Fig. 27 B**). In agreement with the phenotypic characterization of T_{ML} , *Sell* (encoding CD62L) and *Ii7r* (CD127) were preferentially expressed in T_{ML} (**Fig. 27 C**), while *Klrg1* and *Gzmb* were predominantly expressed by T_{EX} cells (**Fig. 27 D**).

Pdcd1 expression, which encodes PD-1, was not different between WT and PD-1 ko cells, indicating that the gene was still expressed. However, the sequence was disrupted as surface PD-1 expression was not detected (**Fig. 27 E**). *Lag3* expression was high in both T_{ML} and T_{EX} cells while Tim3 (encoded by *Havcr2*) was preferentially expressed by T_{EX} (**Fig. 27 E**). In agreement with the flow analyses of selected markers, the gene expression analysis did not show major differences amongst the three types of T_{ML} or T_{EX} cells.

3.13 PD-1 deficiency impairs the expression of TCR downstream genes

In order to address whether gene expression changes affected specific pathways, we used the differentially expressed genes to perform gene set enrichment analysis (GSEA) relative to the "Pathway Interaction Database" (PID) and Hallmark sets available on the Molecular Signatures Database (MSigDB, v.7.4). This analysis revealed that PD-1 ko T_{ML} cells had reduced overlaps with "HALLMARK_TNFA_SIGNALING_VIA_NFKB", the PID_AP-1_pathway, PID_NFAT_TFPATHWAY, PID_BCR_5_PATHWAY, PID_FRA_PATHWAY and PID_CD8_TCR_DOWNSTREAM_PATHWAY signatures compared to WT T_{ML} (adj. p value <0.05) (**Fig. 27 F**). None of the PID pathways were significantly differentially enriched among anti-PD-L1 treated WT compared to untreated WT T_{ML} cells (adj. p value <0.05) (**Fig. 27 G**). On the other hand, a reduced overlap with the "HALLMARK_TNFA_SIGNALING_VIA_NFKB" signature was observed following PD-L1 blockade.

Further PD-1 ko T_{EX} had a reduced overlaps with the HALLMARK_TNFA_SIGNALING_VIA_NFKB and HALLMARK_WNT_BETA_CATENIN_SIGNALING, PID_NFAT_TFPATHWAY, PID_BCR_5PATHWAY, PID_TCR_CALCIIUM_PATHWAY, PID_AP1_PATHWAY, PID_TGFBR_PATHWAY, PID_HIF1_TFPATHWAY signatures compared to WT T_{EX} cells (adj. p value <0.05) (**Fig. 27 H**). While reduced overlaps with the HALLMARK_TNFA_SIGNALING_VIA_NFKB and HALLMARK_WNT_BETA_CATENIN_SIGNALING were also observed among anti-PD-L1 treated WT compared to untreated WT T_{EX} , none of PID pathways were differentially enriched between anti-PD-L1 WT and untreated T_{EX} cells (adj. p value <0.05) (**Fig. 27 I**).

Sandu *et al.*¹¹² recently reported a set of genes upregulated in chronically stimulated CD8⁺ T cells in response to CD3/CD28 re-stimulation. The set of upregulated genes was highly enriched for the "HALLMARK_TNFA_SIGNALING_VIA_NFKB" pathway. Thus, in T cells the "HALLMARK_TNFA_SIGNALING_VIA_NFKB" pathway could be triggered by TCR/CD28 engagement. Therefore, GSEA suggested PD-1 ko T_{ML} cells suffered from impaired TCR downstream signalling, via the NFAT, AP-1 and NF- κ B pathways.

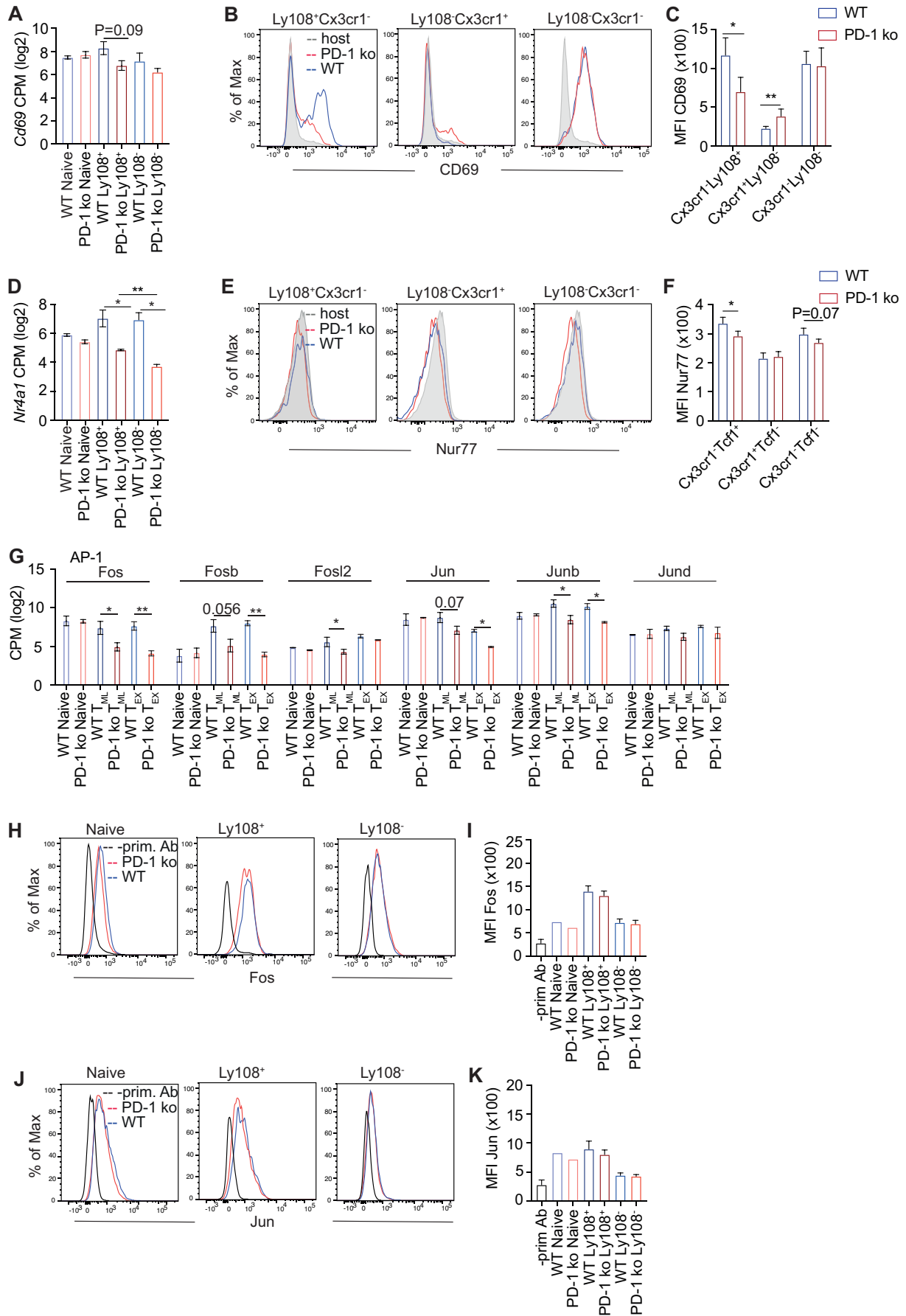


Figure 28: Chronic phase PD-1 ko T_{ML} cells show reduced TCR signalling.

A) Bar graph depicting *Cd69* expression in WT naïve, PD-1 ko naïve WT and PD-1 ko Ly108⁺ T_{ML} and WT and PD-1 ko Ly108⁺ T_{EX} cells, based on RNA-Seq analysis (Log2 counts per million (CPM)). **B)** Representative histograms

comparing CD69 expression by WT (blue) and PD-1 ko (red) Ly108⁺ Cx3cr1⁻, Ly108⁻Cx3cr1⁺ and Ly108⁻Cx3cr1⁻ populations compared to host (grey). **C**) Bar graphs show the MFI of CD69 staining on the different populations. **D**) Bar graph depicting *Nr4a1* expression (encoding Nur77) by WT naïve, PD-1 ko naïve WT and PD-1 ko Ly108⁺ T_{ML} and WT and PD-1 ko Ly108⁻ T_{EX} cells, based on RNA-Seq analysis (Log2 counts per million (CPM)). **E**) Representative histograms comparing Nur77 expression by WT (blue) and PD-1 ko (red) Ly108⁺Cx3cr1⁻, Ly108⁻Cx3cr1⁺ and Ly108⁻Cx3cr1⁻ populations compared to host (grey). **F**) Bar graph shows the MFI of Nur77 staining on the different populations. **G**) Expression of AP-1 family genes in the WT and PD-1 ko cells based on RNA-Seq analysis (CPM; log2). **H,J**) Representative histograms depict **(G)** Fos or **(J)** Jun expression in naïve, Ly108⁺ or Ly108⁻ WT and PD-1 ko P14 cells. (black: -prim. Ab, blue: WT, red: PD-1 ko) **I, K**) Bar graphs depict the **(I)** MFI of Fos or **(K)** MFI of Jun in the indicated populations.

A,D,G) Data are derived from two replicates per population. **B-C,E-F**) Data are representative of 2 experiments with n=4-5 replicates per group. Bar graphs show the mean percentage (±SD). Two-tailed t-test was performed to determine significant differences between two comparisons (*p<0.05, **p<0.01, ***p<0.001, ns=not significant p>0.5). One-way ANOVA was performed to determine significant differences between more than two groups (*p<0.05, **p<0.01, ***p<0.001, ns=not significant p>0.5).

G) Statistics are based on Two-Way ANOVA with Tukey's multiple comparison corrections. (*p<0.05, **p<0.01, ***p<0.001, ns=not significant p>0.5).

I,K) Bar graphs show the mean percentage (±SD). Two-tailed t-test was performed to determine significant differences between two comparisons (WT vs PD-1) (*p<0.05, **p<0.01, ***p<0.001, ns=not significant p>0.5). Data are derived from one experiment with n=3-5 mice per group.

TCR downstream targets include *Nr4a1* (encoding Nur77)^{164,165} and CD69¹⁶⁶. Based on RNA-Seq, *Nr4a1* was significantly reduced in PD-1 ko T_{ML} cells, while CD69 expression was reduced although not significantly in PD-1 ko versus WT T_{ML} cells (**Fig. 28 A,D**). Both Nur77 and CD69 protein expression were significantly reduced in PD-1 ko T_{ML} cells (**Fig. 28 C,F**), confirming that TCR downstream signalling was impaired in PD-1 ko T_{ML} cells.

3.14 PD-1 deficiency impairs downstream TCR signalling

To begin to address the basis for the impaired TCR downstream signalling in the absence of PD-1, we first investigated the expression of TCR components. The RNA-Seq data revealed no or only minor differences in the expression of CD3 components (Cd3g,d,e,z), Lck or Zap70 in WT and PD-1 ko T_{ML} cells (not shown). We similarly analysed the expression of NFAT, NF-κB, AP-1 pathway components. The expression levels of NFAT (*Nfac1*, *Nfatc2*) and NF-κB (*Nfkb1*, *Rela*) pathway components had only minor differences between WT and PD-1 ko T_{ML} cells (not shown). However, the expression of multiple AP-1 factors (Fos, Fosb, Fosl2, Jun, Junb, Jund) was reduced in PD-1 ko T_{ML} cells compared to WT (**Fig. 28 G**). However, Fos or Jun protein levels were not different between PD-1 ko and WT T_{ML} cells (**Fig. 28 H-K**). Thus, the expression levels of NFAT, NF-κB and AP-1 did not account for reduced TCR signalling in the absence of PD-1. Therefore, experiments addressing e.g. the activation or nuclear translocation of the above factors will be needed to further address this question.

3.15 Reduced expression of the stemness genes *Myb* and *Klf4* in PD-1 ko T_{ML}

To address reduced stemness we first monitored the expression of transcription factors (TFs) involved in the formation and function of memory or T_{ML} cells. No major differences were observed in the expression of *Tcf7*⁵⁷, *Id3*¹⁶⁷, *Bcl6*^{168,169}, *Bach2*¹⁷⁰ or *Tox*¹¹⁵ in PD-1 ko T_{ML} or PD-L1 treated WT T_{ML} cells compared to WT T_{ML} cells (**Fig. 29 A**). However, another gene

involved in memory formation, *Myb*⁶⁰, was found to be reduced in PD-1 ko T_{ML} or PD-L1 treated WT T_{ML} cells compared to WT T_{ML} cells (**Fig. 29 B**).

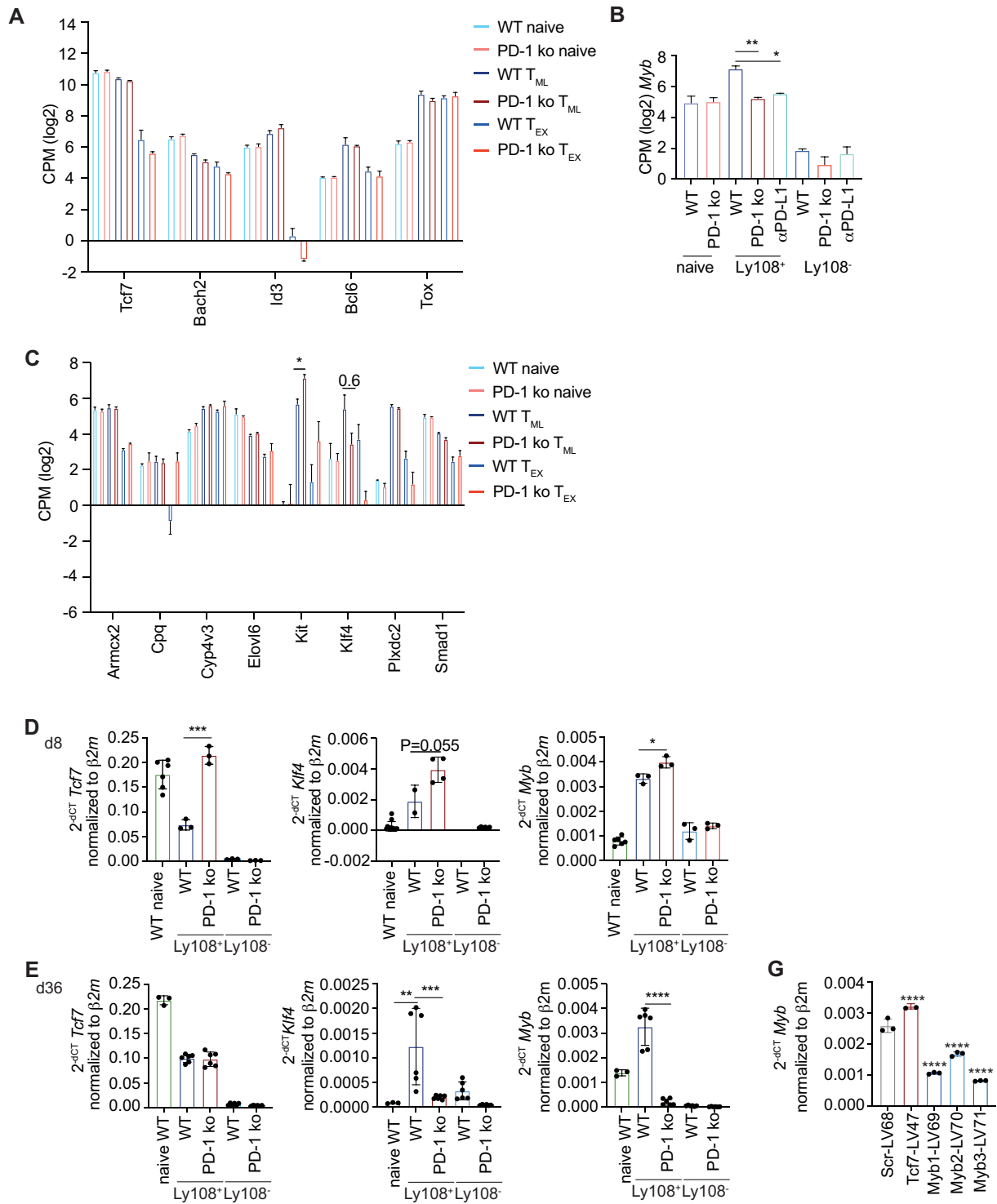


Figure 29: Reduced *Myb* and *Klf4* expression in chronic phase PD-1 ko T_{ML} cells.

The indicated populations of cells were analysed for **A**) Expression of *Tcf7*, *Bach*, *Id3*, *Bcl6* and *Tox* **B**) *Myb* or **C**) *Tcf1*-dependent stemness genes based on RNA-Seq analysis. **D-E**) Expression *Tcf7*, *Klf4* and *Myb* in the indicated populations of cells at **(D)** d8 or **(E)** d36 post infection using RT-qPCR analysis. Bar graphs at d8 depict two samples for the naïve control and technical triplicates of one sample for WT and PD-1 ko Ly108⁺ and Ly108⁻ populations. Bar graphs for d36 depict technical triplicates of the combination of two individual samples. At d36 qPCR analysis was performed using the same RNA as for RNA-Seq analysis. **F**) *Myb* expression upon *in vitro* transduction of

CD8⁺ T cells with *Myb* shRNA. Cells were sorted to obtain transduced mCherry⁺ cells, and RT-qPCR analysis was used to determine *Myb* levels.

A,C) Two-way ANOVA was performed with Tukey's correction to determine significances (*p<0.05, **p<0.01, ***p<0.001, ns=not significant p>0.5) **B)** Statistics are based on One-way ANOVA with Tukey's multiple comparison corrections for each gene. (*p<0.05, **p<0.01, ***p<0.001, ns=not significant p>0.5). **C,D)** Bar graphs show the mean percentage (\pm SD). Two-tailed t-test was performed to determine significant differences between two comparisons (*p<0.05, **p<0.01, ***p<0.001, ns=not significant p>0.5). **E)** Data are representative of one experiment with biological duplicates and technical triplicates. Mean \pm SD are shown. Statistics are based on One-Way ANOVA, comparing the mean of each column to scr sh using uncorrected Fisher's LSD test (p<0.05, **p<0.01, ***p<0.001, ns=not significant p>0.5).

Reduced *Myb* expression in PD-1 ko T_{ML} cells at d36 p.i. was confirmed by RT-qPCR (**Fig. 29 E**). In contrast, WT and PD-1 ko T_{ML} cells comparably expressed *Myb* at d8 p.i. (**Fig. 29 D**). *Myb*, which is part of the PID_AP1 pathway signature, is necessary for the formation and function of conventional memory CD8⁺ T cells arising in response to acute resolved infection⁶⁰. Additionally, an earlier *in vitro* study showed that *Myb* is induced upon TCR stimulation and thus suggests that *Myb* is a downstream target of the TCR¹⁷¹. In addition, this group recently identified a small set of Tcf1-dependent genes that ensure the stemness of central memory precursors arising in response to acute resolved infection⁵⁵. We thus assessed whether the expression of these stemness genes was reduced in PD-1 ko T_{ML} cells (**Fig. 29 C**). This identified reduced expression of *Klf4* in PD-1 ko T_{ML} cells (**Fig. 29 D,E**). *Klf4* is one of the Yamanaka factors whose over-expression can induce pluripotency in human and mouse somatic cells¹⁷². We confirmed reduced *Klf4* expression in PD-1 ko T_{ML} cells at d36 p.i. by RT-qPCR (**Fig. 29 E**). In contrast, at d8 p.i. PD-1 ko T_{ML} cells expressed overexpressed *Klf4* compared to WT (**Fig. 29 D**). Interestingly, *Klf4* is part of the Hallmark TNF- α signalling via NF- κ B pathway. However, *Klf4* is downregulated at least during the initial phase following T cell activation¹⁷³. These data identified *Myb* and *Klf4* as 2 potential stemness genes whose expression was reduced in PD-1 ko T_{ML} cells during the chronic phase of the infection, in line with reduced stemness. In order to investigate their role in T_{ML} stemness, we used lentivirus (LVs) based short-hairpin (sh)RNA constructs to knock down the expression of *Klf4* and *Myb*. As a positive control we included a *Tcf7* shRNA construct and a scrambled (scr) shRNA construct served as a negative control. These constructs also included mCherry to track transduced cells.

Tcf7^{GFP-diphtheria toxin receptor (DTR)} P14 cells (CD45.2⁺, termed *Tcf7*^{GFP-DTR}) were activated *in vitro* and transduced with LV. The transduction and knock down efficiency of the LV constructs was ascertained after 48h of *in vitro* culture. To this end, mCherry⁺ cells were flow sorted and subjected to RT-qPCR analysis. Compared to a scr control construct all three shRNA constructs reduced *Myb* expression, with LV1169 and LV1171 being more effective (**Fig. 29 F**). *Klf4* and *Tcf7* shRNA constructs had been validated before by Pais *et al.*⁵⁵. Of note, in each experiment the transduction efficiency with the scr control, the *Klf4* and *Myb* shRNA constructs *in vitro* were comparable (**Fig. 30 A**).

Next, 24h after transduction, bulk *Tcf7*^{GFP-DTR} P14 (CD45.2⁺) cells (10-30% transduced) (**Fig. 30 A**) were transferred into V β 5 (CD45.1⁺) mice, which had been infected with LCMV cl13 one day before. The impact of the different shRNAs was analysed at d8 p.i. and compared to the scr control construct. *Tcf7* shRNA strongly reduced the abundance of transduced P14 cells (**Fig. 30 B,C**). This was explained by a reduced presence of *Tcf7*^{GFP-DTR+} (T_{ML}) cells and consequently a reduced production of *Tcf7*^{GFP-DTR-} (T_{EX}) cells (**Fig. 30 D,E**). These data confirmed the deficient generation of T_{ML} cells previously observed using *Tcf7* ko cells⁵⁷ and validated our shRNA approach to study the formation of T_{ML} cells.

Myb sh similarly resulted in a reduced abundance of transduced P14 cells at d8 p.i. (**Fig. 30 C**). While *Tcf7*^{GFP-DTR+} (T_{ML}) were present at the expected frequency, *Tcf7*^{GFP-DTR-} (T_{EX}) cells were

strongly reduced (**Fig. 30 D,E**). These data suggest that normal *Myb* levels in T_{ML} cells are required for the generation of differentiated T_{EX} cells.

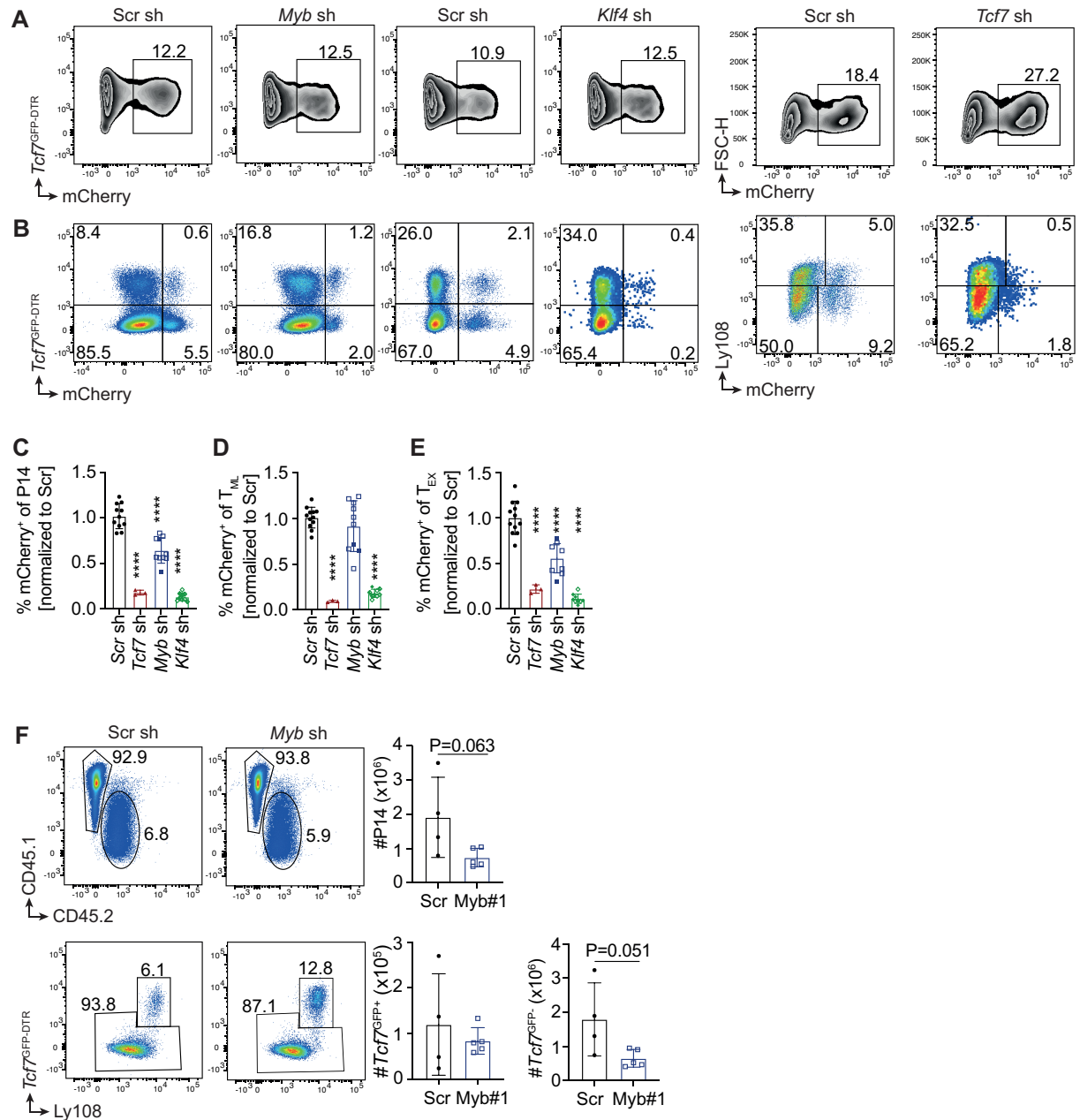


Figure 30: Reduction of *Klf4* and *Myb* expression impairs stemness of P14 cells.

Tcf7^{GFP-diphtheria toxin (DTR)} or WT P14 cells were activated *in vitro* and transduced with control (scr), *Myb* shRNA, *Klf4* shRNA or *Tcf7* shRNA constructs. Cells were cultured O/N and then transferred into Vβ5 mice that had been infected with LCMV cl13 one day earlier. Some cells were kept in culture to analyse transduction efficiency *in vitro*. **A**) P14 cells cultured *in vitro* were analysed for mCherry expression to assess the transduction efficiency *in vitro*. **B**) Splenic P14 cells were analysed on d8 p.i. for the abundance of mCherry⁺ expressing or lacking *Tcf7*^{GFP-DTR} or Ly108. **C**) Fraction of mCherry⁺ P14 cells *Tcf7* shRNA, *Myb* shRNA or *Klf4* shRNA was normalized to that expressing the scrambled (scr) control RNA **(D, E)** Same as C but assessing **(D)** *Tcf7*^{GFP-DTR} or Ly108⁺ T_{ML} cells or **(E)** *Tcf7*^{GFP-DTR} or Ly108⁺ T_{EX} cells. **F**) Splenic mCherry⁺*Tcf7*^{GFP-DTR} P14 cells (CD45.2⁺), expressing scr control or *Myb* shRNA, were flow sorted and transferred into new hosts (Vβ5; CD45.1⁺) which were then infected with LCMV Arm and analysed 8 days later. Representative dot plots depict total P14 cells (CD45.2⁺) and the T_{ML} and T_{EX} populations (*Tcf7*^{GFP-DTR} Ly108⁺ and *Tcf7*^{GFP-DTR} Ly108⁻, respectively). Bar graphs show the number of P14, *Tcf7*^{GFP-DTR} T_{ML} and *Tcf7*^{GFP-DTR} T_{EX} cells at d8+8.

C-F) The data are representative of two independent experiments with n=3-4 mice. Mean \pm SD are shown. Statistics are based on One-Way ANOVA comparing the mean of each column to scr sh using uncorrected Fisher's LSD test ($p < 0.05$, $**p < 0.01$, $***p < 0.001$, ns=not significant $p > 0.5$). **B,I)** Bar graphs show the mean percentage (\pm SD). Two-tailed t-test was performed to determine significant differences between two comparisons ($*p < 0.05$, $**p < 0.01$, $***p < 0.001$, ns=not significant $p > 0.5$).

Klf4 sh also strongly reduced the abundance of transduced P14 cells (**Fig. 30 C**). The presence of $Tcf7^{GFP-DTR+}$ (T_{ML}) and consequently the abundance of $Tcf7^{GFP-DTR-}$ (T_{EX}) were both strongly reduced (**Fig. 30 D,E**). Similar to *Tcf7*, normal *Klf4* expression was thus essential for the generation of T_{ML} cells. *Klf4* and *Myb* thus played essential roles for the generation and differentiation of T_{ML} cells, respectively.

The very low numbers of T_{ML} cells precluded a direct analysis of T_{ML} stemness when *Tcf7* or *Klf4* expression was reduced. In order to investigate the effect of *Myb* sh-RNA expression on stemness, d8 $Tcf7^{GFP-DTR+}mCherry^+$ ($CD45.2^+$) cells were flow sorted and transferred into new $V\beta 5$ hosts ($CD45.1^+$) that were then infected with LCMV Arm. *Myb* shRNA reduced the abundance of secondary P14 cells compared to scr control sh-RNA (**Fig. 30 F**). While the generation of secondary $Tcf7^{DTR-GFP+}$ cells was not different, *Myb* shRNA reduced the generation of secondary $Tcf7^{DTR-GFP-}$ cells (**Fig. 30 F**). Thus, reduced *Myb* expression impacted T_{ML} stemness by reducing the production of differentiated progeny.

These data suggested that reduced expression of *Klf4* and *Myb* during the chronic phase of the infection impaired the stemness of PD-1 ko T_{ML} cells. These data thus provide an explanation for the reduced stemness of PD-1 ko T_{ML} cells.

4. Discussion

The long-term CD8⁺ T cell response to chronic viral infection is sustained by a subpopulation of memory-like CD8⁺ T cells (T_{ML}) that are identified by the expression of PD-1 together with Tcf1. T_{ML} cells possess stem-like properties, i.e. they have the ability to expand, and self-renew or differentiate into cells with cytolytic function that have limited proliferation capacity. The aim of this thesis was to address the role of PD-1 for the generation, maintenance and function of T_{ML} cells.

Comparing LCMV-specific CD8⁺ T cells that lacked PD-1 expression (PD-1 ko) to WT CD8⁺ T cells revealed a significantly higher initial expansion of both PD-1 ko T_{ML} and T_{EX} cells. While the abundance of PD-1 ko T_{ML} cells remained stable until the chronic phase of infection (d28), the abundance of PD-1 ko T_{EX} cells started to decrease slightly. Both acute and chronic phase PD-1 ko and WT T_{ML} cells were phenotypically and functionally remarkably similar, while both acute and chronic phase PD-1 ko T_{EX} cells were more exhausted than their WT counterparts. This was true in both, individual and mixed transfer models, excluding the possibility that this was due to a distinct infectious or inflammatory environment. Most importantly, the stemness of acute phase PD-1 ko T_{ML} cells was increased compared to WT, while that of chronic phase PD-1 ko T_{ML} cells was decreased. Moreover, the transient interruption of the PD-1 signalling, using PD-L1 blockade, reduced the stemness of T_{ML}.

Gene expression analyses of WT, PD-1 ko and anti-PD-L1 treated T_{ML} and T_{EX} cells revealed major reductions in the expression of genes that are part of the NFAT, AP-1 or NF-κB pathways and thus downstream of the TCR. In particular, NF-κB target genes were reduced in all of the above conditions. We further analysed differentially expressed genes for candidate stemness genes and found that PD-1 ko T_{ML} cells expressed less *Myb* and *Klf4*. Interestingly, *Myb* and *Klf4* are part of the AP-1 and NFκB pathway genes, respectively, and are thus likely downstream of the TCR. Reducing the expression of *Myb* and *Klf4* in WT T_{ML} cells, using and sh RNA approach, impaired the differentiation of T_{ML} cells into T_{EX} cells and prevented the generation of T_{ML} cells, respectively. Thus, reduced *Myb* and *Klf4* expression explained at least in part the reduced stemness of chronic phase PD-1 ko T_{ML} cells.

We find that continuous PD-1 engagement during the chronic phase of the infection is necessary to preserve the stemness of T_{ML} cells and thus to ensure a sustained immune response to chronic viral infection. We propose that PD-1 serves as a physiological negative feedback mechanism to prevent overstimulation of T_{ML} cells during the chronic phase of infection. In the absence of PD-1, when overstimulation occurs over a prolonged period of time, CD8⁺ T cells adapt by reducing the transduction of signals via the TCR.

4.1 Phenotypic changes in T_{ML} and T_{EX} cells lacking PD-1

Comparing LCMV-specific CD8⁺ T cells that lacked PD-1 expression to WT CD8⁺ T cells, revealed significantly higher initial expansion of both PD-1 ko T_{ML} and T_{EX} cells (5-fold) (**Fig. 17**). The increased abundance of PD-1 ko T_{ML} and T_{EX} cells was still evident at the chronic phase of the infection (**Fig. 11**). However, the fraction of PD-1 ko T_{EX} cells was only 2-fold higher, whereas the fraction of PD-1 ko T_{ML} cells was still 4-fold higher than WT. Thus, PD-1 ko T_{ML} cells appeared to initially expand more than WT but were maintained slightly less efficiently. Either their differentiation into T_{EX} cells occurred less efficiently or PD-1 ko T_{EX} cells were less well maintained. The increased abundance of PD-1 ko T_{ML} cells seems to be due the increased expansion during the acute phase of the infection.

Table 1: Phenotypic comparison of PD-1 ko vs WT and of anti-PD-L1 treated vs isotype treated T_{ML} and T_{EX} cells in individual and mixed transfer models.

individual transfer	Acute phase (d8)		Chronic phase (d28)		Chronic phase (d41)	
	PD-1 ko vs WT		PD-1 ko vs WT		anti-PD-L1 vs isotype	
	T _{ML}	T _{EX}	T _{ML}	T _{EX}	T _{ML}	T _{EX}
CD62L	↓	/	↓	/	↓	/
CD127	~	~	↑	/	~	/
KLRG1	/	~	/	↓	/	↓
GzmB	/	↓	/	↓	/	↓
PD-1	/	/	/	/	↑	↑
Lag3	↑	~	~	↑	~	~
Tim3	/	~	/	↑	/	↑
IFN-γ	~	↓	~	↓	~	~
TNF-α	~	↓	~	↓	~	~
IL-2	~	/	~	/	↑	/
mixed transfer	PD-1 ko vs WT		PD-1 ko vs WT			
	T _{ML}	T _{EX}	T _{ML}	T _{EX}		
CD62L			↓	/	↑: higher expressed	
CD127			↓	/	↓: lower expressed	
KLRG1		↓	/	↓	~: similar expressed	
GzmB			/	↓	not expressed	
PD-1			/	/	not analysed	
Lag3	↑	↑	~	↑		
Tim3	/	~	/	↑		
IFN-γ			~	↓		
TNF-α			↓	↓		
IL-2			~	~		

The difference between WT and PD-1 ko cells was greater in mixed transfers than in the individual transfer. In mixed transfers we found a 30-fold and a 11-fold difference for T_{ML} and T_{EX} cells, respectively, while the corresponding differences in the individual transfers were 4-fold and 3.7-fold. While WT and PD-1 ko cells can maximally use the available space in individual transfers, in a mixed situation, PD-1 ko cells seemed to be considerably more competitive than WT cells at d28 p.i.. Previously published data comparing mixes of unfractionated WT and PD-1 ko P14 cells showed that the contribution of PD-1 ko P14 cells was reduced at d42 compared to d22 p.i.¹³⁸. This suggests that the contribution of PD-1 ko P14 cells will eventually decline, which is consistent with the reduced stemness of PD-1 ko T_{ML} cells at d28 p.i.

Even though, WT and PD-1 ko T_{ML} cells were phenotypically remarkably similar, we did observe some differences. For example, fewer PD-1 ko T_{ML} cells expressed CD62L, both in the acute and chronic phase of infection, both in the individual and the mixed transfer model. Also, transient PD-L1 blockade, resulted in reduced CD62L expression. No consistent changes were observed in the expression of CD127. Acute phase PD-1 ko T_{ML} cells (individual and mixed transfer) expressed increased levels of Lag3, which was no longer observed at the chronic phase of the infection. WT and PD-1 ko T_{ML} cells expressed similar cytokine levels, only anti-PD-L1 treatment increased IL-2 secretion by T_{ML} cells.

In comparison, more phenotypic differences were observed among T_{EX} cells. While acute phase PD-1 ko T_{EX} cells generally expressed similar levels of inhibitory receptors, chronic phase PD-1 ko T_{EX} cells expressed more Lag3 and Tim3. Further, acute phase PD-1 ko T_{EX} cells showed similar expression of KLRG1, but reduced expression of GzmB and cytokines (IFN-γ and TNF-α) in the individual transfers. During the chronic phase, KLRG1, GzmB and cytokine (IFN-γ and

TNF- α) expression was consistently reduced by PD-1 ko T_{EX} cells. Thus, while PD-1 ko T_{EX} cells appeared more exhausted than WT, in agreement with prior analysis of unfractionated CD8⁺ T cells (Odorizzi *et al.*¹³⁸), T_{ML} cells were comparable.

While PD-1 expression impairs TCR downstream signalling, Tim-3 expression initially enhances TCR downstream signalling and modulates the T cell response depending on signalling strength and timing¹⁷⁴. Even though Lag3 is highly expressed in chronic LCMV infection, its blockade does not improve the expansion of antigen-specific CD8⁺ T cells¹⁷⁵. However, in the absence of PD-1, Lag3 was shown to associate with the CD3 complex, thereby impairing T cell proliferation, cytokine production and calcium influx¹⁷⁶. Further, combined Lag3 and PD-L1 blockade improves antigen-specific CD8⁺ T cell expansion and decreases viral load compared to either therapy alone¹⁷⁷. Finally, CTLA4 deficiency or CTLA4 blockade does not impact the CD8⁺ T cell response to chronic LCMV infection^{78,178} and was therefore not analysed.

Recently, Hudson *et al.* found that T_{EX} cells can be further separated by their Cx3cr1 expression into a Cx3cr1⁺ “transitory” population and a Cx3cr1⁻ terminally exhausted population⁹⁸. When using this separation, we found that PD-1 ko P14 cells had a significantly smaller Ly108⁺Cx3cr1⁺ transitory but an expanded terminally exhausted Ly108⁺Cx3cr1⁻ population at the chronic but not the acute phase of the infection. This may account in part for the higher exhaustion and the reduced functionality of PD-1 ko T_{EX} cells.

4.2 Reduced stemness of PD-1 ko T_{ML} cells

Stemness defines the ability of antigen-specific memory CD8⁺ T cells to expand, self-renew and differentiate upon restimulation. This concept derives from memory cells that persist in the absence of antigen and then re-expand upon secondary antigen encounter. However, it can also be applied to cells responding to chronic infection. In this cases, relevant cells are sorted and re-transferred into new hosts that are then infected with a LCMV strain causing acute resolved infection.

PD-1 ko T_{ML} cells had an impaired stemness, compared to WT during the chronic phase of the infection. Chronic phase PD-1 ko T_{ML} cells derived from individual transfers suffered from impaired self-renewal rather than reduced expansion/differentiation (**Fig. 13**). On the other hand, self-renewal and expansion/differentiation of chronic phase PD-1 ko T_{ML} cells derived from mixed transfers was comparably reduced. Therefore, the presence of responding WT P14 cells during chronic infection may impact the self-renewal or differentiation of PD-1 ko T_{ML} cells. Further, it was possible that we underestimated the difference between WT and PD-1 ko cells during the recall response as PD-1 inhibited only the WT cells. Indeed PD-1 blockade during the recall response further improved the expansion of WT T_{ML} cells derived from the chronic phase of infection (**Fig. 16**). This strengthened the conclusion that lack of PD-1 impairs the stemness of T_{ML} cells and consequently that PD-1 expression preserves the stemness of chronic phase T_{ML} cells.

Contrary to chronic phase PD-1 ko T_{ML} cells, acute phase PD-1 ko T_{ML} cells had a greater stemness than WT T_{ML} cells in individual (**Fig. 19**) and a comparable stemness in mixed transfer (**Fig. 21**). When PD-1 was blocked during the mixed recall response the stemness of WT T_{ML} cells was only slightly better than that of PD-1 ko T_{ML} cells (**Fig. 21**).

Together, these findings suggested that PD-1 ko T_{ML} cells become functionally compromised during the chronic phase of the infection. Therefore, PD-1 expression seemed to protect T_{ML} cells from overstimulation and this might allow them to sustain the CD8⁺ T cell response during

chronic infections. This likely explains the diminished population of PD-1 ko compared to WT P14 cells at a very late stage of chronic infection (d300 p.i.)¹³⁸.

Classical work showed that PD-1 blockade resulted in CD8⁺ T cell expansion and increased virus control⁷⁸. The proliferative burst in response to PD-1 blockade depends on the presence of T_{ML} cells, which yield an expanded pool of T_{EX} cells⁵⁷. Based on the above data, we thus analysed whether repeated PD-1 blockade would impact the stemness of T_{ML} cells (**Fig. 22**).

After 4 treatment cycles with anti-PD-L1 Ab, mice harboured 6-fold more virus-specific T_{ML} cells and >2.6-fold more T_{EX} cells compared to control-treated mice, confirming the efficacy of PD-1 blockade. Anti-PD-L1- and control-treated T_{ML} cells were phenotypically similar and expressed similar percentages of effector cytokines 4 days after the last treatment cycle. Only IL-2 expression was higher upon immune checkpoint blockade. Increased cytokine production by Barber *et al.* was detected at their last day of treatment⁷⁸. Thus, the checkpoint blockade had the expected effects on virus-specific CD8⁺ T cells and differences to other studies are likely explained by testing the cells when they had returned to steady state. Indeed, Pauken *et al.*, have shown that PD-1 blockade has only a temporary effect on virus-specific CD8⁺ T cells and that the epigenetic state of these cells did not change¹³³.

We then tested the stemness of T_{ML} cells derived from anti-PD-L1- and control-treated mice using recall stimulation. This showed that T_{ML} cells derived from anti-PD-L1-treated mice had reduced stemness, whereby self-renewal was particularly affected (**Fig. 23**). These data suggested that a temporary disruption of the inhibitory PD1-PD-L1 interaction was sufficient to reduce the T_{ML} stemness.

4.3 Cycling, survival and metabolism of T_{ML} cells lacking PD-1

In order to define how the absence of PD-1 protein impacts the stemness of T_{ML} cells, we investigated their cycling, survival and metabolic properties. WT and PD-1 ko T_{ML} cells had similar cell cycling during the chronic phase of the infection, but that of acute phase PD-1 ko T_{ML} cells was increased (**Fig. 24**). This suggested that increased expansion of PD-1 ko T_{ML} cells during the acute phase of the infection was based on increased cycling.

Acute phase PD-1 ko T_{EX} cells had a tendency to increased cycling, while the fraction of cycling chronic phase PD-1 ko T_{EX} cells was reduced compared to WT. This is in line with Odorizzi *et al.* who showed decreased proliferation of unfractionated PD-1 ko cells at the chronic phase (d42 p.i.)¹³⁸.

We further compared the survival of PD-1 ko and WT T_{ML} cells. We observed that chronic phase PD-1 ko T_{ML} cells were significantly more prone to undergo apoptosis than WT. We did not observe any difference among chronic phase T_{EX} cells or acute phase populations (**Fig. 25**). Thus, decreased survival correlated with the reduced stemness of chronic phase PD-1 ko T_{ML} cells. Further investigation of the apoptosis pathway will be necessary to better understand the correlation of PD-1 deficiency and increased apoptosis.

Chronically stimulated CD8⁺ T cells have an increased cellular need for glycolysis and OXPHOS during chronic infection, compared to acutely stimulated effector cells¹²¹. However, despite increased mTOR expression chronically stimulated CD8⁺ T cells fail to answer their metabolic demand, therefore this metabolic dysregulation induces mitochondrial depolarization and higher ROS production¹²¹. However, chronically infected acute phase PD-1 ko T_{EX} cells, have further increased glucose uptake and glycolytic activity compared to WT, and thereby resemble T_{EFF} cells from LCMV Armstrong infection¹²¹. This indicates a regulatory role for PD-1

in metabolism, glycolysis and mitochondrial function of CD8⁺ T cells early during chronic infection¹²¹. However, these experiments did not separate T_{ML} and T_{EX} cells.

We found that WT T_{ML} cells have higher mitochondrial mass than WT T_{EX} cells. Further, acute phase PD-1 ko and WT T_{ML} cells had a similar mitochondrial mass and membrane potential. However, chronic phase PD-1 ko T_{ML} cells had a higher mitochondrial mass and membrane potential than WT (**Fig. 26 A-F**). On the other hand, the mitochondrial mass and potential of PD-1 ko and WT T_{EX} cells was not different.

While this work was in progress, metabolic differences between T_{ML} and T_{EX} cells were reported¹⁷⁹. T_{ML} cells had a high mitochondrial content while mitochondria of T_{EX} cells were largely depolarised and underwent metabolic exhaustion over time¹⁷⁹.

Activated T cells undergo a metabolic switch towards glycolysis, which leads to increased production of reactive oxygen species (ROS). One producer of large amounts of ROS are mitochondria during glycolysis and fatty acid oxidation (FAO), others are the transmembrane proteins NOX that transport electrons from NAD(P)H to oxygen and generate superoxide anion¹⁸⁰. In agreement with increased mitochondrial function, total ROS levels were significantly increased in PD-1 ko compared to WT T_{ML} cells (**Fig. 26 G-J**). Additional experiments will be needed to show whether the increased ROS in PD-1 ko T_{ML} cells indeed derives from mitochondria. Even though ROS is necessary for adequate cellular functions, excessive ROS leads to impaired cellular functions and even induction of apoptosis^{180,181}. It is thus tempting to speculate that PD-1 ko T_{ML} cells have excessive ROS levels, which impairs their function and, which could explain in part the increased apoptosis of these cells.

4.4 Transcriptome of T_{ML} cells lacking PD-1 or after PD-1 blockade

To further investigate the basis for reduced stemness, WT, PD-1 ko and anti-PD-L1 treated T_{ML} and T_{EX} cells were subjected to RNA-Seq analysis. The T_{ML} populations from all these conditions were distinct from their respective T_{EX} and similar to each other, indicating that PD-1 deficiency or blockade did not lead to massive transcriptome changes. Notwithstanding, >200 genes were differentially expressed by any pairwise comparison of the T_{ML} populations generated in the three different conditions. A corresponding comparison of T_{EX} cells revealed larger differences i.e >450 genes in any pairwise comparison.

Pathway analysis using GSEA revealed significant differences in selected signalling pathways. In particular, PD-1 ko T_{ML} cells had reduced overlaps with “HALLMARK_TNFA_SIGNALING_VIA_NFKB”, the PID_AP-1_pathway, PID_NFAT_TFPATHWAY, and the PID_CD8_TCR_DOWNSTREAM_PATHWAY signatures compared to WT T_{ML} (adj. p value < 0.05). A reduced overlap with the “HALLMARK_TNFA_SIGNALING_VIA_NFKB was also observed among anti-PD-L1 treated WT compared to untreated WT T_{ML} cells. The reanalysis of published gene expression data¹¹² revealed that the HALLMARK_TNFA_SIGNALING_VIA_NFKB is a major pathway triggered by TCR signalling. Collectively, pathway analysis thus suggested that PD-1 ko T_{ML} cells suffered from reduced NFAT, AP-1 and NF-κB signalling downstream of the TCR, while anti-PD-L1 treated T_{ML} cells suffered from reduced NF-κB signalling. Reduced TCR signalling was confirmed based on the reduced expression of Nur77 and CD69 in PD-1 ko T_{ML} cells.

AP-1 factors are expressed based on TCR signals but AP-1 complex formation (heterodimers of Fos and Jun proteins form) is chiefly dependent on co-stimulatory signals, and these are needed for the expression of IL-2 and effector molecules^{182,183}. Original RNA-Seq data found reduced expression of AP-1 factors (Fos and Jun family genes) in exhausted compared to

memory-like T cells⁵⁷. We found that also PD-1 ko T_{ML} cells had a reduced expression of AP-1 factors compared to WT T_{ML} cells. However, when we verified the Fos and Jun protein levels we did not find significant differences between PD-1 ko and WT T_{ML} cells (**Fig. 28 H-K**). Thus, in addition to transcriptional regulation (which seemed different in PD-1 ko and WT T_{ML}), posttranscriptional mechanisms seemed to affect Fos/Jun protein levels (which seemed similar in PD-1 ko and WT T_{ML}).

Previous studies correlated CD8⁺ T cell exhaustion with impaired AP-1 function. Martinez *et al.* found that a NFAT1 construct that cannot interact with AP-1 (partnerless NFAT) promotes exhaustion of activated CD8⁺ T cells based on the upregulation of inhibitory receptors and the reduction of cytokine expression¹⁰⁸. Additional work has expanded this observation, showing that partnerless NFAT induces TOX and NR4A family proteins that contribute to the expression of inhibitory receptors and the inhibition of effector functions¹¹⁰. Based on the reduced gene expression of AP-1 family genes in exhausted cells it was proposed that reduced AP-1 leads to excess NFAT and thus partnerless NFAT signalling. As AP-1 proteins appear normal, it should thus be verified whether AP-1 function is indeed reduced in exhausted cells.

Interestingly, Agnellini *et al.* found that exhausted CD8⁺ T cells have a defect in the nuclear translocation of NFAT. On the other hand, Ca²⁺ influx, NF-κB translocation or ERK phosphorylation were normal¹⁰⁹. Therefore, it will be important to address whether the nuclear translocation of AP-1 complexes is normal in T_{EX} and T_{ML} cells or if the phenotype observed could be linked to an impaired cellular localisation of these proteins. Further, it will be of interest whether NFAT and AP-1 function is further reduced in PD-1 ko T_{ML} cells. Finally, based on the reduced expression of NF-κB targets, it will be of great interest to address whether NF-κB function is impaired in PD-1 ko T_{ML} cells.

4.5 Reduced *Myb*- and *Klf4* expression explains the impaired stemness of PD-1 ko T_{ML} cells

To find an explanation for the reduced stemness of PD-1 ko T_{ML} cells, we analysed the expression of TFs involved in the formation and function of conventional memory cells or of T_{ML} cells. This did not reveal significant differences in the expression of *Tcf7*, *Id3*, *Bcl6* or *Bach2* in PD-1ko vs WT T_{ML} cells. However, we noted a reduced expression of *Myb* in PD-1 ko vs WT T_{ML} cells, a gene described for its role in restraining terminal differentiation of CD8⁺ T cells and required for central memory formation⁶⁰. We also addressed whether Tcf1-dependent CD8 stemness genes, recently described by Pais *et al.*⁵⁵, were expressed normally in PD-1ko T_{ML} cells. *Klf4*, one of the four Yamanaka factors whose overexpression can convert mouse fibroblasts into pluripotent stem cells¹⁷², is part of the Tcf1 dependent stemness-gene pool⁵⁵. We first addressed whether *Myb* and *Klf4* could be linked to impaired TCR signalling. Indeed, *Myb* is part of PID_AP1 pathway. Further, *Myb* expression is induced by the engagement of the TCR on activated T lymphocytes¹⁷¹. Indeed, preliminary experiments using *in vitro* stimulation of naive CD8⁺ T cells with anti-CD3/CD28 increased *Myb* mRNA expression (data not shown). *Klf4* was found to be part of the HALLMARK_TNFA_SIGNALING_VIA_NFKB and may thus also be downstream of the TCR. However, *Klf4* expression was decreased shortly after TCR activation¹⁷³. Even though there is some evidence for a connection between TCR stimulation and *Myb* and *Klf4* expression, further experiments are needed to establish a more direct link.

We then tested whether reduced expression of *Myb* or *Klf4* reproduced the phenotype of PD-1 ko T_{ML} cells. Therefore, we transduced virus-specific CD8⁺ T cells with shRNA constructs to *Tcf7*, *Myb* or *Klf4* prior to transfer into mice and chronic LCMV infection. As expected, based

on the analysis of virus-specific *Tcf7* ko CD8⁺ T cells, *Tcf7* knock down impaired the formation of T_{ML} cells. On the other hand, *Myb* knock down did not alter formation of the T_{ML} population but reduced their differentiation into T_{EX} (Fig. 30 D). Further, recall stimulation of T_{ML} cells revealed that *Myb* knock down did not impact the self-renewal of T_{ML} cells but again reduced their differentiation into T_{EX} cells. Thus, normal *Myb* levels played a role for T_{ML} stemness, ensuring normal differentiation into T_{EX} cells. Chen *et al.* have enforced *Myb* expression in virus specific CD8⁺ T cells responding to chronic viral infection⁶². They found that enforced *Myb* expression expanded T_{ML} cells and also reduced the formation of T_{EX} cells. Together the data suggest that *Myb* levels play an important role for the self-renewal versus differentiation of T_{ML} cells. Indeed, both increased and reduced *Myb* levels seem to reduce T_{ML} cells differentiation. Irrespectively, reduced *Myb* levels can thus account for the observation that chronic phase PD-1 ko T_{ML} cells have a reduced propensity to generate transitory exhausted cells.

Klf4 knock down severely impaired the generation of T_{ML} and consequently of T_{EX} cells (Fig. 30 C-E). The absence of T_{ML} cells prevented us from directly testing the stemness of *Klf4* knock down T_{ML} cells. Notwithstanding the data show that normal *Klf4* expression is essential for the self-renewal (generation and/or maintenance) of T_{ML} cells. Thus, reduced *Klf4* levels can explain the reduced self-renewal of chronic phase PD-1 ko T_{ML} cells.

These results are in line with the reduced stemness of *Klf4* knock down central memory precursors responding to in acute LCMV infection⁵⁵. Conversely, it was shown that *Klf4* ko CD8⁺ T cells have an improved ability to form memory in response to *Listeria monocytogenes* (Lm) infection. While the recall response was also increased, the increase seemed to correspond to the increased abundance of *Klf4* ko memory CD8⁺ T cells and was not tested on a per cell basis¹⁸⁴. Differences between *Listeria monocytogenes* and acute LCMV infections, such as the dependence of CD8⁺ differentiation on IL-12 and type I IFN signals, respectively, may explain this discrepancy. Despite some caveats, we were able to show that reduced *Klf4* and *Myb* expression are detrimental to the normal self-renewal and differentiation of T_{ML} cells. Thereby these findings can account for the altered stemness of PD-1 ko T_{ML} cells.

Proposed Model:

PD-1 is a central inhibitory receptor negatively regulating CD8⁺ T cell effector function in chronic viral infection, but the role of PD-1 in modulating the function of the memory-like subset has not been defined. To address this question, we compared the phenotypic and the function of wild-type (WT) and PD-1 deficient (PD-1 ko) T_{ML} cells during chronic LCMV infection. PD-1 ko T_{ML} cell were significantly more abundant compared to WT T_{ML} cells both in the acute and the chronic phase of infection. Even though WT and PD-1 ko T_{ML} cells had similar phenotypical and functional characteristics, PD-1 ko T_{ML} cells present at the chronic phase of infection had reduced stemness (recall expansion, differentiation and self-renewal) compared to WT cells. This seemed to be acquired, since PD-1 ko and T_{ML} cells obtained from the acute phase of the infection had comparable stemness. Based on transcriptome analysis we find that transcriptional targets downstream of the TCR are reduced in PD-1 ko T_{ML} cells. We thus propose that PD-1 serves as a physiological negative feedback mechanism to prevent overstimulation of T_{ML} cells during chronic phase of infection. If overstimulation occurs over prolonged periods of time, CD8⁺ T cells respond by reducing the transduction of signals via the TCR. This seems to reduce the maintenance of stemness genes such as *Myb* and *Klf4*. The mechanism underlying the reduced transduction of signals via the TCR remains to be elucidated. In this context, it will be important to further analyse the activity of the key TCR signalling mediators NFAT, AP-1 and NF-κB in PD-1 ko T_{ML} cells. This would include the analysis

of their nuclear translocation in T_{ML} cells as well as the analysis of their transcriptional response following restimulation.

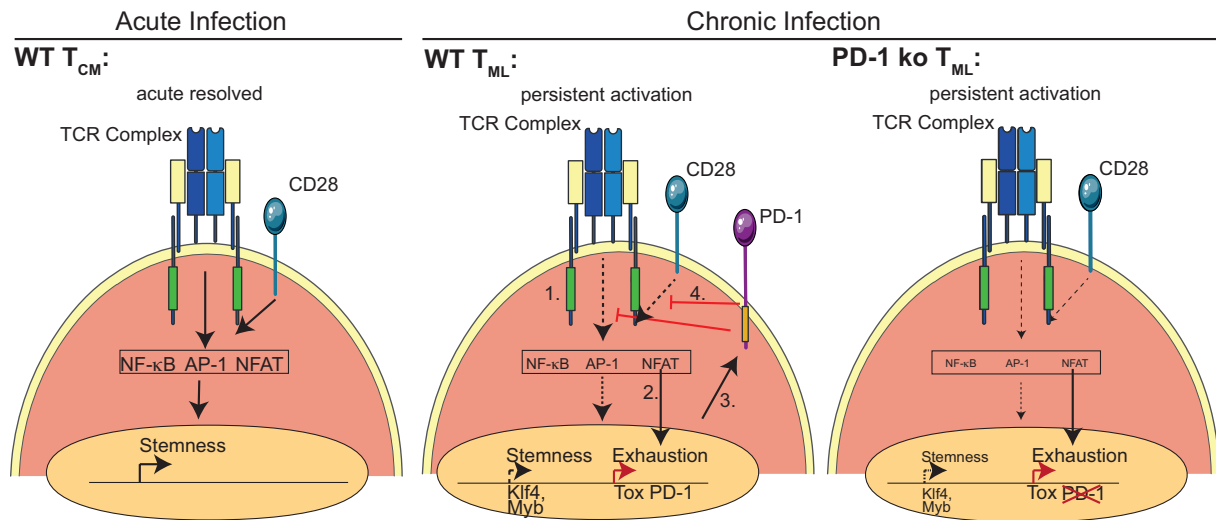


Figure 31: PD-1 serves as a negative feedback mechanism to prevent overstimulation of T_{ML} cells.

In chronic WT T_{ML} cells PD-1 inhibits TCR and CD28 downstream signalling compared to T_{CM} in acute infection, which results in reduced NFAT, AP-1 (Fos/Jun) and NF- κ B signalling and reduced expression of stemness genes *Myb* and *Klf4*. Persistent antigen-stimulation in chronic infection thereby drives constant PD-1 expression through NFAT signalling and leads to increased expression of inhibitory receptors (e.g. Lag3, PD-1) and exhaustion programs (e.g. *Tox*). PD-1 deficiency of chronic phase T_{ML} cells results in even further reduced TCR and CD28 downstream signalling and thereby impairs the expression of the stemness genes *Myb* and *Klf4* even further.

4.6 Perspective

Our data on chronic viral infection have implications for cancer immunotherapy. Blockade of PD-1 or PD-L1 is a key therapeutic approach to treat cancer, such as melanoma. This therapy approach is able to eradicate previously untreatable metastatic melanoma in a significant fraction of patients. Similar to chronic infection, the expansion of tumour-specific $CD8^+$ T cells in response to PD-1 blockade depends on the presence of T_{ML} cells. Ablation of T_{ML} cells precludes the proliferative burst, prevents the formation of an expanded pool of T_{EX} cells and impedes tumour control¹⁴³. Unfortunately, checkpoint blockade still only benefits a fraction of patients and the reasons for treatment resistance is a very important area of research^{185,186,187,188,189,190}. Our data raise the possibility of a novel type of resistance to treatment. Repeated cycles of PD-1 blockade may gradually impair the stemness of T_{ML} and thus reduce the efficacy of immunotherapy. This effect may eventually “exhaust” the tumour immune response. Thus, the short-term interruption of PD-1:PD-L1 signalling seems to be beneficial, if it allows to clear an infection or eradicate a tumour. However, prolonged PD-1:PD-L1 blockade in the face of remaining antigen (infection or cancer) are expected to gradually reduce the efficacy of immunotherapy and may even have a detrimental effect on immune control of infection or cancer. One possible improvement could be a better timing and duration of PD-1 blockade. Fewer and milder treatments may limit the negative effect on T_{ML} stemness while still improving the $CD8^+$ T cell response. A better understanding of the impact of the PD-1 signalling pathway in T_{ML} cells, especially the effects on TCR downstream signals may be necessary to enhance the activity of T_{ML} cells without reducing their stemness.

References

1. Chaplin, D.D. Overview of the immune response. *J Allergy Clin Immunol* **125**, S3-23 (2010).
2. Amanna, I.J., Messaoudi, I. & Slifka, M.K. Protective immunity following vaccination: how is it defined? *Hum Vaccin* **4**, 316-319 (2008).
3. Forthal, D.N. Functions of Antibodies. *Microbiol Spectr* **2**, AID-0019-2014 (2014).
4. Zanetti, M. & Franchini, G. T cell memory and protective immunity by vaccination: is more better? *Trends Immunol* **27**, 511-517 (2006).
5. Klenerman, P. & Zinkernagel, R.M. What can we learn about human immunodeficiency virus infection from a study of lymphocytic choriomeningitis virus? *Immunol Rev* **159**, 5-16 (1997).
6. Zinkernagel, R.M. Lymphocytic choriomeningitis virus and immunology. *Curr Top Microbiol Immunol* **263**, 1-5 (2002).
7. Lee, K.J., Novella, I.S., Teng, M.N., Oldstone, M.B. & de La Torre, J.C. NP and L proteins of lymphocytic choriomeningitis virus (LCMV) are sufficient for efficient transcription and replication of LCMV genomic RNA analogs. *J Virol* **74**, 3470-3477 (2000).
8. Durbeej, M., Henry, M.D., Ferletta, M., Campbell, K.P. & Ekblom, P. Distribution of dystroglycan in normal adult mouse tissues. *J Histochem Cytochem* **46**, 449-457 (1998).
9. Saito, T. & Gale, M., Jr. Differential recognition of double-stranded RNA by RIG-I-like receptors in antiviral immunity. *J Exp Med* **205**, 1523-1527 (2008).
10. Suprunenko, T. & Hofer, M.J. Complexities of Type I Interferon Biology: Lessons from LCMV. *Viruses* **11** (2019).
11. Schoggins, J.W. *et al.* A diverse range of gene products are effectors of the type I interferon antiviral response. *Nature* **472**, 481-485 (2011).
12. McNab, F., Mayer-Barber, K., Sher, A., Wack, A. & O'Garra, A. Type I interferons in infectious disease. *Nat Rev Immunol* **15**, 87-103 (2015).
13. Clingan, J.M., Ostrow, K., Hosiawa, K.A., Chen, Z.J. & Matloubian, M. Differential roles for RIG-I-like receptors and nucleic acid-sensing TLR pathways in controlling a chronic viral infection. *J Immunol* **188**, 4432-4440 (2012).
14. Virgin, H.W., Wherry, E.J. & Ahmed, R. Redefining chronic viral infection. *Cell* **138**, 30-50 (2009).

15. Kalia, V., Sarkar, S. & Ahmed, R. CD8 T-cell memory differentiation during acute and chronic viral infections. *Adv Exp Med Biol* **684**, 79-95 (2010).
16. Beier, K.C., Kallinich, T. & Hamelmann, E. Master switches of T-cell activation and differentiation. *Eur Respir J* **29**, 804-812 (2007).
17. Xu, X., Li, H. & Xu, C. Structural understanding of T cell receptor triggering. *Cell Mol Immunol* **17**, 193-202 (2020).
18. Samelson, L.E. Signal transduction mediated by the T cell antigen receptor: the role of adapter proteins. *Annu Rev Immunol* **20**, 371-394 (2002).
19. Borroto, A., Abia, D. & Alarcon, B. Crammed signaling motifs in the T-cell receptor. *Immunol Lett* **161**, 113-117 (2014).
20. Hwang, J.R., Byeon, Y., Kim, D. & Park, S.G. Recent insights of T cell receptor-mediated signaling pathways for T cell activation and development. *Exp Mol Med* **52**, 750-761 (2020).
21. Dustin, M.L. The immunological synapse. *Cancer Immunol Res* **2**, 1023-1033 (2014).
22. Agrawal, S.G. *et al.* Multiple co-stimulatory signals are required for triggering proliferation of T cells from human secondary lymphoid tissue. *Int Immunol* **13**, 441-450 (2001).
23. Francisco, L.M., Sage, P.T. & Sharpe, A.H. The PD-1 pathway in tolerance and autoimmunity. *Immunol Rev* **236**, 219-242 (2010).
24. Chen, L. & Flies, D.B. Molecular mechanisms of T cell co-stimulation and co-inhibition. *Nat Rev Immunol* **13**, 227-242 (2013).
25. Curtsinger, J.M. & Mescher, M.F. Inflammatory cytokines as a third signal for T cell activation. *Curr Opin Immunol* **22**, 333-340 (2010).
26. Haring, J.S., Badovinac, V.P. & Harty, J.T. Inflaming the CD8+ T cell response. *Immunity* **25**, 19-29 (2006).
27. Kolumam, G.A., Thomas, S., Thompson, L.J., Sprent, J. & Murali-Krishna, K. Type I interferons act directly on CD8 T cells to allow clonal expansion and memory formation in response to viral infection. *J Exp Med* **202**, 637-650 (2005).
28. Vella, L.A., Herati, R.S., Wherry, E.J. CD4+ T Cell Differentiation in Chronic Viral Infection: The Tfh Perspective. *Trends in Molecular Medicine* **23**, 1072-1087 (2017).
29. Matloubian, M., Concepcion, R.J. & Ahmed, R. CD4+ T cells are required to sustain CD8+ cytotoxic T-cell responses during chronic viral infection. *J Virol* **68**, 8056-8063 (1994).

30. Szabo, S.J. *et al.* A novel transcription factor, T-bet, directs Th1 lineage commitment. *Cell* **100**, 655-669 (2000).
31. Bategay, M. *et al.* Enhanced establishment of a virus carrier state in adult CD4+ T-cell-deficient mice. *J Virol* **68**, 4700-4704 (1994).
32. Huang, Q., Hu, J., Tang, J., Xu, L. & Ye, L. Molecular Basis of the Differentiation and Function of Virus Specific Follicular Helper CD4(+) T Cells. *Front Immunol* **10**, 249 (2019).
33. Reinhardt, R.L., Liang, H.E. & Locksley, R.M. Cytokine-secreting follicular T cells shape the antibody repertoire. *Nat Immunol* **10**, 385-393 (2009).
34. Hirota, K. *et al.* Plasticity of Th17 cells in Peyer's patches is responsible for the induction of T cell-dependent IgA responses. *Nat Immunol* **14**, 372-379 (2013).
35. Gong, F., Zheng, T. & Zhou, P. T Follicular Helper Cell Subsets and the Associated Cytokine IL-21 in the Pathogenesis and Therapy of Asthma. *Front Immunol* **10**, 2918 (2019).
36. Gorentla, B.K. & Zhong, X.P. T cell Receptor Signal Transduction in T lymphocytes. *J Clin Cell Immunol* **2012**, 5 (2012).
37. Vierbuchen, T. *et al.* AP-1 Transcription Factors and the BAF Complex Mediate Signal-Dependent Enhancer Selection. *Mol Cell* **68**, 1067-1082 e1012 (2017).
38. Eferl, R. & Wagner, E.F. AP-1: a double-edged sword in tumorigenesis. *Nat Rev Cancer* **3**, 859-868 (2003).
39. Shaulian, E. & Karin, M. AP-1 as a regulator of cell life and death. *Nat Cell Biol* **4**, E131-136 (2002).
40. Garces de Los Fayos Alonso, I. *et al.* The Role of Activator Protein-1 (AP-1) Family Members in CD30-Positive Lymphomas. *Cancers (Basel)* **10** (2018).
41. Macian, F., Lopez-Rodriguez, C. & Rao, A. Partners in transcription: NFAT and AP-1. *Oncogene* **20**, 2476-2489 (2001).
42. Macian, F., Im, S.H., Garcia-Cozar, F.J. & Rao, A. T-cell anergy. *Curr Opin Immunol* **16**, 209-216 (2004).
43. Knudson, K.M. *et al.* NFkappaB-Pim-1-Eomesodermin axis is critical for maintaining CD8 T-cell memory quality. *Proc Natl Acad Sci U S A* **114**, E1659-E1667 (2017).
44. Kaech, S.M. *et al.* Selective expression of the interleukin 7 receptor identifies effector CD8 T cells that give rise to long-lived memory cells. *Nat Immunol* **4**, 1191-1198 (2003).

45. Martin, M.D. *et al.* Phenotypic and Functional Alterations in Circulating Memory CD8 T Cells with Time after Primary Infection. *PLoS Pathog* **11**, e1005219 (2015).
46. Eberlein, J. *et al.* Aging promotes acquisition of naive-like CD8+ memory T cell traits and enhanced functionalities. *J Clin Invest* **126**, 3942-3960 (2016).
47. Yuzefpolskiy, Y., Baumann, F.M., Kalia, V. & Sarkar, S. Early CD8 T-cell memory precursors and terminal effectors exhibit equipotent in vivo degranulation. *Cell Mol Immunol* **12**, 400-408 (2015).
48. Chang, J.T. *et al.* Asymmetric T lymphocyte division in the initiation of adaptive immune responses. *Science* **315**, 1687-1691 (2007).
49. Williams, M.A. & Bevan, M.J. Effector and memory CTL differentiation. *Annu Rev Immunol* **25**, 171-192 (2007).
50. Wherry, E.J. & Ahmed, R. Memory CD8 T-cell differentiation during viral infection. *J Virol* **78**, 5535-5545 (2004).
51. Homann, D., Teyton, L. & Oldstone, M.B. Differential regulation of antiviral T-cell immunity results in stable CD8+ but declining CD4+ T-cell memory. *Nat Med* **7**, 913-919 (2001).
52. Prlic, M., Williams, M.A. & Bevan, M.J. Requirements for CD8 T-cell priming, memory generation and maintenance. *Curr Opin Immunol* **19**, 315-319 (2007).
53. Sallusto, F., Geginat, J. & Lanzavecchia, A. Central memory and effector memory T cell subsets: function, generation, and maintenance. *Annu Rev Immunol* **22**, 745-763 (2004).
54. Topham, D.J. & Reilly, E.C. Tissue-Resident Memory CD8(+) T Cells: From Phenotype to Function. *Front Immunol* **9**, 515 (2018).
55. Pais Ferreira, D. *et al.* Central memory CD8(+) T cells derive from stem-like Tcf7(hi) effector cells in the absence of cytotoxic differentiation. *Immunity* **53**, 985-1000 e1011 (2020).
56. Abbas, A.K.L., A.H.; Andrew, H.; Pillai, S. *Cellular and Molecular IMMUNOLOGY*, 7th edn. ELSEVIER Saunders: Philadelphia, USA, 2012.
57. Utzschneider, D.T. *et al.* T Cell Factor 1-Expressing Memory-like CD8(+) T Cells Sustain the Immune Response to Chronic Viral Infections. *Immunity* **45**, 415-427 (2016).
58. Welsh, R.M. Blimp hovers over T cell immunity. *Immunity* **31**, 178-180 (2009).
59. Omilusik, K.D. *et al.* Sustained Id2 regulation of E proteins is required for terminal differentiation of effector CD8(+) T cells. *J Exp Med* **215**, 773-783 (2018).

60. Gautam, S. *et al.* The transcription factor c-Myb regulates CD8(+) T cell stemness and antitumor immunity. *Nat Immunol* **20**, 337-349 (2019).
61. Martin, M.D. & Badovinac, V.P. Defining Memory CD8 T Cell. *Front Immunol* **9**, 2692 (2018).
62. Chen, Z. *et al.* miR-150 Regulates Memory CD8 T Cell Differentiation via c-Myb. *Cell Rep* **20**, 2584-2597 (2017).
63. McLane, L.M., Abdel-Hakeem, M.S. & Wherry, E.J. CD8 T Cell Exhaustion During Chronic Viral Infection and Cancer. *Annu Rev Immunol* **37**, 457-495 (2019).
64. Zhao, X., Shan, Q. & Xue, H.H. TCF1 in T cell immunity: a broadened frontier. *Nat Rev Immunol* (2021).
65. Zhou, X. *et al.* Differentiation and persistence of memory CD8(+) T cells depend on T cell factor 1. *Immunity* **33**, 229-240 (2010).
66. Banerjee, A. *et al.* Cutting edge: The transcription factor eomesodermin enables CD8+ T cells to compete for the memory cell niche. *J Immunol* **185**, 4988-4992 (2010).
67. Zajac, A.J. *et al.* Viral immune evasion due to persistence of activated T cells without effector function. *J Exp Med* **188**, 2205-2213 (1998).
68. Gallimore, A. *et al.* Induction and exhaustion of lymphocytic choriomeningitis virus-specific cytotoxic T lymphocytes visualized using soluble tetrameric major histocompatibility complex class I-peptide complexes. *J Exp Med* **187**, 1383-1393 (1998).
69. Cornberg, M. *et al.* Clonal exhaustion as a mechanism to protect against severe immunopathology and death from an overwhelming CD8 T cell response. *Front Immunol* **4**, 475 (2013).
70. Bergthaler, A. *et al.* Viral replicative capacity is the primary determinant of lymphocytic choriomeningitis virus persistence and immunosuppression. *Proc Natl Acad Sci U S A* **107**, 21641-21646 (2010).
71. Wherry, E.J. T cell exhaustion. *Nat Immunol* **12**, 492-499 (2011).
72. Wherry, E.J., Blattman, J.N., Murali-Krishna, K., van der Most, R. & Ahmed, R. Viral persistence alters CD8 T-cell immunodominance and tissue distribution and results in distinct stages of functional impairment. *J Virol* **77**, 4911-4927 (2003).
73. Hashimoto, M. *et al.* CD8 T Cell Exhaustion in Chronic Infection and Cancer: Opportunities for Interventions. *Annu Rev Med* **69**, 301-318 (2018).

74. Smith, L.K. *et al.* Interleukin-10 Directly Inhibits CD8(+) T Cell Function by Enhancing N-Glycan Branching to Decrease Antigen Sensitivity. *Immunity* **48**, 299-312 e295 (2018).
75. Tinoco, R., Alcalde, V., Yang, Y., Sauer, K. & Zuniga, E.I. Cell-intrinsic transforming growth factor-beta signaling mediates virus-specific CD8+ T cell deletion and viral persistence in vivo. *Immunity* **31**, 145-157 (2009).
76. Brooks, D.G. *et al.* Interleukin-10 determines viral clearance or persistence in vivo. *Nat Med* **12**, 1301-1309 (2006).
77. Ejrnaes, M. *et al.* Resolution of a chronic viral infection after interleukin-10 receptor blockade. *J Exp Med* **203**, 2461-2472 (2006).
78. Barber, D.L. *et al.* Restoring function in exhausted CD8 T cells during chronic viral infection. *Nature* **439**, 682-687 (2006).
79. Schmitz, J.E. *et al.* Control of viremia in simian immunodeficiency virus infection by CD8+ lymphocytes. *Science* **283**, 857-860 (1999).
80. Jin, X. *et al.* Dramatic rise in plasma viremia after CD8(+) T cell depletion in simian immunodeficiency virus-infected macaques. *J Exp Med* **189**, 991-998 (1999).
81. Jamieson, B.D. *et al.* Epitope escape mutation and decay of human immunodeficiency virus type 1-specific CTL responses. *J Immunol* **171**, 5372-5379 (2003).
82. Wherry, E.J. & Kurachi, M. Molecular and cellular insights into T cell exhaustion. *Nat Rev Immunol* **15**, 486-499 (2015).
83. Wherry, E.J. *et al.* Molecular signature of CD8+ T cell exhaustion during chronic viral infection. *Immunity* **27**, 670-684 (2007).
84. Velu, V. *et al.* Elevated expression levels of inhibitory receptor programmed death 1 on simian immunodeficiency virus-specific CD8 T cells during chronic infection but not after vaccination. *J Virol* **81**, 5819-5828 (2007).
85. Radziewicz, H. *et al.* Liver-infiltrating lymphocytes in chronic human hepatitis C virus infection display an exhausted phenotype with high levels of PD-1 and low levels of CD127 expression. *J Virol* **81**, 2545-2553 (2007).
86. Brooks, D.G., Teyton, L., Oldstone, M.B. & McGavern, D.B. Intrinsic functional dysregulation of CD4 T cells occurs rapidly following persistent viral infection. *J Virol* **79**, 10514-10527 (2005).
87. Snell, L.M. *et al.* Overcoming CD4 Th1 Cell Fate Restrictions to Sustain Antiviral CD8 T Cells and Control Persistent Virus Infection. *Cell Rep* **16**, 3286-3296 (2016).

88. Lindqvist, M. *et al.* Expansion of HIV-specific T follicular helper cells in chronic HIV infection. *J Clin Invest* **122**, 3271-3280 (2012).
89. Petrovas, C. *et al.* CD4 T follicular helper cell dynamics during SIV infection. *J Clin Invest* **122**, 3281-3294 (2012).
90. Wang, L. *et al.* Increased numbers of CD5+CD19+CD1d^{high}IL-10⁺ Bregs, CD4+Foxp3⁺ Tregs, CD4+CXCR5+Foxp3⁺ follicular regulatory T (TFR) cells in CHB or CHC patients. *J Transl Med* **12**, 251 (2014).
91. Gerlach, J.T. *et al.* Recurrence of hepatitis C virus after loss of virus-specific CD4(+) T-cell response in acute hepatitis C. *Gastroenterology* **117**, 933-941 (1999).
92. Im, S.J. *et al.* Defining CD8⁺ T cells that provide the proliferative burst after PD-1 therapy. *Nature* **537**, 417-421 (2016).
93. Jeannet, G. *et al.* Essential role of the Wnt pathway effector Tcf-1 for the establishment of functional CD8 T cell memory. *Proc Natl Acad Sci U S A* **107**, 9777-9782 (2010).
94. Charmoy, M., Wyss, T., Delorenzi, M. & Held, W. PD-1(+) Tcf1(+) CD8(+) T cells from established chronic infection can form memory while retaining a stable imprint of persistent antigen exposure. *Cell Rep* **36**, 109672 (2021).
95. Wu, T. *et al.* The TCF1-Bcl6 axis counteracts type I interferon to repress exhaustion and maintain T cell stemness. *Sci Immunol* **1** (2016).
96. Teijaro, J.R. *et al.* Persistent LCMV infection is controlled by blockade of type I interferon signaling. *Science* **340**, 207-211 (2013).
97. Wilson, E.B. *et al.* Blockade of chronic type I interferon signaling to control persistent LCMV infection. *Science* **340**, 202-207 (2013).
98. Hudson, W.H. *et al.* Proliferating Transitory T Cells with an Effector-like Transcriptional Signature Emerge from PD-1(+) Stem-like CD8(+) T Cells during Chronic Infection. *Immunity* **51**, 1043-1058 e1044 (2019).
99. Beltra, J.C. *et al.* Developmental Relationships of Four Exhausted CD8(+) T Cell Subsets Reveals Underlying Transcriptional and Epigenetic Landscape Control Mechanisms. *Immunity* **52**, 825-841 e828 (2020).
100. Kumar, B.V. *et al.* Human Tissue-Resident Memory T Cells Are Defined by Core Transcriptional and Functional Signatures in Lymphoid and Mucosal Sites. *Cell Rep* **20**, 2921-2934 (2017).
101. Wieland, D. *et al.* TCF1(+) hepatitis C virus-specific CD8(+) T cells are maintained after cessation of chronic antigen stimulation. *Nat Commun* **8**, 15050 (2017).

102. Man, K. *et al.* Transcription Factor IRF4 Promotes CD8(+) T Cell Exhaustion and Limits the Development of Memory-like T Cells during Chronic Infection. *Immunity* **47**, 1129-1141 e1125 (2017).
103. Dominguez, C.X. *et al.* The transcription factors ZEB2 and T-bet cooperate to program cytotoxic T cell terminal differentiation in response to LCMV viral infection. *J Exp Med* **212**, 2041-2056 (2015).
104. Kao, C. *et al.* Transcription factor T-bet represses expression of the inhibitory receptor PD-1 and sustains virus-specific CD8+ T cell responses during chronic infection. *Nat Immunol* **12**, 663-671 (2011).
105. Utzschneider, D.T. *et al.* Early precursor T cells establish and propagate T cell exhaustion in chronic infection. *Nat Immunol* **21**, 1256-1266 (2020).
106. Chen, Z. *et al.* TCF-1-Centered Transcriptional Network Drives an Effector versus Exhausted CD8 T Cell-Fate Decision. *Immunity* **51**, 840-855 e845 (2019).
107. Yao, C. *et al.* BACH2 enforces the transcriptional and epigenetic programs of stem-like CD8(+) T cells. *Nat Immunol* **22**, 370-380 (2021).
108. Martinez, G.J. *et al.* The transcription factor NFAT promotes exhaustion of activated CD8(+) T cells. *Immunity* **42**, 265-278 (2015).
109. Agnellini, P. *et al.* Impaired NFAT nuclear translocation results in split exhaustion of virus-specific CD8+ T cell functions during chronic viral infection. *Proc Natl Acad Sci U S A* **104**, 4565-4570 (2007).
110. Seo, H. *et al.* TOX and TOX2 transcription factors cooperate with NR4A transcription factors to impose CD8(+) T cell exhaustion. *Proc Natl Acad Sci U S A* **116**, 12410-12415 (2019).
111. Kim, K. *et al.* Single-cell transcriptome analysis reveals TOX as a promoting factor for T cell exhaustion and a predictor for anti-PD-1 responses in human cancer. *Genome Med* **12**, 22 (2020).
112. Sandu, I., Cerletti, D., Claassen, M. & Oxenius, A. Exhausted CD8(+) T cells exhibit low and strongly inhibited TCR signaling during chronic LCMV infection. *Nat Commun* **11**, 4454 (2020).
113. Chen, J. *et al.* NR4A transcription factors limit CAR T cell function in solid tumours. *Nature* **567**, 530-534 (2019).
114. Liu, X. *et al.* Genome-wide analysis identifies NR4A1 as a key mediator of T cell dysfunction. *Nature* **567**, 525-529 (2019).
115. Khan, O. *et al.* TOX transcriptionally and epigenetically programs CD8(+) T cell exhaustion. *Nature* **571**, 211-218 (2019).

116. Alfei, F. *et al.* TOX reinforces the phenotype and longevity of exhausted T cells in chronic viral infection. *Nature* **571**, 265-269 (2019).
117. Yao, C. *et al.* Single-cell RNA-seq reveals TOX as a key regulator of CD8(+) T cell persistence in chronic infection. *Nat Immunol* **20**, 890-901 (2019).
118. Gupta, S.S., Wang, J. & Chen, M. Metabolic Reprogramming in CD8(+) T Cells During Acute Viral Infections. *Front Immunol* **11**, 1013 (2020).
119. Buck, M.D., O'Sullivan, D. & Pearce, E.L. T cell metabolism drives immunity. *J Exp Med* **212**, 1345-1360 (2015).
120. van der Windt, G.J. *et al.* CD8 memory T cells have a bioenergetic advantage that underlies their rapid recall ability. *Proc Natl Acad Sci U S A* **110**, 14336-14341 (2013).
121. Bengsch, B. *et al.* Bioenergetic Insufficiencies Due to Metabolic Alterations Regulated by the Inhibitory Receptor PD-1 Are an Early Driver of CD8(+) T Cell Exhaustion. *Immunity* **45**, 358-373 (2016).
122. Zhu, Y., Yao, S. & Chen, L. Cell surface signaling molecules in the control of immune responses: a tide model. *Immunity* **34**, 466-478 (2011).
123. Bardhan, K., Anagnostou, T. & Boussiotis, V.A. The PD1:PD-L1/2 Pathway from Discovery to Clinical Implementation. *Front Immunol* **7**, 550 (2016).
124. Hui, E. *et al.* T cell costimulatory receptor CD28 is a primary target for PD-1-mediated inhibition. *Science* **355**, 1428-1433 (2017).
125. Zuazo, M. *et al.* Molecular mechanisms of programmed cell death-1 dependent T cell suppression: relevance for immunotherapy. *Ann Transl Med* **5**, 385 (2017).
126. Sheppard, K.A. *et al.* PD-1 inhibits T-cell receptor induced phosphorylation of the ZAP70/CD3zeta signalosome and downstream signaling to PKCtheta. *FEBS Lett* **574**, 37-41 (2004).
127. Patsoukis, N. *et al.* Selective effects of PD-1 on Akt and Ras pathways regulate molecular components of the cell cycle and inhibit T cell proliferation. *Sci Signal* **5**, ra46 (2012).
128. Arasanz, H. *et al.* PD1 signal transduction pathways in T cells. *Oncotarget* **8**, 51936-51945 (2017).
129. Ahn, E. *et al.* Role of PD-1 during effector CD8 T cell differentiation. *Proc Natl Acad Sci U S A* **115**, 4749-4754 (2018).
130. Utzschneider, D.T. *et al.* T cells maintain an exhausted phenotype after antigen withdrawal and population reexpansion. *Nat Immunol* **14**, 603-610 (2013).

131. Youngblood, B. *et al.* Cutting edge: Prolonged exposure to HIV reinforces a poised epigenetic program for PD-1 expression in virus-specific CD8 T cells. *J Immunol* **191**, 540-544 (2013).
132. Bally, A.P.R. *et al.* PD-1 Expression during Acute Infection Is Repressed through an LSD1-Blimp-1 Axis. *J Immunol* **204**, 449-458 (2020).
133. Pauken, K.E. *et al.* Epigenetic stability of exhausted T cells limits durability of reinvigoration by PD-1 blockade. *Science* **354**, 1160-1165 (2016).
134. Odorizzi, P.M. & Wherry, E.J. Inhibitory receptors on lymphocytes: insights from infections. *J Immunol* **188**, 2957-2965 (2012).
135. Raju, S., Verbaro, D.J. & Egawa, T. PD-1 Signaling Promotes Control of Chronic Viral Infection by Restricting Type-I-Interferon-Mediated Tissue Damage. *Cell Rep* **29**, 2556-2564 e2553 (2019).
136. Frebel, H. *et al.* Programmed death 1 protects from fatal circulatory failure during systemic virus infection of mice. *J Exp Med* **209**, 2485-2499 (2012).
137. Speiser, D.E. *et al.* T cell differentiation in chronic infection and cancer: functional adaptation or exhaustion? *Nat Rev Immunol* **14**, 768-774 (2014).
138. Odorizzi, P.M., Pauken, K.E., Paley, M.A., Sharpe, A. & Wherry, E.J. Genetic absence of PD-1 promotes accumulation of terminally differentiated exhausted CD8+ T cells. *J Exp Med* **212**, 1125-1137 (2015).
139. Sakuishi, K. *et al.* Targeting Tim-3 and PD-1 pathways to reverse T cell exhaustion and restore anti-tumor immunity. *J Exp Med* **207**, 2187-2194 (2010).
140. Herbst, R.S. *et al.* Predictive correlates of response to the anti-PD-L1 antibody MPDL3280A in cancer patients. *Nature* **515**, 563-567 (2014).
141. Pircher, H. *et al.* T cell tolerance to Mlsa encoded antigens in T cell receptor V beta 8.1 chain transgenic mice. *EMBO J* **8**, 719-727 (1989).
142. Dillon, S.R., Jameson, S.C. & Fink, P.J. V beta 5+ T cell receptors skew toward OVA+H-2Kb recognition. *J Immunol* **152**, 1790-1801 (1994).
143. Siddiqui, I. *et al.* Intratumoral Tcf1(+)/PD-1(+)/CD8(+) T Cells with Stem-like Properties Promote Tumor Control in Response to Vaccination and Checkpoint Blockade Immunotherapy. *Immunity* **50**, 195-211 e110 (2019).
144. Gairin, J.E., Mazarguil, H., Hudrisier, D. & Oldstone, M.B. Optimal lymphocytic choriomeningitis virus sequences restricted by H-2Db major histocompatibility complex class I molecules and presented to cytotoxic T lymphocytes. *J Virol* **69**, 2297-2305 (1995).

145. Hudrisier, D., Oldstone, M.B. & Gairin, J.E. The signal sequence of lymphocytic choriomeningitis virus contains an immunodominant cytotoxic T cell epitope that is restricted by both H-2D(b) and H-2K(b) molecules. *Virology* **234**, 62-73 (1997).
146. Battegay, M. *et al.* Quantification of lymphocytic choriomeningitis virus with an immunological focus assay in 24- or 96-well plates. *J Virol Methods* **33**, 191-198 (1991).
147. Martin, M. Cutadapt removes adapter sequences from high-throughput sequencing reads. *EMBnet Journal* **17**, 10-12 (2011).
148. Davis, M.P., van Dongen, S., Abreu-Goodger, C., Bartonicek, N. & Enright, A.J. Kraken: a set of tools for quality control and analysis of high-throughput sequence data. *Methods* **63**, 41-49 (2013).
149. Dobin, A. *et al.* STAR: ultrafast universal RNA-seq aligner. *Bioinformatics* **29**, 15-21 (2013).
150. Anders, S., Pyl, P.T. & Huber, W. HTSeq--a Python framework to work with high-throughput sequencing data. *Bioinformatics* **31**, 166-169 (2015).
151. Wang, L., Wang, S. & Li, W. RSeQC: quality control of RNA-seq experiments. *Bioinformatics* **28**, 2184-2185 (2012).
152. Team, R.C. R: A language and environment for statistical computing. 2017 [cited] Available from: <https://www.R-project.org/>
153. Robinson, M.D. & Oshlack, A. A scaling normalization method for differential expression analysis of RNA-seq data. *Genome Biol* **11**, R25 (2010).
154. Ritchie, M.E. *et al.* limma powers differential expression analyses for RNA-sequencing and microarray studies. *Nucleic Acids Res* **43**, e47 (2015).
155. Law, C.W., Chen, Y., Shi, W. & Smyth, G.K. voom: Precision weights unlock linear model analysis tools for RNA-seq read counts. *Genome Biol* **15**, R29 (2014).
156. Phipson, B., Lee, S., Majewski, I.J., Alexander, W.S. & Smyth, G.K. Robust Hyperparameter Estimation Protects against Hypervariable Genes and Improves Power to Detect Differential Expression. *Ann Appl Stat* **10**, 946-963 (2016).
157. Benjamini, Y.a.H., Y. Controlling the False Discovery Rate: a Practical and Powerful Approach to Multiple Testing. *Journal of the Royal Statistical Society Series B* **57**, 289-300 (1995).
158. Wu, T., Hu, E., Xu, S., Chen, M., Guo, P., Dai, Z., Feng, T., Zhou, L., Tang, W., Zhan, L., Fu, X., Liu, S., Bo, X., Yu, G. clusterProfiler 4.0: A universal enrichment tool for interpreting omics data. *The Innovation* **2** (2021).

159. Schaefer, C.F., Anthony, K., Krupa, S., Buchoff, J., Day, M., Hannay, T., Buetow, K.H. PID: the Pathway Interaction Database. *Nucleic Acids Res.* **37**, D674-679 (2009).
160. Subramanian, A. *et al.* Gene set enrichment analysis: a knowledge-based approach for interpreting genome-wide expression profiles. *Proc Natl Acad Sci U S A* **102**, 15545-15550 (2005).
161. Blattman, J.N. *et al.* Estimating the precursor frequency of naive antigen-specific CD8 T cells. *J Exp Med* **195**, 657-664 (2002).
162. Scholzen, T. & Gerdes, J. The Ki-67 protein: from the known and the unknown. *J Cell Physiol* **182**, 311-322 (2000).
163. Tkachev, V. *et al.* Programmed death-1 controls T cell survival by regulating oxidative metabolism. *J Immunol* **194**, 5789-5800 (2015).
164. Zhou, T. *et al.* Inhibition of Nur77/Nurr1 leads to inefficient clonal deletion of self-reactive T cells. *J Exp Med* **183**, 1879-1892 (1996).
165. Calnan, B.J., Szychowski, S., Chan, F.K., Cado, D. & Winoto, A. A role for the orphan steroid receptor Nur77 in apoptosis accompanying antigen-induced negative selection. *Immunity* **3**, 273-282 (1995).
166. Ziegler, S.F., Ramsdell, F. & Alderson, M.R. The activation antigen CD69. *Stem Cells* **12**, 456-465 (1994).
167. Yang, C.Y. *et al.* The transcriptional regulators Id2 and Id3 control the formation of distinct memory CD8+ T cell subsets. *Nat Immunol* **12**, 1221-1229 (2011).
168. Ichii, H. *et al.* Role for Bcl-6 in the generation and maintenance of memory CD8+ T cells. *Nat Immunol* **3**, 558-563 (2002).
169. Liu, Z. *et al.* Cutting Edge: Transcription Factor BCL6 Is Required for the Generation, but Not Maintenance, of Memory CD8(+) T Cells in Acute Viral Infection. *J Immunol* **203**, 323-327 (2019).
170. Roychoudhuri, R. *et al.* BACH2 regulates CD8(+) T cell differentiation by controlling access of AP-1 factors to enhancers. *Nat Immunol* **17**, 851-860 (2016).
171. Churilla, A.M., Braciale, T.J. & Braciale, V.L. Regulation of T lymphocyte proliferation. Interleukin 2-mediated induction of c-myc gene expression is dependent on T lymphocyte activation state. *J Exp Med* **170**, 105-121 (1989).
172. Takahashi, K. & Yamanaka, S. Induction of pluripotent stem cells from mouse embryonic and adult fibroblast cultures by defined factors. *Cell* **126**, 663-676 (2006).

173. Yamada, T., Park, C.S., Mamonkin, M. & Lacorazza, H.D. Transcription factor ELF4 controls the proliferation and homing of CD8+ T cells via the Kruppel-like factors KLF4 and KLF2. *Nat Immunol* **10**, 618-626 (2009).
174. Avery, L., Filderman, J., Szymczak-Workman, A.L. & Kane, L.P. Tim-3 co-stimulation promotes short-lived effector T cells, restricts memory precursors, and is dispensable for T cell exhaustion. *Proc Natl Acad Sci U S A* **115**, 2455-2460 (2018).
175. Richter, K., Agnellini, P. & Oxenius, A. On the role of the inhibitory receptor LAG-3 in acute and chronic LCMV infection. *Int Immunol* **22**, 13-23 (2010).
176. Hannier, S., Tournier, M., Bismuth, G. & Triebel, F. CD3/TCR complex-associated lymphocyte activation gene-3 molecules inhibit CD3/TCR signaling. *J Immunol* **161**, 4058-4065 (1998).
177. Blackburn, S.D. *et al.* Coregulation of CD8+ T cell exhaustion by multiple inhibitory receptors during chronic viral infection. *Nat Immunol* **10**, 29-37 (2009).
178. Bachmann, M.F. *et al.* Normal responsiveness of CTLA-4-deficient anti-viral cytotoxic T cells. *J Immunol* **160**, 95-100 (1998).
179. Gabriel, S.S. *et al.* Transforming growth factor-beta-regulated mTOR activity preserves cellular metabolism to maintain long-term T cell responses in chronic infection. *Immunity* **54**, 1698-1714 e1695 (2021).
180. Rashida Gnanaprakasam, J.N., Wu, R. & Wang, R. Metabolic Reprogramming in Modulating T Cell Reactive Oxygen Species Generation and Antioxidant Capacity. *Front Immunol* **9**, 1075 (2018).
181. Franchina, D.G., Dostert, C. & Brenner, D. Reactive Oxygen Species: Involvement in T Cell Signaling and Metabolism. *Trends Immunol* **39**, 489-502 (2018).
182. Papavassiliou, A.G. & Musti, A.M. The Multifaceted Output of c-Jun Biological Activity: Focus at the Junction of CD8 T Cell Activation and Exhaustion. *Cells* **9** (2020).
183. Karin, M. The regulation of AP-1 activity by mitogen-activated protein kinases. *J Biol Chem* **270**, 16483-16486 (1995).
184. Mamonkin, M. *et al.* Differential roles of KLF4 in the development and differentiation of CD8+ T cells. *Immunol Lett* **156**, 94-101 (2013).
185. Robert, C. *et al.* Nivolumab in previously untreated melanoma without BRAF mutation. *N Engl J Med* **372**, 320-330 (2015).
186. Ansell, S.M. *et al.* PD-1 blockade with nivolumab in relapsed or refractory Hodgkin's lymphoma. *N Engl J Med* **372**, 311-319 (2015).

187. Kammerer-Jacquet, S.F. *et al.* Targeting the PD-1/PD-L1 Pathway in Renal Cell Carcinoma. *Int J Mol Sci* **20** (2019).
188. Rizvi, N.A. *et al.* Activity and safety of nivolumab, an anti-PD-1 immune checkpoint inhibitor, for patients with advanced, refractory squamous non-small-cell lung cancer (CheckMate 063): a phase 2, single-arm trial. *Lancet Oncol* **16**, 257-265 (2015).
189. Jenkins, R.W., Barbie, D.A. & Flaherty, K.T. Mechanisms of resistance to immune checkpoint inhibitors. *Br J Cancer* **118**, 9-16 (2018).
190. Sharma, P., Hu-Lieskovan, S., Wargo, J.A. & Ribas, A. Primary, Adaptive, and Acquired Resistance to Cancer Immunotherapy. *Cell* **168**, 707-723 (2017).